BIOGEOCHEMICAL ANALYSIS OF LEAF WAX FATTY ACIDS FROM LAKE SURFACE SEDIMENTS IN MESOAMERICA

by

Damara Jade Strong

Bachelor's of Environmental Science, Northern Arizona University, 2011

Submitted to the Graduate Faculty of

The Dietrich School of Arts and Sciences in partial fulfillment

of the requirements for the degree of

Master of Science

University of Pittsburgh

2017

UNIVERSITY OF PITTSBURGH

DIETRICH SCHOOL OF ARTS AND SCIENCES

This dissertation was presented

by

Damara Jade Strong

It was defended on

July 5th, 2017

and approved by

Dr. Emily Elliott, Associate Professor, Department of Geology and Environmental Science

Dr. Nadine McQuarrie, Associate Professor, Department of Geology and Environmental Science

Thesis Advisor: Dr. Josef Werne, Professor, Department of Geology and Environmental Science

BIOGEOCHEMICAL ANALYSIS OF LEAF WAX FATTY ACIDS FROM LAKE SURFACE SEDIMENTS IN MESOAMERICA

Damara Jade Strong, M.Sc.

University of Pittsburgh, 2017

Leaf wax hydrogen isotope (δD) values in paleoclimate records are a rapidly developing tool to determine how precipitation has changed through time. Previous studies have demonstrated a variation in fractionation of δD from precipitation and biomarker hydrogen isotope values due to biosynthesis and other environmental factors including elevation, precipitation patterns, and vegetation types, varying from region to region. This study focuses on identifying factors contributing to variations in leaf wax fatty acid abundances and meteoric δD across a Mesoamerican lake transect, as well as preliminary data identifying patterns in δD fractionation from meteoric waters to fatty acids.

Lake core top samples were taken from over 150 sites throughout Mesoamerica. These samples span environmental, elevational, and longitudinal gradients, and vary among lake types. All samples exhibited an even-over-odd predominance of fatty acid chain lengths across Mesoamerica, indicating little degradation of terrestrial input and successful recovery of leaf waxes for δD analysis. Most samples exhibited a dominance in terrigenous fatty acid input into the lake with short-chained fatty acids in relatively low abundance, assuring little contamination to the lake sediment surface samples from petroleum byproducts and successful recovery of fatty acids for δD analysis.

δD from lake waters (δD_{water}) from approximately 85 lake sites was analyzed for comparison with leaf wax δD for quantifying fractionation during incorporation of δD into the

leaf wax compounds. This study found an overall decline in δD_{water} values further from the coast westward and an overall decline in δD_{water} values with increasing elevation, however the correlations were insignificant with R^2 values of 0.19 and 0.08, respectively. However, the p-value of longitude and elevation vs δD_{water} is 0.024, indicating a significant impact of these independent factors on δD_{water}. δD_{water} analyses across elevational and longitudinal transects demonstrate no clear uniform effects on δD_{water} values, indicating stronger local effects than regional effects on δD_{water}.

Preliminary data demonstrate the potential for successful analysis of δD leaf waxes due to the robust recovery of fatty acids from the lake sediments and initial results of effects on δD_{water} for future interpretation in the δD leaf wax/water calibration and downcore lake sediment paleoclimate studies.

TABLE OF CONTENTS

LIST OF TABLES

LIST OF FIGURES

ACKNOWLEDGEMENTS

I want to thank everyone who has supported me throughout this process. First, I would like to thank Dr. Josef Werne for bringing me to Pittsburgh to start my graduate education process, as well as for advising me through my passion in climate and speaking about science, leading me to a career of science outreach. I would also like to thank Elisabeth Svensson, Molly O'Beirne, and more recently Dr. T.E. Arnold for always being there when I have a question and when I need help fixing yet another instrument. I want to thank our entire lab group, former and current members, Troy Ferland, Dervla Kumar, Arielle Woods, Tyler Myers, Evan Scott, Elizabeth Holmes, Christina Puhtany, and many others for helping me when I worked long hours in the lab, from typical clean-up to lab maintenance. I also want to thank my friends in the Geology and Environmental Science Department and Barbara Paul for the mental and emotional support. Last, but not least, I want to thank my husband, Jason Strong, and my son, Aiden Strong, sticking with me through the ups and downs of being a graduate student while trying to maintain a family life. Thank you for all your love and support through this process.

1.0 INTRODUCTION

With the ongoing international concern of global climate change, understanding Earth's climate variability and the impact it has on ecosystems is crucial for mitigation and adaption in response to future climate scenarios. It is projected by 2080 more than 17% of the Earth's surface will be occupied by no-analog climates, with 80% of these regions in the tropical and subtropical northern hemisphere (García-Lopez and Allue, 2013). To understand modern climate change, it is important to acquire paleoclimatic records and to develop climate models based on past climate patterns and associated environments and analyze their link to changing global temperatures. Based on the most recent collaborative climate models, warming temperatures related to modern climate change are expected to alter the amount of regional precipitation and strength of storm systems within the next 20 years, causing drought in many locations in subtropical regions, including the American Southwest, Mexico, and northern Central America (IPCC, 2013).

Mexico and Central America is very sensitive to subtle changes in global climate due to modern water stress, which can become progressively worse by increasing global temperatures and the increased anticipated drought across the region (IPCC, 2013). Most areas in the Trans-Mexican Volcanic Belt (TMVB) in central Mexico are already experiencing a decline in water availability due to increasing populations and are projected to become more arid in response to anthropogenically-driven climate change (Mendoza et al., 1997; Lounejeva Baturina et al., 2006;

IPCC, 2007; Seager et al., 2007). Mesoamerica is expected to warm between 2 and 4ºC by the end of the 21st century, with decreases in precipitation of 10-20% and more warming predicted in the northern section of Mesoamerica with a larger decrease in precipitation during the wet season in Guatemala and the dry season in the TMVB (IPCC, 2007).

To understand how changing climates could impact the future, researchers must study how previous global temperature changes influenced climate systems in the past. Previous studies have indicated varying sources of moisture during the last glacial period in Mexico. Using pollen and diatom proxies in a 48,000-year lake sediment record from Lake Patzcuaro, Jalisco, Mexico, Bradbury (2000) found wetter conditions prior to 10,000 years ago. Bradbury (2000) hypothesizes the dominance of westerly winds pushed south by the Laurentide ice sheet, increasing precipitation in central Mexico. Lyle et al. (2012) also suggested the continental ice sheet caused differences in atmospheric circulation patterns 17,000 years before present, which would have influenced precipitation across North America as far south as Northwestern Mexico (Figure 1), with little mention of the extent of the influence on the Trans-Mexican Volcanic Belt through the Yucatan Peninsula. Paleoehydrological studies using paleorecords spanning longer than the Last Glacial Maximum are sparse across Mesoamerica, and researchers have yet to confirm Bradbury's (2000) hypothesis in this region.

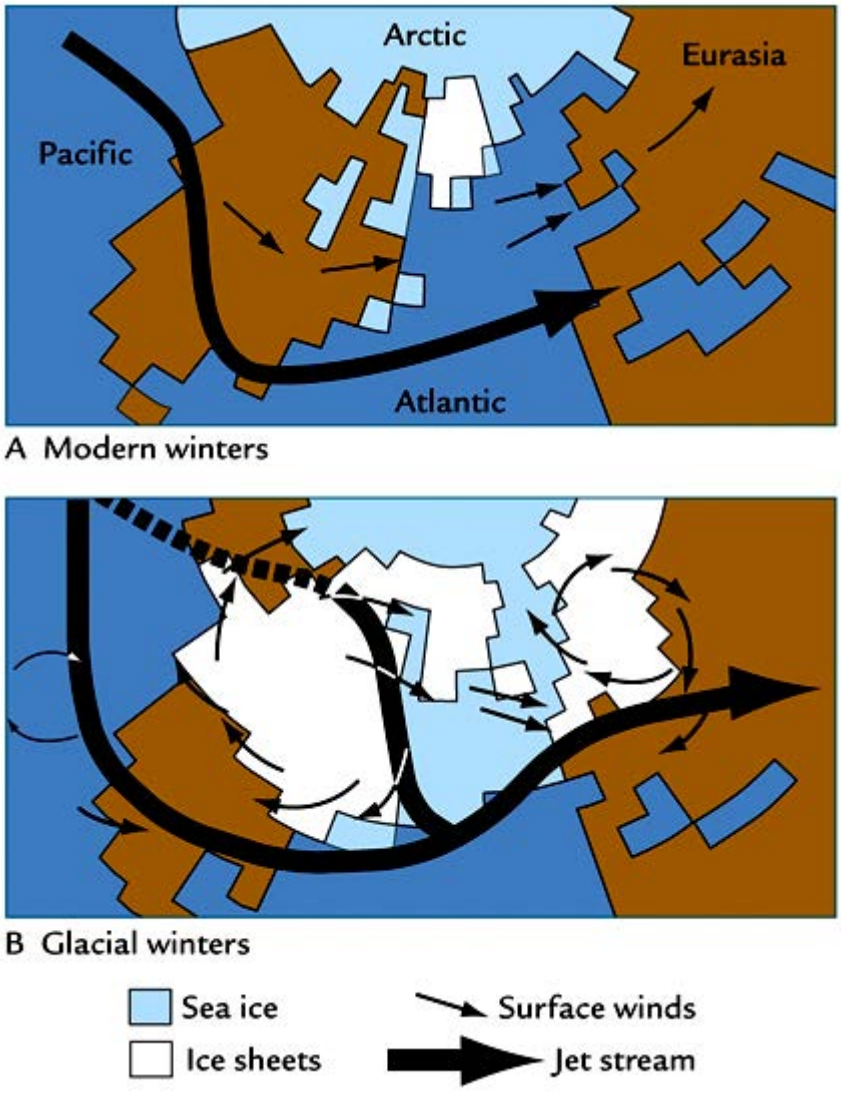

Figure 1 – The jet stream shown in modern winters (A) vs winters during the Last Glacial Maximum in the presence of the Laurentide ice sheet (B; from Ruddiman, 2013). This model shows a split in the jet stream due to the continental ice sheet, and therefore a southern storm path during the Last Glacial Maximum, bringing rain much further south than in modern winters.

Paleoprecipitation and aridity can be evaluated using various proxies, including pollen type, sedimentation rates, magnetic susceptibility, diatom productivity, and X-ray fluorescence. However, any paleoclimate proxy must be vetted by a modern study to understand the climate-proxy relationship. The long-term goal of this study is to determine interpretation of the novel proxy of terrestrially-derived leaf wax biomarkers across Mesoamerica from lake surface sediments and their corresponding hydrogen isotope value. Many environmental factors influence the hydrogen isotope values of biomarkers, which could cause unclear interpretation downcore. Determining how environmental factors influence these proxies is important in understanding the accuracy of its use in paleoclimate research.

Previous studies have looked at the fidelity of leaf-wax biomarkers and the interpretation of corresponding hydrogen isotopes from lake surface sediments across a wide range of climate systems, including the Tibetan Plateau (Bai et al., 2015), the Andes and the Amazon (Feakins et al., 2016), Cameroon (Garcin, et al., 2012), Europe (Sachse et al., 2004) and North America (Huang et al., 2004; Hou et al., 2008; Feakins and Sessions, 2010). Leaf wax biomarker hydrogen isotopes have been shown to be a promising proxy for meteoric water interpretation in modern lake sediment surface samples and paleo lake sediment samples, however this approach requires a local calibration of how leaf wax hydrogen isotope values translate meteoric water hydrogen isotope values to interpret lake sediment core paleoclimate data (Aichner et al., 2010).

1.1 MODERN MESOAMERICAN CLIMATE

To interpret δD values of meteoric water and biomarkers in terms of past climatic conditions, it is critical to understand how climate forcings across the region alter precipitation source,

distributions, and magnitude. Mean annual precipitation (MAP) varies widely across Mesoamerica with much drier regions in the TMVB, getting progressively wetter eastward into the lowlands of the Yucatan Peninsula and Guatemala. In western Mesoamerica, the primary driver of precipitation is the southern extent of the North American Monsoon (NAM), bringing significant summer rainfall across much of Mexico, with moisture coming from the Pacific and Gulf of Mexico (Figure 2; Higgins et al., 1998; Metcalfe et al., 2000). The NAM is centered in the southwestern United States and northwestern Mexico; however, the winter phase of the NAM brings winter precipitation to western Mexico, delivering most of the annual rainfall to the region (Metcalfe et al., 2000). Despite the increase in rainfall in the winter, the amount of precipitation remains low in the region throughout most of the year.

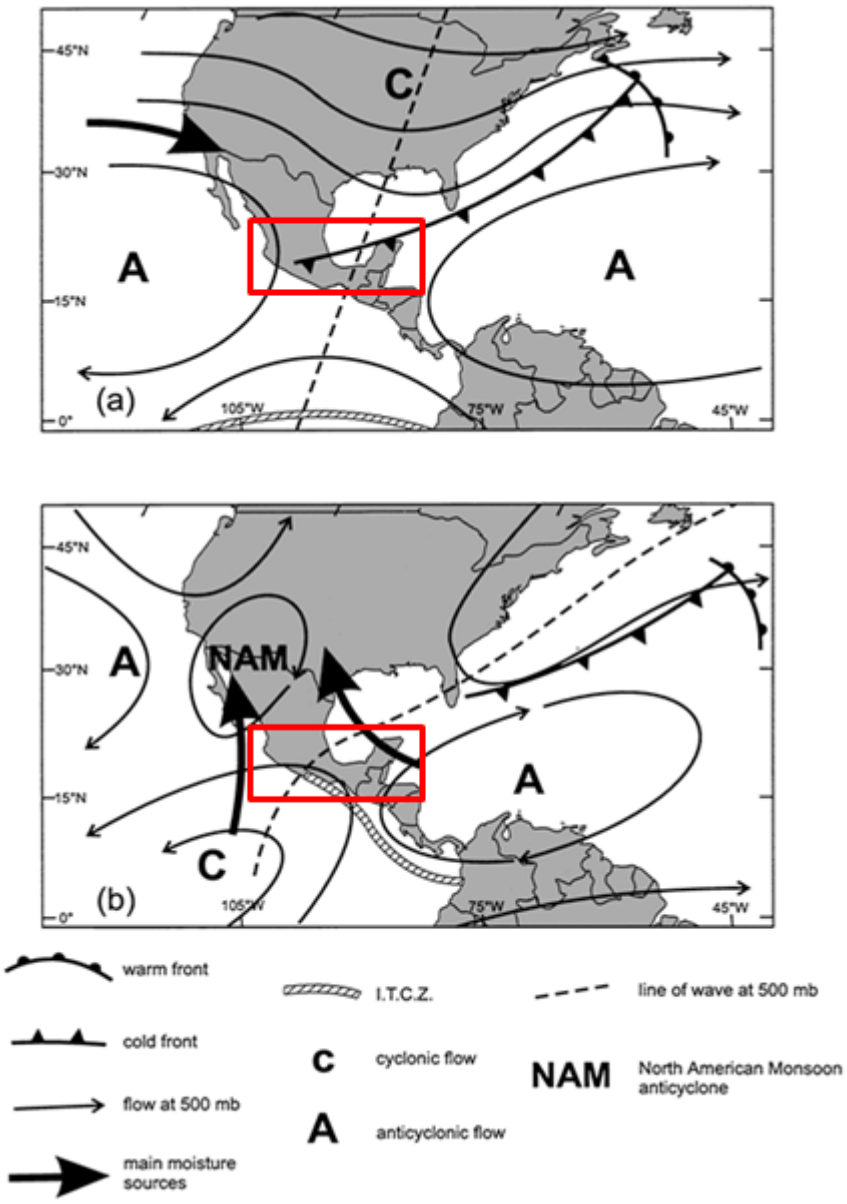

Figure 2 – The major hydrological systems that deliver sources of moisture to southern North America and Central American during the winter (above) and summer (below). The heavy arrows display the dominant sources of moisture (modified from Metcalfe et al., 2000).

The NAM, in turn, is influenced by many other atmospheric circulation systems including the trade winds/Intertropical Convergence Zone (ITCZ; Adams and Comrie, 1997). The ITCZ is a low-pressure belt in the equatorial zone, shifting seasonally following maximum insolation, which brings the ITCZ into the northern hemisphere in the boreal summer and into the southern hemisphere in the boreal winter (Figure 2; Metcalfe et al., 2000). The ITCZ is further impacted by long-term changes in climate, causing shifts of the ITCZ further north or further south depending on sea surface temperatures and atmospheric heat transport near the equator (McGee et al., 2014). The extent of the ITCZ in paleostudies should be interpreted along with regional climate forcings, as the impact on precipitation can vary both locally and seasonally (McGee et al., 2014). The strength of the NAM and position of the ITCZ are affected by the variability in insolation, with stronger boreal summer insolation shifting the ITCZ further northward, increasing the intensity of the NAM (Haug et al., 2001). The ITCZ is the main driver of precipitation in central and eastern Mesoamerica, including the Basin of Mexico and Guatemala, delivering most of the region's annual precipitation during its northernmost extent in the boreal summer (Figure 2; Hodell et al., 2008).

1.2 IMPORTANCE AND SUCCESS OF LEAF WAX HYDROGEN ISOTOPE COMPOSITION CALIBRATIONS

Previous studies have examined past ecosystems, lake changes, and climate across Mesoamerica; however, these proxies are limited due to hiatuses in lake sediment cores, lake sediment cores not extending far past the Holocene (12,000 years ago), or due to environmental limitations. For example, the high-desert ecosystems in the TMVB are dominated by pine, which tend to overproduce pollen, skewing the pollen records retrieved for vegetation reconstruction in paleoecology studies (Lozano-García and Xelhuantzi-López, 1997; Metcalfe, 1997). A consistent proxy is needed to determine climate and environmental change across Mesoamerica, along with long, continuous records reaching as far into the past as the Last Glacial Maximum for a clearer understanding of impacts associated with global climate change in the region. The novel leaf wax biomarker and corresponding δD proxy has the potential to quantitatively assess hydroclimate through time and is robust across a range of different climate conditions. However, a potential problem with the δD leaf wax proxy is the extent to which the precipitation signal is masked by factors such as changing vegetation and elevation.

To address potential issues with the δD leaf wax proxy, biome type and elevation analyses will be included in the interpretation of my abundances of leaf waxes from lake surface sediments and the δD values of meteoric waters. This will assist in the interpretation of leaf wax δD seen in the calibration and future downcore analyses. Douglas et al. (2012) recently conducted a δD calibration study across Guatemala and part of eastern Mexico and Honduras, and found that although meteoric water δD exerts a strong influence on δD of leaf waxes, there are other environmental factors influencing leaf wax δD. Douglas et al. (2012) resolved these environmental effects by analyzing aridity and $\delta^{13}C$ values of leaf waxes to determine additional

effects of differing vegetation contribution to sedimentary leaf wax δD. By focusing on the environmental and elevation effects on δD of leaf wax fatty acids of lake sediments, the long-term goals of this study can contribute to the interpretation of downcore δD analysis in the future. The short-term goal of this study is to quantify fatty acid leaf wax abundances and origins to provide a clear interpretation of future δD leaf wax analysis, including information about watershed environments, climate, and leaf wax contributions to the lake sediments covering the range of the Trans-Mexican Volcanic Belt to the Yucatan Peninsula and part of Central America. While a precise calibration between leaf wax and rainfall hydrogen isotopes is lacking in Mesoamerica, preliminary data from this region suggests a strong likelihood of success (Douglas et al., 2012).

1.3 CALIBRATION PROXIES

1..1 *N*-alkanoic acids

Organic material from living organisms in and around a basin can be preserved in lake sediments and thus used as proxies for paleoanalysis. Organic material is washed into lacustrine and marine basins primarily by runoff and river transport, but can also travel by wind (Killops and Killops, 2004; Eglinton and Eglinton, 2008). The organic matter undergoes degradation in the water column due to chemical and physical weathering, dependent on the chemical parameters of the water and the heterotrophs present in the aquatic basin (Killops and Killops, 2004). The most stable organic compounds, typically lipid-derived due to their structural stability, are unaltered or partly altered during deposition but retain structural similarity to their biological precursor

molecules (Cranwell, 1982; Killops and Killops, 2004). The organic compounds that survive with little to no degradation and are deposited and preserved in the sedimentary record are called biomarkers.

Biomarkers are derived from both aquatic and terrestrial sources. They can provide a range of information about water sources, watershed environments, climate, and community types. Depending on the specificity of the biomarker and its extent of preservation, the source organism of the biomarker could be identified, and estimates of organism community contribution to the sediments can be quantified (Killops and Killops, 2004).

This study focuses on the use of leaf waxes, the fatty acid lipids derived from the surface of terrestrial and aquatic plant leaves, and their isotopic composition. Leaf waxes are a thin layer of wax consisting of a mixture of esters of long-chain fatty acids with long-chain fatty alcohols (Rezanka and Sigler, 2009). Leaf waxes can be abraded from the plant via wind or washed off by precipitation and carried by atmospheric deposition, runoff, or stream water to an aquatic basin for final deposition in lake or marine sediments (Figure 3; Eglinton and Eglinton, 2008).

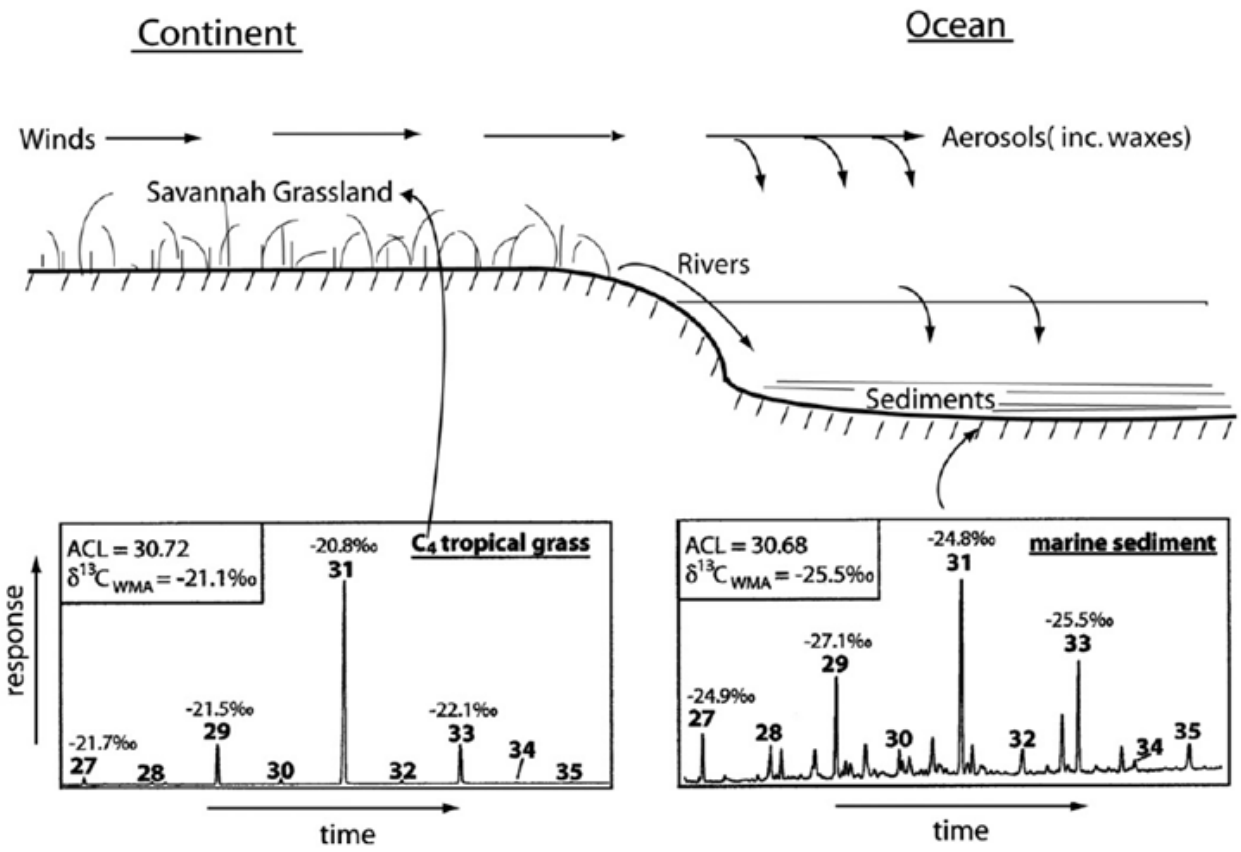

Figure 3 – Transportation of terrestrial leaf waxes/lipid biomarkers to a basin (from Eglinton and Eglinton, 2008). The biomarkers identified in this figure are *n*-alkanes, but fatty acid leaf waxes, or *n*-alkanoic acids, are transported via the same mechanisms. Above diagram displays oceanic sediments, however transportation is similar into lacustrine basins.

Fatty acids, or more specifically *n*-alkanoic acids, are composed of a long chain of covalently-bound carbon and hydrogen atoms with a carboxyl end group, written as $CH_3(CH_2)_nCO_2H$ (Eglinton and Eglinton, 2008). The number of carbon atoms in fatty acids from leaf waxes typically range from C_{20} to C_{30} or more in sediments and has an even-over-odd predominance of carbon chain lengths indicating a vegetative source of leaf wax fatty acids (Rezanka and Sigler, 2009). If an even-over-odd predominance is not observed in leaf wax fatty acids deriving from lake surface sediments, there is likely a contribution of petroleum or plastic fatty acids in the depositional environment and/or during the extraction process of the fatty acids from the lake surface sediments. This study uses *n*-alkanoic acids, as opposed to *n*-alkanes, due to their typically high abundance in terrestrial vegetation, including both angiosperms and gymnosperms – *n*-alkanes are typically found in low abundances in gymnosperms, limiting the use of the specific biomarker (Diefendorf et al., 2011). Quantifying abundances of specific chain-lengths of fatty acids, and other biomarkers, assists in identifying the relative distribution and contributions of various sources of fatty acids to the sediments. Fatty acid abundances coupled with their corresponding isotopic values further identifies environmental effects on the compound, such as determining local climate effects using hydrogen isotopes.

1.3.2 δD values of meteoric water and leaf waxes

Hydrogen isotope composition (δD) refers to the deuterium/protium (D/H) ratio within a given molecule. The δD value that is ultimately recorded in a leaf wax is a function of both the δD of meteoric waters as well as the alteration of that value through evaporation from the soil and transpiration and biosynthesis in plants (Figures 4 and 5). This study focuses on the changes in

δD values between meteoric waters to better understand the impacts of these processes on δD leaf wax values and the final fractionation values (ε).

The δD of precipitation varies depending on the source of the moisture and the path traveled to the area of deposition (Alley and Cuffey, 2001). The isotopic composition of a condensing air mass is affected by the composition of the source water, often an ocean surface, providing the vapor, as well as the fractionation that occurs during the change of state from a liquid to a vapor via evaporation (Dansgaard, 1964; Ingraham, 1998; Alley and Cuffey, 2001). The isotopic fractionation occurring during evaporation and condensation are temperature dependent, and can vary greatly in different regions (Alley and Cuffey, 2001). There are several observed effects on the δD values of water related to patterns and history of evaporation & condensation of a given atmospheric water mass.

i. Continental effect: Meteoric water is more D-depleted farther from the source of the water vapor. Condensing precipitation tends to be more D-enriched than the remaining vapor due to fractionation during condensation (Figure 4; Ingraham, 1998; Alley and Cuffey, 2001).
ii. Elevation effect: Meteoric water is more D-depleted at higher elevations, caused by increased rain at the higher elevations due to continuous cooling of the air mass to below dew point and the orographic effect (Figure 4; Ingraham, 1998; Alley and Cuffey, 2001).
iii. Latitude effect: Meteoric water is more D-depleted at higher latitudes, caused by increased rainout at higher latitudes and greater isotopic fractionation at the cooler temperatures, generally at higher latitudes (Ingraham, 1998).
iv. Amount effect: Water from smaller rainstorms is generally more D-enriched than the water collected during larger rainstorms. In smaller rainstorms, liquid reaching the

ground can become more D-enriched by evaporation during its descent (Ingraham, 1998).

v. Seasonal effect: When an air mass reaches a more advanced stage of rainout, precipitation condenses at cooler temperatures, causing winter precipitation to be more D-depleted than summer precipitation (Simpson et al., 1972; Ingraham, 1998). Summer may experience more evapotranspiration from higher temperature during the decent of the rain drop, resulting in D-enriched precipitation (Ingraham, 1998), which is often seen in arid environments, causing isotopically heavier rain.

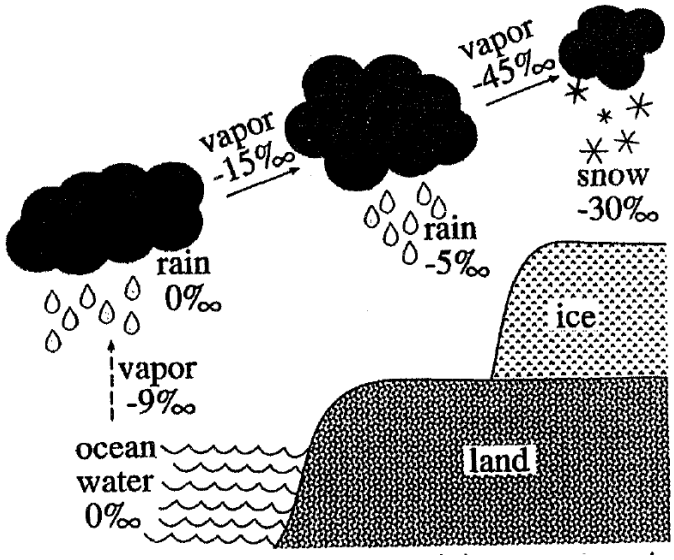

Figure 4– An illustration of continental and elevation effects on δD of meteoric water, not representing concrete values, starting with evaporation from the oceanic source to its site of deposition (Alley and Cuffey, 2001).

It is important to quantify the difference between the meteoric/local water δD values and the δD of leaf waxes across varying environmental and climatic regimes due to the multiple fractionation effects occurring from the uptake from the source water to incorporation into the final biomarker product.

When precipitation is deposited onto the surface and infiltrated into the groundwater, plants take up the water for biosynthetic processes to create necessary compounds, including leaf waxes. The hydrogen (H) and oxygen (O) isotopes are fractionated during biosynthesis, preferably incorporating the lighter isotope of hydrogen (^{1}H) into the final product, as a lighter mass requires the plant to use less energy (Sachse et al., 2012). The hydrogen isotope composition of lipid biomarkers is controlled by three main factors: isotopic compositions of biosynthetic precursors, fractionation and exchange accompanying biosynthesis, and hydrogenation during biosynthesis (Figure 5; Sessions et al., 1999; Sachse et al., 2012). Once incorporated into the leaf, the hydrogen atoms of leaf wax biomarker compounds are covalently bonded to the carbon atoms and therefore not exchangeable (Schimmelmann et al., 1999).

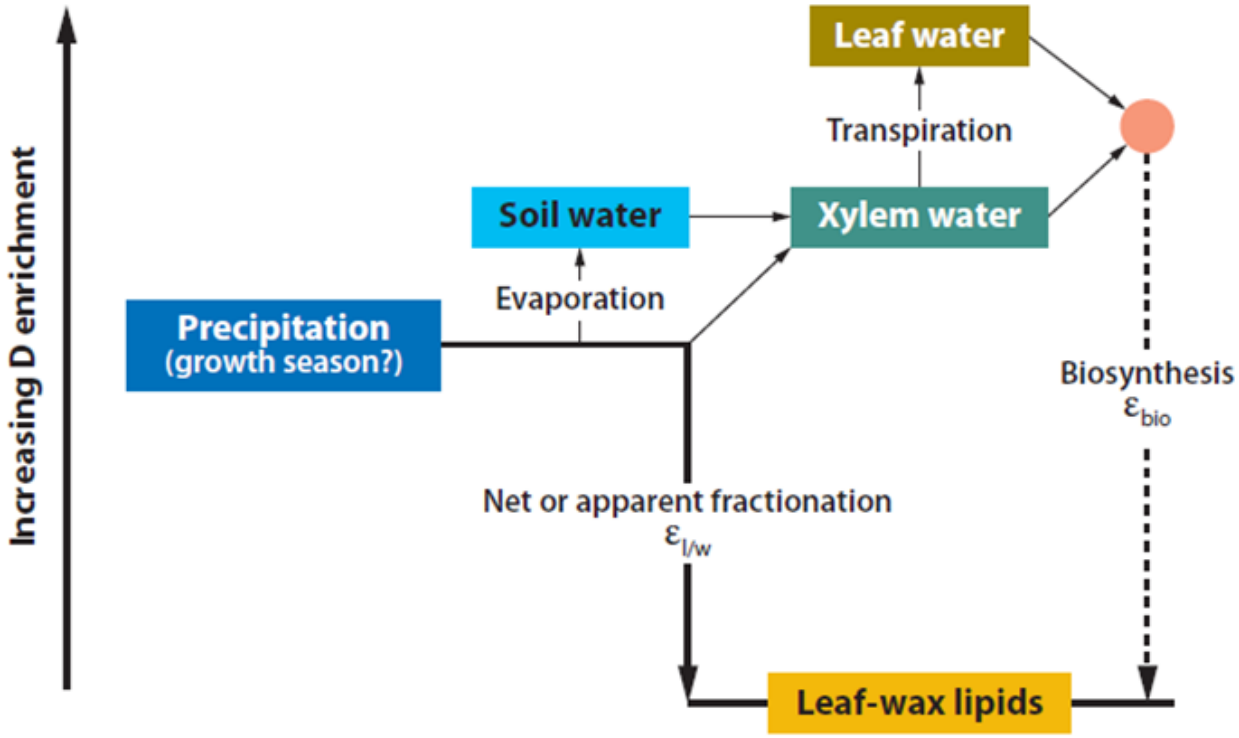

Figure 5 – A conceptual diagram describing the hydrogen isotope relationship between precipitation and leaf-wax lipids (from Sachse et al., 2012). The red dot represents the hypothetical source water for the plant.

The δD of leaf waxes is further impacted by environmental factors before and after the water is incorporated into the lipid compound. The amount of fractionation varies widely due to potential evapotranspiration from soil and leaf water, relative humidity, plant life form (e.g. tree, shrub, grass), and physiological differences of plant types such as photosynthetic pathways or water-use efficiency (Sessions et al., 1999; Hou et al., 2008; Castaneda and Schouten, 2011; McInerney et al., 2011; Sachse et al., 2012; Gotsch, et a., 2014).

The apparent fractionation of individual species differs due to their varying biosynthetic processes. Feakins and Sessions (2010) found ranges in fractionation from -41‰ to -55‰ (for a few shrub species) to approximately -140‰ (for trees and grasses) in the same locality. Many other studies have found a similar spread in apparent fractionation between species (e.g. Sachse et al., 2006; Hou et al., 2007; Feakins and Sessions, 2010). Although the apparent fractionation of individual terrestrial species is widely variable, observations of the leaf wax δD values of vegetation communities give an average of values that agree with climate trends in modern studies (e.g. Sachse et al., 2004; Hou et al., 2008; Xia et al., 2008). Overall, vegetative community mean-weighted leaf isotopic compositions reflect the isotopic composition of meteoric waters (Figure 6; Feakins and Sessions, 2010; Polissar and Freeman, 2010, Feakins et al., 2016).

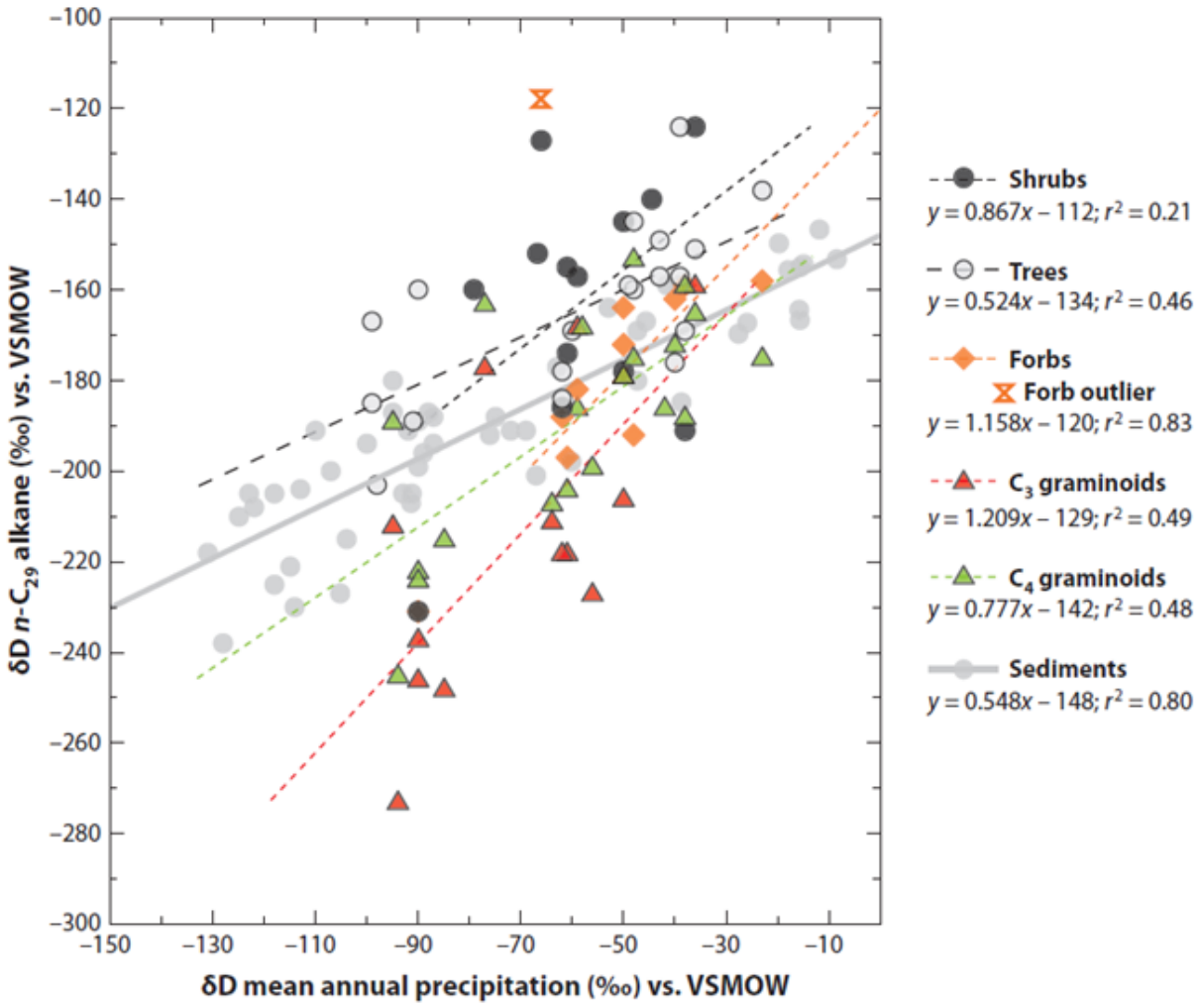

Figure 6 – The site-averaged δD of *n*-alkanes vs the δD of the mean annual precipitation for vegetation source-specific comparison to sedimentary average data (from Sachse et al., 2012). Although δD values of leaf waxes vary by plant functional type, the average of the leaf waxes found in surface sediment lake deposits have a strong correlation with the δD of mean annual precipitation.

Understanding the hydrogen isotope fractionation value of a vegetative community is more important than the fractionation of individual species when applying these values to lipid biomarker δD values in the paleorecord. Net fractionation of δD values within terrestrial plants in arid to semi-arid regions is typically much smaller than temperate, alpine, and tropical forests due to higher evapotranspiration (Feakins and Sessions, 2010). Feakins and Sessions (2010) demonstrated apparent fractionation of leaf wax biomarkers from meteoric waters in arid to semi-arid sites from the Southern California coast to the Mojave Desert to be -94±21‰ δD. This is similar to the findings from Hou et al. (2008), who determined an average fractionation of -99±8‰ using sedimentary C_{28} *n*-alkanoic acids along a transect from Texas to New Mexico. Previous studies of more humid and temperate climates in the central and northeastern United States, southeastern Asia, and northern Asia demonstrate apparent fractionation values of leaf wax lipids to range up to -160‰ (Sachse et al., 2006; Hou et al., 2007; Feakins and Sessions, 2010). The apparent fractionation of leaf wax δD of different ecosystem types and within different climate regions is important in applying the fractionation value of δD to lipid biomarkers in the paleorecord. Quantifying the fractionation value between δD of meteoric waters and leaf wax δD in modern sediments allows us to more accurately estimate the δD of the source water in downcore leaf wax δD studies.

Apparent fractionation between meteoric water δD and leaf wax δD has recently been measured by Bai et al. (2015) using different elevation transects across the Tibetan Plateau. The Tibetan Plateau exhibits large amount of rainfall just south of the Himalayan Mountains, but mild to arid conditions on the plateau. The apparent fractionation values remained fairly constant with values ranging from -99‰ to -110‰ throughout the region (86^{o}E to 98^{o}E), with varying elevation effects on different transects (Bai et al., 2015). The leaf wax δD values from

each transect exhibited an altitudinal lapse rate with increasing elevation (Figure 7). The soil δD of leaf waxes in the Southern Himalayan transect, furthest west in their study site with an altitude range of 1660 to 5050 meters, had an altitudinal lapse rate of -2.4‰/100m due to the significant change in altitude over short distances (Bai et al., 2015). The Bayi-Lhasa transect, with an altitude of 3050 to 4970 meters and just east of the Southern Himalayan transect, had a soil δD leaf wax altitudinal lapse rate of -1.4‰/100m reflecting the combination of local continental and altitudinal effects (Bai et al., 2015). The Zayu-Bomi transect, furthest east in the study region with an altitude of 1468 to 4800 meters, had a soil δD leaf wax altitudinal lapse rate of -3.3‰/100m above 3000 meters and -1.35‰/100m below 3000 m (Bai et al., 2015).

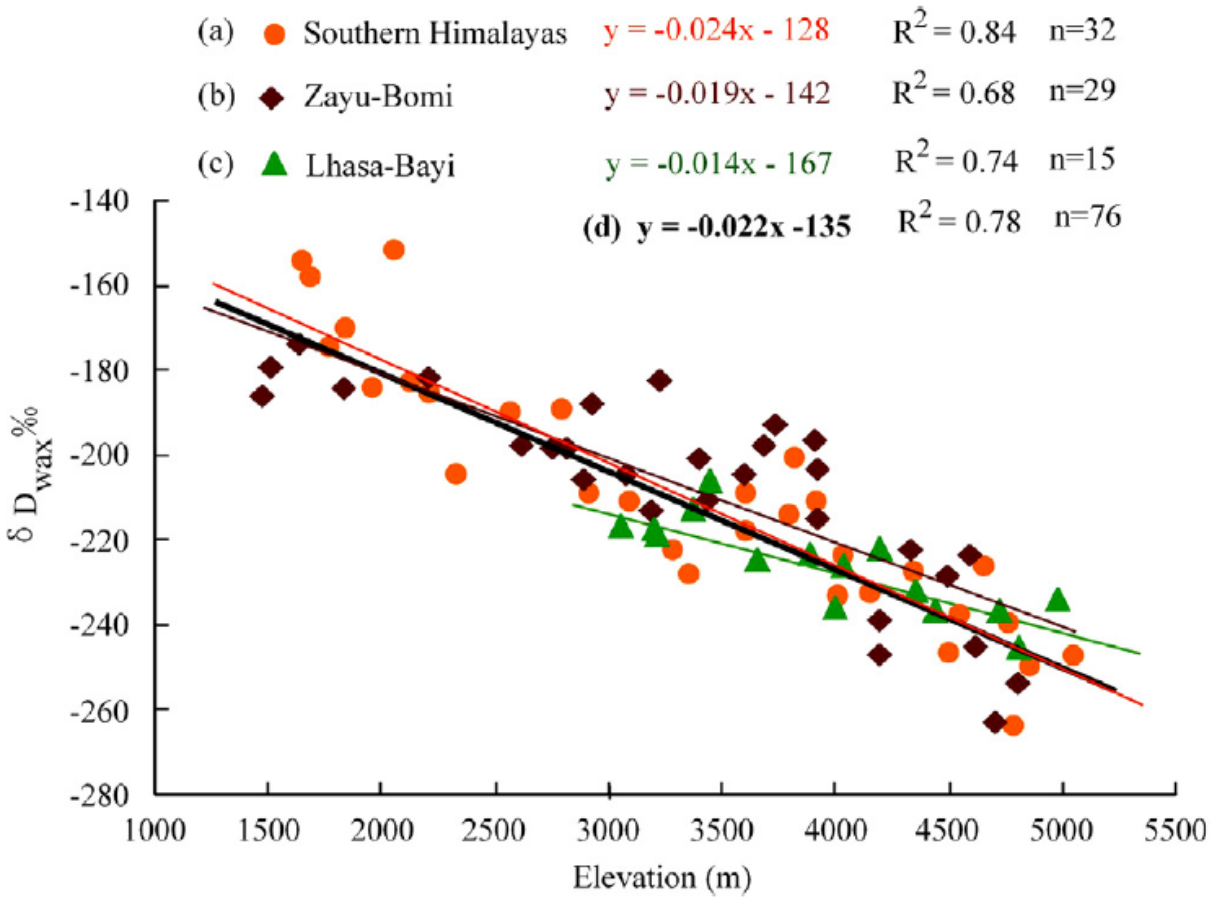

Figure 7– Soil δD leaf wax values vs. elevation along the Southern Himalayan, Zayo-Bomi, and Lhasa-Bayi transects (from Bai et al., 2015).

Bai et al. (2015) concluded that the variation in the lapse rate in the Zayu-Bomi transect is due to the latitudinal effect counteracting the elevation effect in the lower part of the transect. Bai et al. (2015) concluded that the isotopic effects of meteoric waters control the leaf wax δD values; however, various moisture sources and other local environmental conditions still influence the rate at which the elevation can influence the leaf wax δD. The Bai et al. (2012) study introduces the impacts of elevation and continental effects on leaf wax δD values across a mountainous region. This study will analyze the effects on δD values of meteoric water across a region of varying elevations and intensity of climate systems.

1.4 RESEARCH OBJECTIVES AND APPLICATION

The short-term goal of this study is to determine the success of leaf wax recovery and initial assessment of the extent to which the hydrogen isotope composition of meteoric waters track precipitation regionally, and how they are affected by local (e.g. orographic) effects. Analyses include abundances of leaf wax fatty acids from modern lake surface sediments across Mesoamerica based on biome type and the hydrogen isotopic composition (δD) of meteoric waters. This work will contribute to the understanding of how climate, particularly precipitation, has changed through time in Mesoamerica when the long-term research goal of a δD leaf wax/water calibration is applied to downcore studies.

Specifically, this calibration analysis is comprised of two main parts: 1) interpretation of fatty acid leaf wax abundance and distribution across Mesoamerica, the proposed complete region of the δD calibration, to determine the successful recovery of leaf wax fatty acids from the lake surface sediments and 2) the δD analysis of meteoric waters across Mesoamerica to

determine the effects on δD values across the region, particularly the continental and elevation effects. This study sets the stage for utilizing leaf wax δD analyses for paleoclimate reconstructions in the TMVB and Yucatan Peninsula and Central America.

I expect to find abundant terrestrial FAMES in lake sediment surface samples across the Mesoamerican region for δD analyses. Leaf waxes are extremely abundant across all terrestrial plant types and therefore provide a strong signal of leaf wax contribution to lakes in their watershed. I also expect to find various factors contributing to the water δD values across Mesoamerica, including a continental effect and elevation effect causing lower δD values of meteoric waters as moving away from the water vapor source. Due to the significant variation in MAP and climate systems across the region (Metcalfe, 2000), δD values will be expressed differently based on factors such as distance from the source of water vapor, elevation, and lake conditions. Evaporative enrichment in lakes may also have a large impact on δD water values depending on the year-round conditions of the lakes, for example, in the Trans-Mexican Volcanic Belt where it is typically dry nearly year-round, more evaporative enrichment would be expected relative to the wetter Eastern Mesoamerican lowlands.

2.0 METHODS

2.1 STUDY SITES AND SAMPLE COLLECTION

Approximately 150 lake surface sediment samples were collected in glass jars or whirlpaks between 2005 and 2013 by researchers from Universidad Nacional Autonoma de Mexico (UNAM) and Technische Universitat Braunschweig (Figure 8). The sample sites range from 15 to 22 degrees latitude and about -87 to -105 degrees longitude, spanning Central and Southern Mexico, Guatemala, Belize, Honduras, and El Salvador. Samples varied in size from site to site and among different sampling trips. Several samples were taken from the same lake or reservoir at different lake sediment surface depths to compare the signatures given from the littoral zone and the deepest part of the lake for the long-term goal of leaf wax δD analysis.

Figure 8 – The lake sample sites of Mesoamerican Lake Calibration project. Sites are represented by red dots.

Some sets of sediment and water samples were taken along longitudinal, latitudinal, and elevation gradients and across varying biomes to help quantify the response of leaf wax δD composition in different environments. The biome map shape file from Olsen et al. (2001) was used for biome classification for each study site. Five different biome types were identified across the study region: tropical and subtropical moist broadleaf forests, tropical and subtropical dry broadleaf forests, tropical and subtropical coniferous forests, deserts and xeric shrublands, and mangroves (Figure 9). The Trans-Mexican Volcanic Belt and Eastern Mesoamerican transects both had lake surface sample sites in tropical and subtropical moist broadleaf forests, tropical and subtropical dry broadleaf forests, and tropical and subtropical coniferous forests, however the deserts and xeric shrubland and mangrove sites were only located in the TMVB/Central Mexican transect (Figure 9).

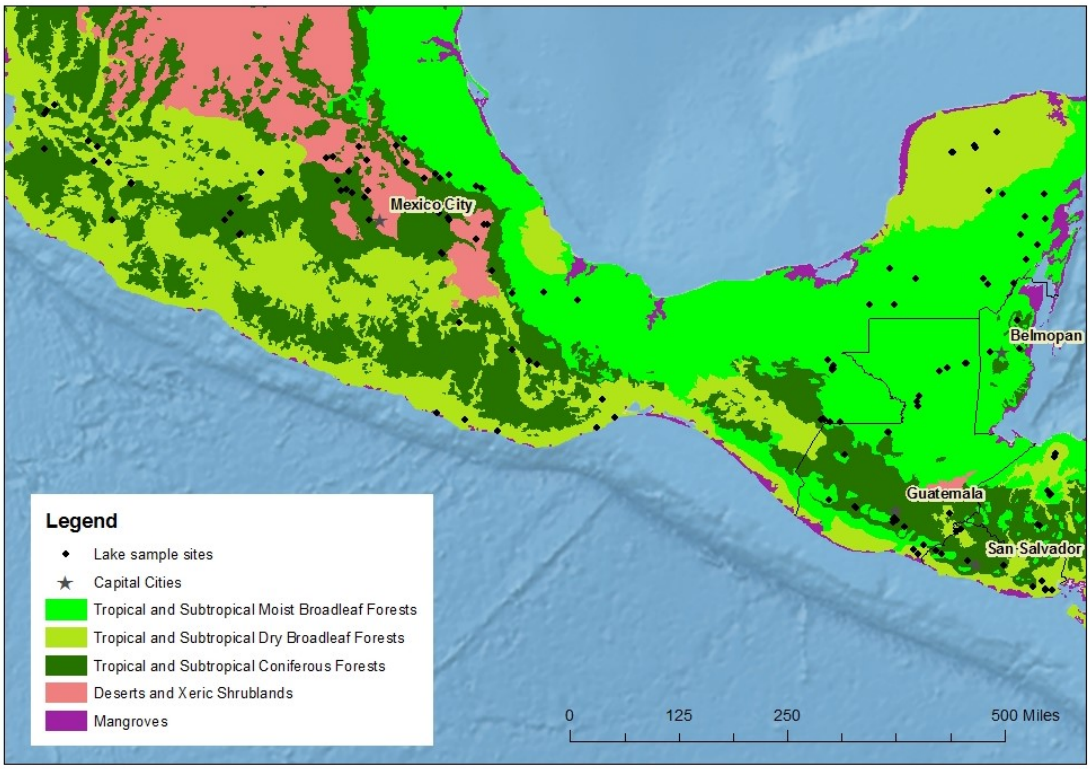

Figure 9 – The biomes and lake sample sites across Mesoamerica (biome map file from Olson et al., 2001).

All sediment samples used for this study were extracted for δD leaf wax analysis and all water samples were used for water isotope analysis. Approximately 80% of samples were kept in or transferred to glass jars and frozen at the Large Lakes Observatory at the University of Minnesota Duluth until shipped to the University of Pittsburgh. All samples were kept frozen at the University of Pittsburgh until ready for biomarker extraction.

2.2 SAMPLE PREPARATION AND EXTRACTION

The samples were freeze-dried in glass containers using activated carbon pellets between filters to prevent organic biomarker contamination from oil used in the vacuum pump. The samples were homogenized by mortar and pestle, further dried before extraction, and stored in a desiccator to assure recording of an accurate dry mass. Sediment subsamples were weighed for use in this project with the goal of 5 grams of sediment, except where sample size was below 5 g, in which case the entire sample was extracted. All analyses are normalized based on their respective sediment mass used for extraction.

The sediment samples were extracted using a Dionex Accelerated Solvent Extractor (ASE) 350 to obtain the Total Lipid Extract (TLE) using 9:1 (v:v) methanol:dichloromethane. The 9:1 (v:v) methanol:dichloromethane was flushed through the samples three times at 100 ºC and a pressure of $7.6X10^6$ Pa. Copper beads, activated by a small amount of 2N HCl and cleaned with solvents, were added to the TLE in 9:1 (v:v) methanol:dichloromethane for several days to completely remove inorganic sulfur from each sample.

After the sulfur was removed, the resulting TLE was volumetrically and quantitatively split into 3 fractions: one designated for solid phase extraction (SPE) using aminopropyl for

analysis of n-alkanoic acids, one designated for alumina column chromatography for n-alkane preparation, and a third fraction was archived for future use. The quantitative split was determined based on the maximum loading capacity of the specific columns used in these methods. A maximum of 5 milligrams of TLE can be loaded onto alumina columns for accurate analysis, and a maximum of 25 milligrams of TLE can be loaded onto aminopropyl SPE columns for accurate chromatography and analysis. This study solely focuses on the use of the aminopropyl SPE split.

The SPE bulk sorbent aminopropyl is dried overnight at 60^{o}C and placed in a desiccator to cool. Six-mL glass columns were plugged with pre-extracted cotton wool and packed with approximately 500mg of aminopropyl. Six mL of methanol were eluted through the column to clean the solid phase. Six mL of 2:1 dichloromethane (DCM):2-propanol was then eluted through the aminopropyl solid phase to condition the column for elution of the TLE. Six mL each of 2:1 DCM:2-proponal, 4% distilled glacial acetic acid in ethyl ether, and methanol was then used to elute the neutral/polar lipid, fatty acid, and phospholipid fatty acid fractions, respectively.

The fatty acid fraction from the aminopropyl SPE columns was methylated prior to gas chromatography. First, 0.5 mL of BF_3 in methanol was added to each sample and incubated at 60^{o}C for 10 minutes. Extracted Milli-Q water (0.5 mL) was then added to the sample along with approximately 1 mL of DCM. The samples were capped with a solvent-cleaned liner, vortexed thoroughly, and allowed to sit and separate. After complete density separation of the liquid, the bottom DCM layer containing the fatty acid fraction was pipetted out and placed in its own vial. This procedure was repeated two more times to ensure complete recovery of fatty acid methyl esters (FAMES). The samples were eluted through sodium sulfate columns with DCM to remove

traces of water. Small silica columns were then used to remove the unsaturated fraction of FAMES, leaving only the saturated fraction for quantification and analysis of δD. The samples were eluted through extracted silica gel using ethyl acetate to retrieve the saturated fraction. The saturated FAMES fraction from each sample was then analyzed for compound identification and quantification as described below.

2.3 FATTY ACID INSTRUMENTAL ANALYSIS

Individual FAME compounds were identified by gas chromatography mass spectrometry (GC-MS) using a Thermo Scientific Trace 1310 Gas Chromatograph (using a HP-1 column, 30 m length, 0.32 mm ID, and 0.25 um film thickness) coupled to a Thermo Scientific ISQ Series Single Quadrupole Mass Spectrometer with helium as the carrier gas. The autosampler injected 0.5ul to 1ul of one sample in ethyl acetate at a time into the instrument using a Programmed Temperature Vaporization inlet and glass liner. The GC oven temperature was set at 70^{o}C and increasing at a rate of 10^{o}C/min until reaching 130^{o}C. Temperature was then increased at a rate of 4^{o}C/min until reaching 320^{o}C, where temperature is held for 10 minutes. The Mass Spectrometer was in the electron ionization mode with an ion source temperature of 275^{o}C with a start mass of 50 amu and an end mass of 650 amu. Fatty acid methyl ester and α-androstane (standard) peaks were identified based on their retention times and mass spectra, using XCalibur software and NIST mass spectral library.

Compounds of interest were quantified using a Thermo Scientific Trace 1310 Gas Chromatograph with a Flame Ionization Detector (GC-FID) with the same conditions as the Gas Chromatograph/Mass Spectrometer (GC/MS). Samples with large concentrations of compounds

and co-elution of peaks were re-analyzed with oven temperature increasing from 70ºC to 130ºC at a rate of 5ºC/min to help separate specific compounds of interest.

Due to the varying concentrations of FAMES in different samples, between 30 and 300ul of 5α-androstane was added to each sample as the internal standard. Each sample was then transferred to a >2mL autosampler vial (some with a 200ul insert and some without based on respective dilutions due to specific FAME concentrations), then the solvent evaporated using a stream of nitrogen. Each sample was quantitatively diluted in 100 to 400 ul of ethyl acetate before final analysis on the GC-FID.

The FAMES and 5α-androstane peaks were identified based on comparison with mass spectra of peaks from the GC/MS and matching retention times of each peak with the chromatogram produced by the GC-FID. Each peak from the GC-FID chromatograms were integrated using Chromeleon software to calculate area of each peak. Compound concentrations were determined using the known internal standard 5α-androstane, using the following calculations (pA = peak area; min = minute):

i. Androstane concentration (ng/pA x min) =

([40 ng/ul] x [ng added to sample]) / [androstane pA x min]

ii. FAME abundance (ng) =

[androstane concentration (ng/pA x min)] x [FAME pA x min]

2.4 HYDROGEN ISOTOPE COMPOSITION OF LOCAL WATER

Lake water samples were collected from 85 of the lakes across Mesoamerica – 57 were collected in Eastern Mesoamerica by our collaborators at Technische Universitat Braunschweig between the wet and dry seasons of August and October 2013, and 28 samples were collected in the Trans-Mexican Volcanic Belt by our collaborators at UNAM in the wet season of June 2011 (Figure 10).

The δD of lake water samples from the Trans-Mexican Volcanic Belt were analyzed at UNAM and the $\delta^{18}O$ of lake water samples from Eastern Mesoamerica were analyzed at Technische Universitat Braunschweig. The δD of the Eastern Mesoamerica lake water samples were extrapolated using the local evaporation line based on the water isotopes from three published studies (i.e. Lachniet and Patterson, 2009; Douglas et al., 2012; Hodell et al., 2012).

For analysis of continental and elevational effects on δD of meteoric water, transects across the Mesoamerican region were identified for further analysis (Figure 11; Table 1). Lakes from Transect A were identified based on their location in respect to the southern extent of the NAM. As longitude and elevation increases in Transect A, the lakes move further away from the vapor source of the NAM. Transect B spans the TMVB, thus as longitude decreases, the further from the primary source of precipitation the lake is. Transect C represents a longitudinal and elevational gradient in Eastern Mesoamerica. As longitude decreases and elevation increases for the lakes in Transect C, the further from the source the lakes are. Transect D represents a longitudinal and elevational gradient, however the lakes should be equally impacted by the trade winds/ITCZ.

Figure 10 – Locations of lake water samples collected for δD analysis of meteoric waters across Mesoamerica.

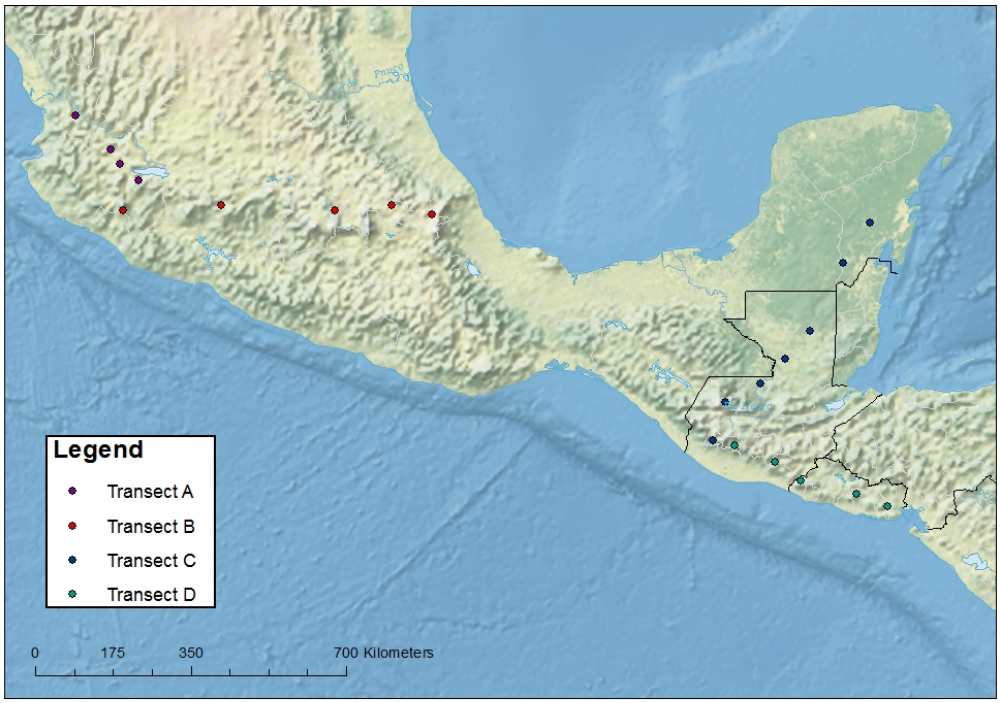

Figure 11 – Elevational and longitudinal transects identified for analysis on effects of δD values of meteoric waters across Mesoamerica.

Table 1 – Descriptions of lakes included in the transect analysis of δD meteoric water analysis across Mesoamerica.

Transect	Region	Lake Water Sample	Longitude	Elevation (m)	δD (‰ VSMOW)
Transect A	Trans-Mexican Volcanic Belt	Santa Maria del Oro	-104.56	799	-16.98
		La Vega	-103.85	1260	-23.42
		Atotonilco	-103.67	1349	-11.07
		Santa Gertrudis	-103.28	1720	-49.51
Transect B	Trans-Mexican Volcanic Belt	Quechulac	-97.35	2333	-20.86
		Atlanglatepec	-98.16	2488	-29.80
		Aljojuca	-99.32	2378	-39.55
		Patzcuaro	-101.63	2039	-10.73
		Sayula	-103.61	1349	-40.91
Transect C	Eastern Mesoamerica	Laguna Emiliano Zapata	-88.47	23	11.34
		Laguna San José	-89.01	118	11.79
		Salpeten litoral1	-89.68	120	15.06
		Petexbatún super	-90.19	120	-26.37
		Lachua 35 m	-90.67	170	-28.76
		Magdalena litoral 2	-91.40	2864	-55.21
		Chicabal litoral 1	-91.65	2739	-36.61
Transect D	Eastern Mesoamerica	Atitlán litoral 2	-91.20	1633	-14.09
		El pino 7m	-90.39	1038	-39.11
		Espino 5m	-89.87	689	-8.18
		Apastepeque litoral 1	-88.74	511	2.58
		Aramuaca litoral	-88.10	96	-0.94

2.5 FURTHER ANALYSES

Statistical analysis was completed using Microsoft Excel for Windows. Aquatic:terrestrial ratios were calculated using the following equation (altered from Meyers, 1997):

iii. Aquatic:terrestrial = ((C20 + C22)/2) / (((C20 + C22)/2) + ((C26 + C28 + C30)/3))

The Carbon Preference Index (CPI), indicating the statistical even-over-odd predominance of carbon chain lengths, was calculated using the following equation (derived from Bray and Evans, 1961):

iv. CPI = (sum (C_{20}-C_{33}) even / 7) / ((sum (C_{20}-C_{33}) odd / 7) + (sum (C_{20}-C_{33}) even / 7))

The Average Chain Length was calculated using the following equation (derived from Poynter and Eglinton, 1990)):

v. ACL = ((26 x C_{26}) + (28 x C_{28}) + (30 x C_{30}) + (32 x C_{32})) / (C_{26} + C_{28} + C_{30} + C_{32})

Each sample site was plotted in ArcMap using Natural Earth shape files, used for figures as well as to determine transects to analyze.

3.0 RESULTS

3.1 ABUNDANCES OF FATTY ACID METHYL ESTERS

The abundance of FAMES follow an even-over-odd predominance across the entire Mesoamerican sampling region (Figure 12). The carbon preference index (CPI) was calculated using carbon chain lengths C_{20} to C_{33}. The CPI ranged from 0.733 to 0.954, indicating a strong even-over-odd carbon predominance. The average chain length (ACL) of the FAMES from all lake surface sediment samples ranged from 26.55 to 29.56 with an average of 27.78. Figure 13 shows ACL vs biome type; no significant correlation or differences are observed between local vegetation and *n*-alkanoic acid carbon chain lengths among the lake sample sites. The p-values for biome type and ACL is 0.092 in Eastern Mesoamerica and 0.61 in the Trans-Mexican Volcanic Belt, indicating no significant impact of biome-type on ACL (Table 2).

Table 2 – Regression analyses of fatty acid abundance calculations.

Region	Independent variable	Dependent variable	R^2 value	p-value
Mesoamerica	Basin type	Aquatic:Terrestrial	0.00076	0.75
Eastern Mesoamerica	Biome type	Average Chain Length	0.032	0.092
	Biome type	Aquatic:Terrestrial	0.029	0.12
Trans-Mexican Volcanic Belt	Biome type	Average Chain Length	0.0047	0.61
	Biome type	Aquatic:Terrestrial	0.0012	0.797

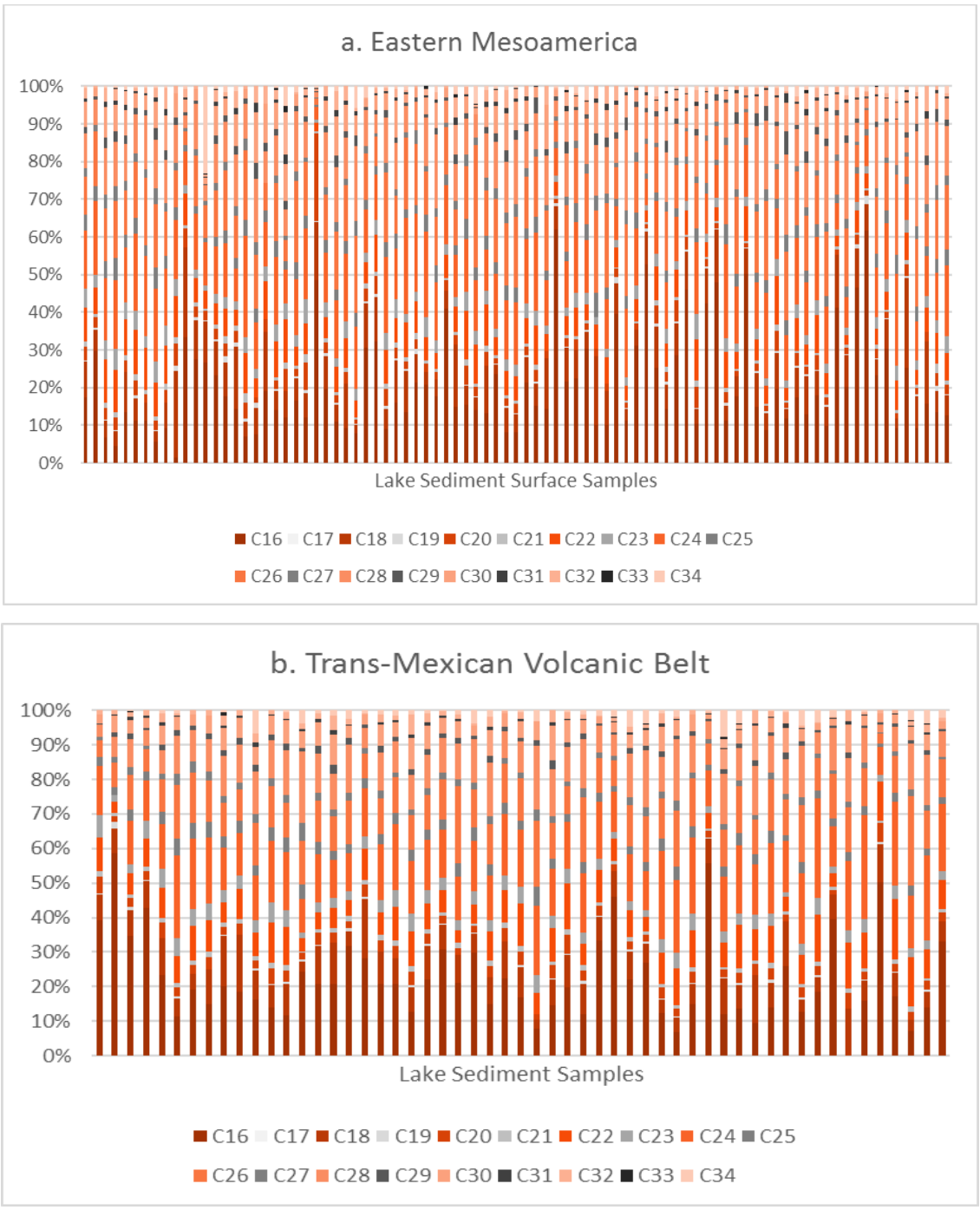

Figure 12 – Percent of C_{16} to C_{34} of each sample in a) Eastern Mesoamerica and the b) Trans-Mexican Volcanic Belt. Each bar represents the FAMES composition of an individual lake sediment surface sample from the region. Red colors represent even carbon chain-length FAMES and greyscale represents odd carbon chain-lengths.

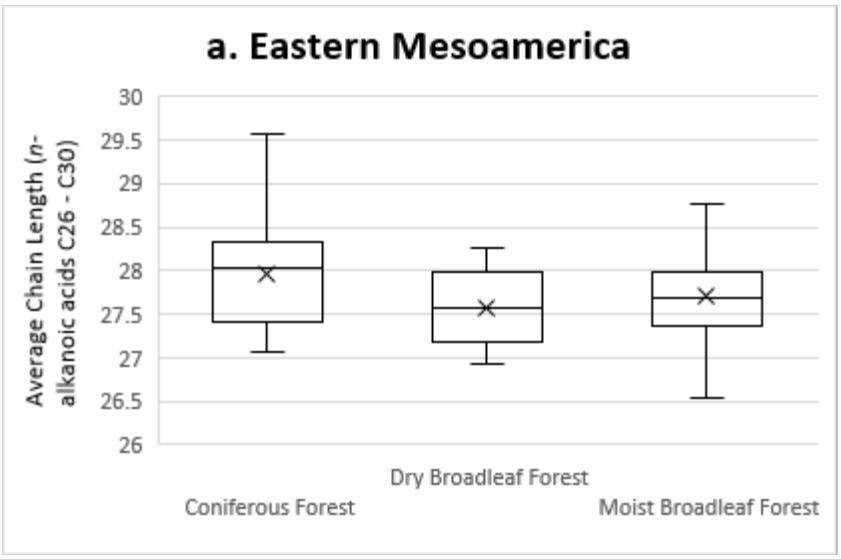

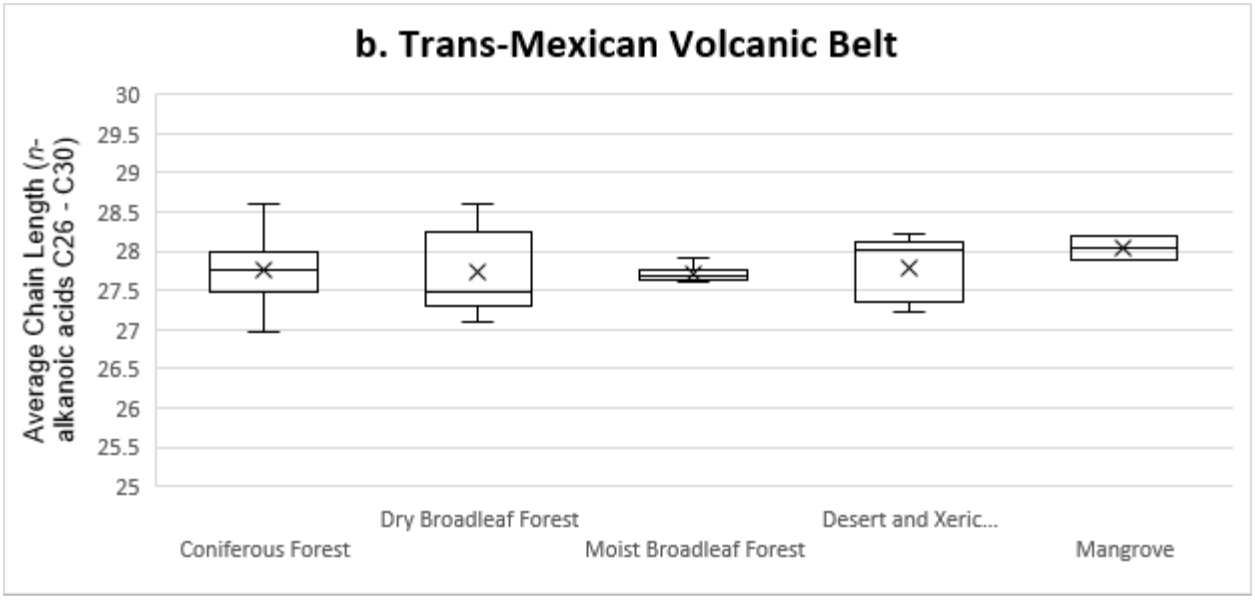

Figure 13 – Average chain length of *n*-alkanoic acids (leaf wax fatty acids) vs biome type in a.) Eastern Mesoamerica, and the b.) Trans-Mexican Volcanic Belt.

Aquatic:terrestrial ratios of the abundance of FAMES were identified to determine their source using C_{20} and C_{22} chain lengths for aquatic sources and C_{26}, C_{28}, and C_{30} for terrestrial sources. Values below 0.5 are dominant in terrestrially-sourced FAMES. Figure 14 shows the aquatic:terrestrial ratio for all lake surface sediment samples based on biome and elevation. There are no trends in biome vs. aquatic:terrestrial ratios, as well as no trends in elevation vs. aquatic:terrestrial ratios. Among the forest biomes in the Trans-Mexican Volcanic Belt and Eastern Mesoamerican transects, aquatic:terrestrial ratios range from 0.15 to around 0.55, with less variability in the moist broadleaf forest biome in the Trans-Mexican Volcanic Belt (Figure 15). However, the differences among the aquatic:terrestrial ratio values are not statistically significant among biomes. In a regression analysis of biome vs. aquatic:terrestrial ratios in Eastern Mesoamerica, the p-value is 0.12 (Table 2). The p-value of biome vs. aquatic:terrestrial ratios in the Trans-Mexican Volcanic Belt is 0.797 (Table 2). With p-values >0.05, this indicates that biome type in Eastern Mesoamerica and the Trans-Mexican Volcanic Belt has no significant impact on aquatic:terrestrial ratios.

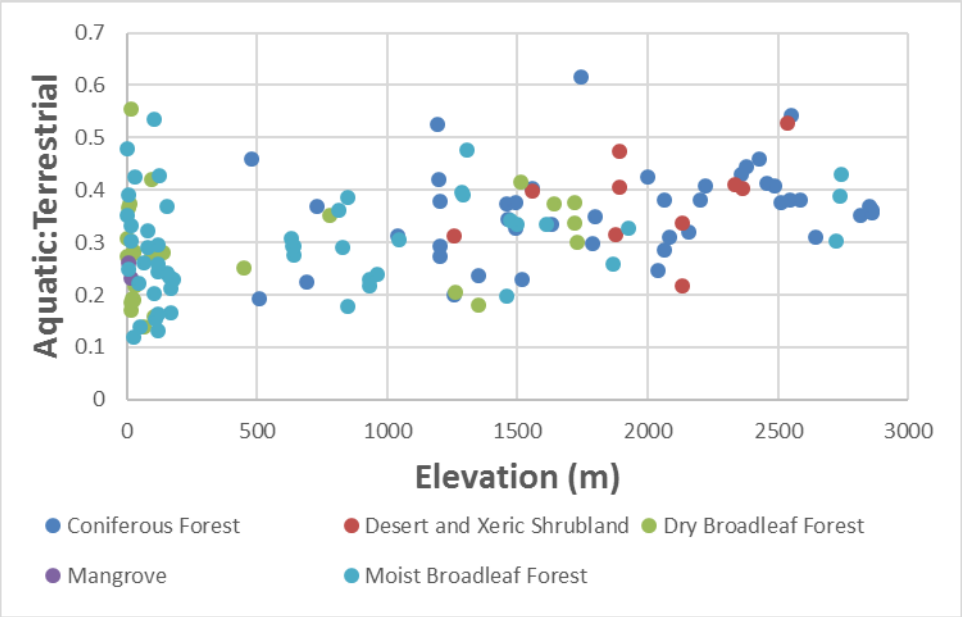

Figure 14 – Elevation of each site vs aquatic: terrestrial ratios of each biome type. Values of aquatic vs terrestrial below 0.5 are more dominant in terrestrial-sourced FAMES.

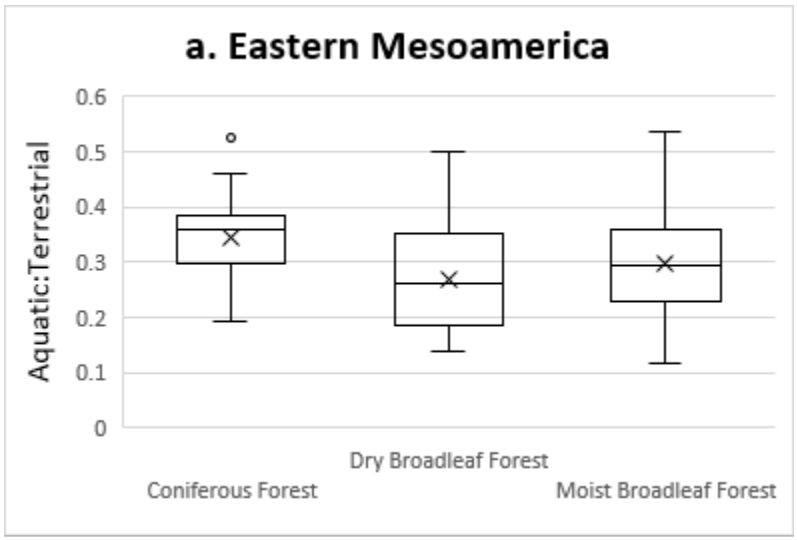

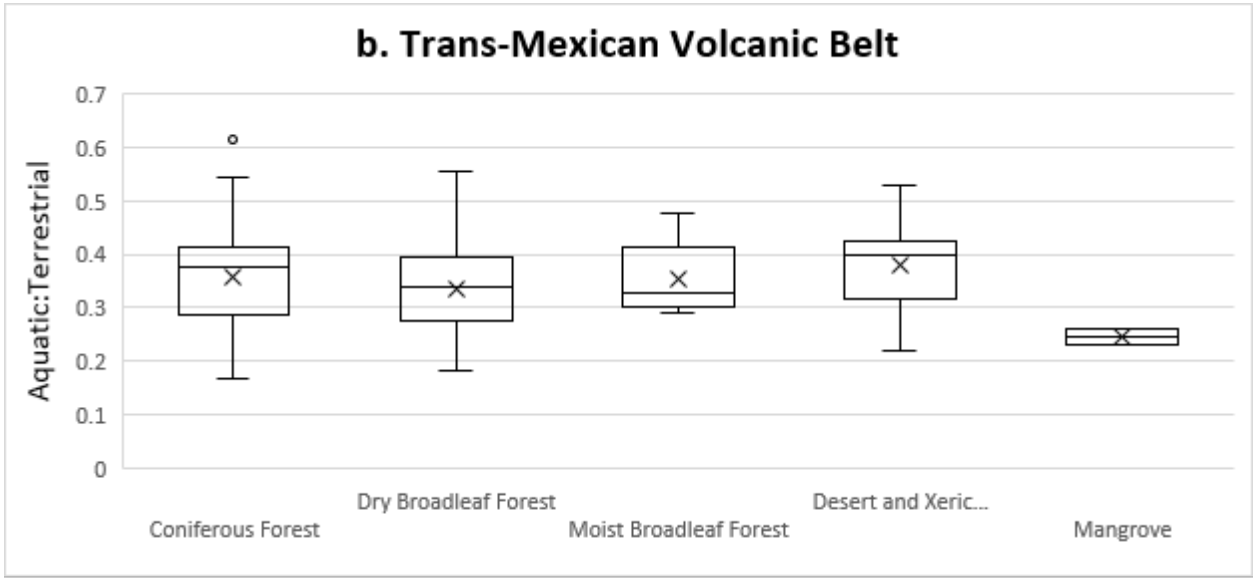

Figure 15 – Box-and-whisker plots of a) Eastern Mesoamerica and the b) Trans- Mexican Volcanic Belt showing the distributions of aquatic vs terrestrial ratios against biome type. The smaller the value of aquatic vs terrestrial, the more dominant the terrestrial-sourced FAMES.

Six samples showed a slightly stronger dominance in aquatically-sourced FAMES with values >0.5 (Figure 14). When the aquatic:terrestrial ratio was compared to basin type, no trend was observed with >0.5 aquatic:terrestrial values in lake basins, lagoons, and one in a reservoir (Figure 16). Again, differences between aquatic:terrestrial ratio values are not statistically significant among basin types based on error bars. A regression analysis of basin type vs. aquatic:terrestrial ratios has a p-value of 0.75, indicating there is no significant impact of basin type on aquatic:terrestrial ratios (Table 2).

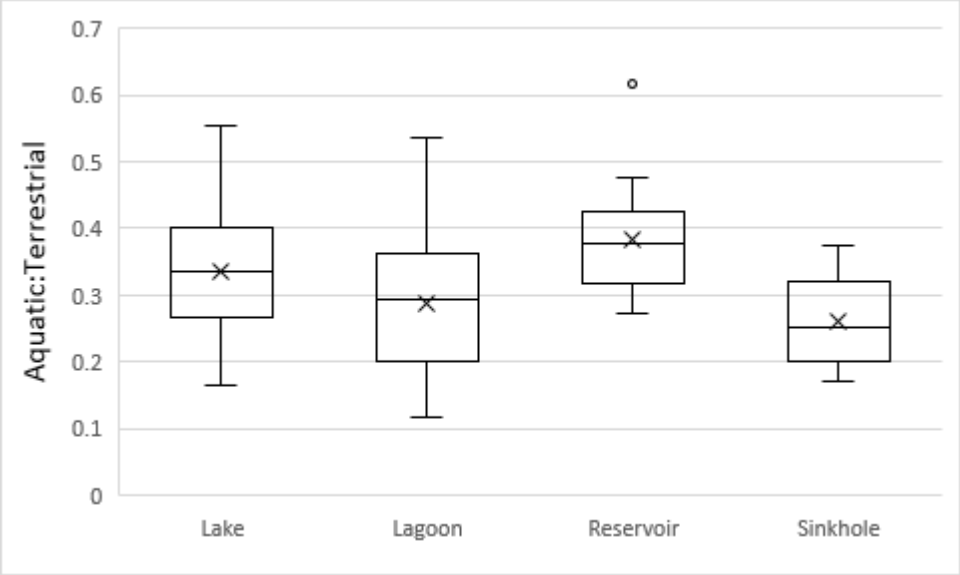

Figure 16 – Box and whisker plots of the aquatic:terrestrial ratio based on sample site type. Values of aquatic vs terrestrial below 0.5 are more dominant in terrestrial-sourced FAMES.

3.2 HYDROGEN ISOTOPE COMPOSITION OF METEORIC WATER SAMPLES

The Trans-Mexican Volcanic Belt and Eastern Mesoamerica both have local evaporation lines that fall below the Global Meteoric Water Line (Figure 17). Figure 17 shows two local evaporation lines plotted against the Global Meteoric Water Line. The Trans-Mexican Volcanic Belt (data from Table 3) has a lower local evaporation line than the lowlands of Eastern Mesoamerica. The Eastern Mesoamerica local evaporation line uses data from three combined studies, Douglas et al. (2012) along with Lachniet and Patterson (2009), and Hodell et al. (2012), for a representation of year-round isotope values (Figure 17). The local evaporation line from these three studies has an R^2 value 0.9573 and a trendline equation of $y = 5.096x - 4.6608$ (Figure 17).

Since δD water values were not measured in Eastern Mesoamerica based on availability of data from our collaborators at Technische Universitat Braunschweig, $\delta^{18}O$ values were used to determine the hydrogen isotope composition. The $\delta^{18}O$ values for lakes in this study are consistently lighter than the $\delta^{18}O$ from the meteoric waters collected from the same lakes in Douglas et al. (2012) and heavier than some of the samples from the same lakes in Lachniet and Patterson (2009) and Hodell et al. (2012), and therefore the trendline equation from the local evaporation line based on the three studies (Lachniet and Patterson, 2009; Douglas et al., 2012; Hodell et al., 2012) was used to extrapolate the δD values of meteoric water from some of the Eastern Mesoamerican lakes in this study (Table 4). The caveats of extrapolating this data for δD values of lake waters in this study would be the differing lake conditions and settings between

the lake waters collected in the studies plotted no the local evaporation lines (Lachniet and Patterson, 2009; Douglas et al., 2012; Hodell et al., 2012) and the lake waters collected and measured for $\delta^{18}O$ water in this study.

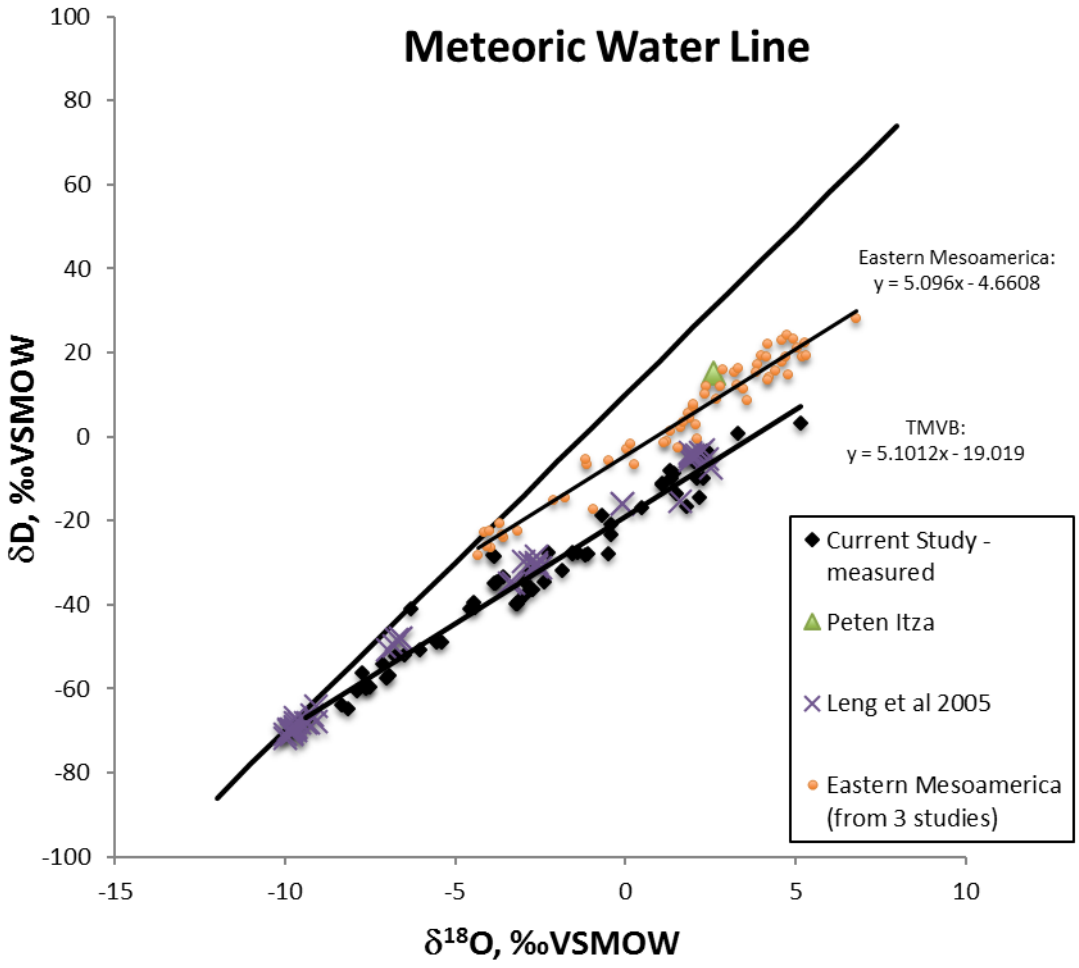

Figure 17 – Water isotope data from lakes in Mesoamerica showing the Local Evaporation Lines of Eastern Mesoamerica (plotted with orange dots and green triangle) vs the Trans-Mexican Volcanic Belt (TMVB; plotted with black dots and purple x's) against the Global Meteoric Water Line (data from Leng et al., 2005; Lachniet and Patterson, 2009; Douglas et al., 2012; Hodell et al., 2012; and our collaborators at UNAM, including Dr. Alexander Correa-Metrio, Dr. Margarita Caballero, and Dr. Liseth Pérez).

Table 3 – List of lake water samples from the Trans-Mexican Volcanic Belt and their corresponding δD_{water} values.

Data from Dr. Alexander Correa-Metrio, Dr. Margarita Caballero, and Dr. Liseth Pérez.

Sample	Code	Longitude	Latitude	Elevation (m)	δD (‰ VSMOW)
Alberca	6 Alb	-101.46	19.21	1491	-59.34
Alchichica	15 Alch	-97.40	19.37	2363	-10.73
Aljojuca	4 Alj	-99.32	19.44	2378	-11.07
Atezca	17 Atcz	-98.75	20.81	1290	-28.44
Atlangatepec	7 Atl	-98.16	19.55	2488	-20.86
Atotonilco	22 Atdlc	-103.67	20.40	1349	-16.98
Camaléon	14 Cmn	-103.28	20.06	N/A	-35.47
Juanacatlán	10 Jnctln	-104.74	20.63	1999	-53.68
La Colorada	6 Ccr	-103.99	20.77	N/A	-59.49
La Vega	12 LaVeg	-103.85	20.67	1260	-49.51
Meztitlán	27 Mztln	-98.87	20.68	1255	-36.46
Patzcuaro	24 Ptzc	-101.63	19.56	2039	-13.33
Quechulac	11 Qchl	-97.35	19.37	2333	-29.24
San Pedro Lagunilla	8 Lag	-104.73	21.21	1256	-34.81
Santa Gertrudis	5 SGer	-103.28	20.04	1720	-59.82
Santa María del Oro	18 SMarDel	-104.56	21.37	779	-4.36
Sayula	20 Svla	-103.61	19.45	1349	-36.02
Tacambaro	13 PTcmb	-101.47	19.21	1517	-39.55
Tecocomulco	9 Tecm	-98.69	20.41	2539	-8.77
Tepeltitic	25 Tpltc	-104.69	21.28	N/A	-40.91
Teremento	21 Trmd	-101.45	19.81	2065	-15.53
Yuriria	14 Yri	-101.13	20.24	1729	-23.42
Zempoala	23 Zmpl	-99.32	19.44	2817	-67.23
Zirahuen	19 Zrhn	-101.73	19.45	2082	-29.80

Table 4 – List of lake water samples from Eastern Mesoamerica and their corresponding δD_{water} values calculated using $\delta^{18}O_{water}$ from the Local Evaporation Line based on data from Douglas et al (2012), Lachniet and Patterson (2009), and Hodell et al (2012). $\delta^{18}O_{water}$ data provided by our collaborators: Dr. Liseth Pérez, Dr. Antje Schwalb, Sergio Cohuo-Duran, and Laura Anahi Macario-Gonzalez.

Sample	Code	Longitude	Latitude	Elevation (m)	$\delta^{18}O$ (‰)	δD extrapolated (‰ VSMOW)
Apastepeque 47m	4 Apq47	-88.74	13.69	509	1.02	0.54
Apastepeque litoral 1	10 Apql1	-88.74	13.69	5112	1.42	2.58
Aramuaca litoral	14 Arm	-88.10	13.43	96	0.73	-0.94
Atitlán 90m	21 Atn	-91.22	14.68	1556	-1.77	-13.68
Atitlán litoral 2	21 Atnl2	-91.20	14.66	1633	-1.85	-14.09
Bahia de Oro Amatitlán 90cm	7 BOA	-90.57	14.49	1203	-6.02	-35.34
Calderas 26m	11 Cds26	-90.59	14.41	1790	-3.56	-22.80
Calderas litoral	6 Cdsl	-90.59	14.41	1800	-3.40	-21.99
Cenote colac	11 Clc	-88.87	20.91	11	-4.10	-25.55
Cenote Oxolá	4 Oxl	-89.24	20.68	18	-4.57	-27.94
Cenote Sabak Ha	16 Sbk	-89.59	20.58	18	-3.66	-23.29
Cenote Yumku	3 Ymk	-89.61	20.58	16	-4.39	-27.01
Chan Laguna	23 CLg	-90.21	18.48	67	2.83	9.77
Chanmico 40m	23 Cmo	-89.35	13.78	477	-1.50	-12.30
Chicabal 10m	22 Ccl10	-91.66	14.79	2726	-6.00	-35.24
Chicabal litoral 1	22 Ccll1	-91.65	14.79	2739	-6.27	-36.61
Chiligatoro 5.5m	6 Cgt	-88.18	14.38	1925	-6.30	-36.77
Comandador litoral	18 Cdr	-90.25	13.96	20	-3.54	-22.70
El pino 7m	12 Epn	-90.39	14.34	1038	-6.76	-39.11
Espino 5m	12 Esp	-89.87	13.95	689	-0.69	-8.18
Este centro Amatitlán 16m	8 ECA	-90.55	14.45	1204	-3.64	-23.21
Finca de Escamilla 1m	3 FdE	-90.53	14.45	1200	-3.92	-24.64
Grande litoral	9 Grdl1	-90.17	13.89	5	-8.09	-45.89
Gruta San Miguel	8 GSM	-89.00	19.93	32	-4.70	-28.60
Ipala 25m	18 Ipl	-89.64	14.56	1495	0.32	-3.03
Jocotal 3m	24 Jct	-88.25	13.34	26	-7.25	-41.61
Jucutuma 2m	12 Juc	-87.90	15.51	27	-1.74	-13.53
Lachua 35 m	19 Lch	-90.67	15.92	170	-4.73	-28.76
Lachua litoral	11 Lchl	-90.66	15.92	177	-5.04	-30.34

Table 4 (continued)

Sample	Code	Longitude	Latitude	Elevation (m)	$\delta^{18}O$ (‰)	δD extrapolated (‰ VSMOW)
Laguna Chichancanab	6 Chn	-88.77	19.88	1	3.78	14.58
Laguna Emiliano Zapata	21 Ezp	-88.47	19.20	23	3.14	11.34
Laguna Kaná	19 Kna	-88.40	19.50	5	3.75	14.46
Laguna Miguel Hidalgo	21 Mhd	-88.37	18.79	31	1.68	3.92
Laguna San José	12 SJs	-89.01	18.37	118	3.23	11.79
Laguna Señor	4 Snr	-88.08	19.88	3	1.94	5.21
Laguna Sijil Noh Ha	10 SNh	-88.06	19.47	0	2.28	6.97
Laguna verde 12m	16 Vrd	-89.79	13.89	1609	-3.09	-20.41
Laguna Yalahau	11 Yhu	-89.22	20.66	2	2.65	8.84
Las pozas 23 m	19 Pzs23	-90.17	16.34	152	-0.31	-6.24
Las pozas 5m	7 Pzs5	-90.17	16.34	152	-7.16	-41.15
Madre vieja 1m	5 MVa	-88.14	14.36	1866	-2.08	-15.26
Magdalena litoral 2	14 Mdl l2	-91.40	15.54	2864	-9.92	-55.21
Metapan 6m	10 Mtp	-89.47	14.31	450	-5.80	-34.22
Negritos super	11 Ngr	-87.94	13.28	102	-2.49	-17.35
Oeste Centro Amatitlán 20 m	8 OCA	-90.59	14.48	1196	-3.74	-23.72
Olomega litoral	17 Olol1	-88.06	13.29	96	-0.24	-5.88
Petexbatún super	19 Ptx	-90.19	16.42	120	-4.26	-26.37
Quexil 25m	7 Qxl25	-89.81	16.92	120	2.59	8.54
Quexil litoral 3	4 Qxll3	-89.81	16.92	120	1.98	5.43
Rio villalobos super	19 RVl	-90.57	14.48	1193	-9.25	-51.80
Rosario litoral	14 Rso	-90.16	16.53	126	-4.69	-28.56
Sacnab 9m	22 Scb	-89.37	17.06	170	1.65	3.75
Salpeten 10m	9 Spnl10	-89.68	16.98	105	3.86	15.01
Salpeten litoral1	17 Spnl1	-89.68	16.99	120	3.87	15.06
San Juan Bautista litoral	5 SJB	-90.08	14.04	1285	-1.97	-14.70
Ticamaya 2m	23 Tcy	-87.89	15.55	17	-1.67	-13.17
Yojoa punto2	21 Yjap2	-87.98	14.86	639	-2.45	-17.15

Figure 18 shows the δD values of the meteoric waters for both regions plotted against longitude. Due to the low R^2 value of 0.21, the weak negative correlation is insignificant. However, in a regression analysis, the p-value of longitude vs δD_{water} is 0.01. With a p-value <0.05, this indicates that longitude has a significant impact on δD_{water} values (Table 5).

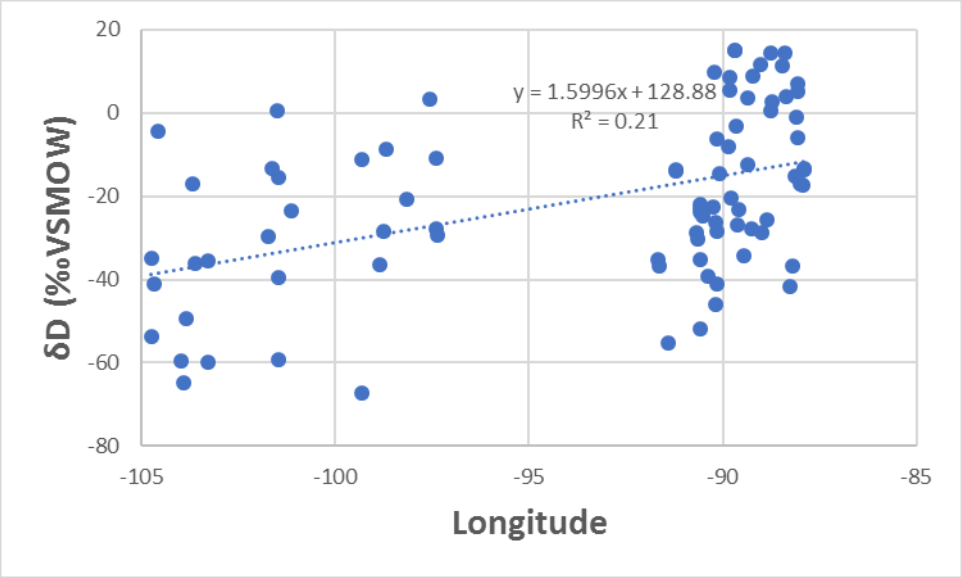

Figure 18 – Longitude of meteoric water samples vs δD of meteoric waters (‰ VSMOW; Vienna Standard Mean Ocean Water = VSMOW; values from Lachniet and Patterson, 2009; Douglas et al., 2012; Hodell et al., 2012). The samples from -105 to -95 are from the Trans-Mexican Volcanic Belt, and the samples from -95 to -85 are from Eastern Mesoamerica.

Table 5 – Regression analysis results for regions and transects across Mesoamerica. Bold numbers indicate a strong significant value.

Region/Transect	Independent variable	Dependent variable	R^2 value	p-value
Mesoamerica	Longitude*	δD_{water}	0.23	**0.01**
	Elevation*	δD_{water}	0.12	0.099
	Longitude + Elevation*	δD_{water}	0.21	**0.024**
Eastern Mesoamerica	Longitude	δD_{water}	0.19	**0.00056**
	Elevation	δD_{water}	0.077	**0.037**
	Longitude + Elevation*	δD_{water}	0.21	**0.0045**
	Basin type	δD_{water}	0.058	0.075
Trans-Mexican Volcanic Belt**	Longitude	δD_{water}	0.16	**0.037**
	Elevation	δD_{water}	0.0033	0.811
	Longitude + Elevation*	δD_{water}	0.083	0.29
Transect A	Longitude	δD_{water}	0.39	0.37
	Elevation	δD_{water}	0.51	0.28
	Longitude + Elevation*	δD_{water}	**0.99**	0.0902
Transect B	Longitude	δD_{water}	0.039	0.75
	Elevation	δD_{water}	0.075	0.66
	Longitude + Elevation*	δD_{water}	0.09	0.84
Transect C	Longitude	δD_{water}	**0.81**	**0.006**
	Elevation	δD_{water}	0.57	**0.049**
	Longitude + Elevation*	δD_{water}	**0.81**	0.089
Transect D	Longitude	δD_{water}	0.41	0.24
	Elevation	δD_{water}	0.29	0.35
	Longitude + Elevation*	δD_{water}	0.52	0.43

* = p-values calculated with multiple regression analysis

** = Trans-Mexican Volcanic Belt has no variability in Basin type

When the δD values were compared to elevation in Eastern Mesoamerica, there was a weak negative trend and an R^2 value of 0.20 (Figure 19). The low R^2 values imply the correlation seen between δD_{water} and elevation is insignificant. Based on a regression analysis, longitude has a significant impact on Eastern Mesoamerica δD_{water} with a p-value of 0.0039. Elevation has an insignificant impact on Eastern Mesoamerica δD_{water} with a p-value of 0.34. However, the p-value for longitude and elevation combined vs. δD_{water} is 0.0045 (Table 5), indicating a significant impact of longitude and elevation in tandem to the δD_{water} values in Eastern Mesoamerica.

Regression analyses of longitude and elevation in the TMVB vs δD_{water} have R^2 values of 0.16 and 0.0033, respectively, showing no significant correlation (Table 5). However, longitude vs δD_{water} has a p-value of 0.037, indicating a significant impact of longitude on δD_{water} values (Table 5).

Figure 20 shows a relative scale of δD_{water} values in a bubble plot vs longitude and elevation in Eastern Mesoamerica and the Trans-Mexican Volcanic Belt. The size of the bubbles range from small to large, giving a relative scale of lighter δD_{water} values to heavier δD_{water} values, respectively. In a multiple regression analysis of longitude, elevation, and δD_{water}, the p-value is 0.024, with a p-value of 0.01 for longitude vs δD_{water} and a p-value of 0.099 for elevation vs δD_{water} (Table 5).

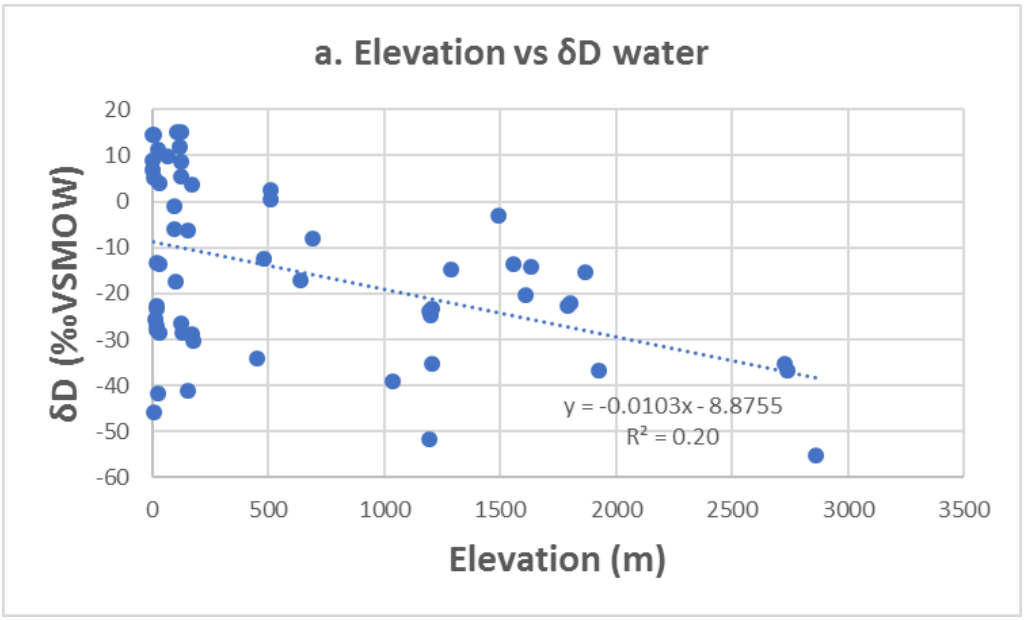

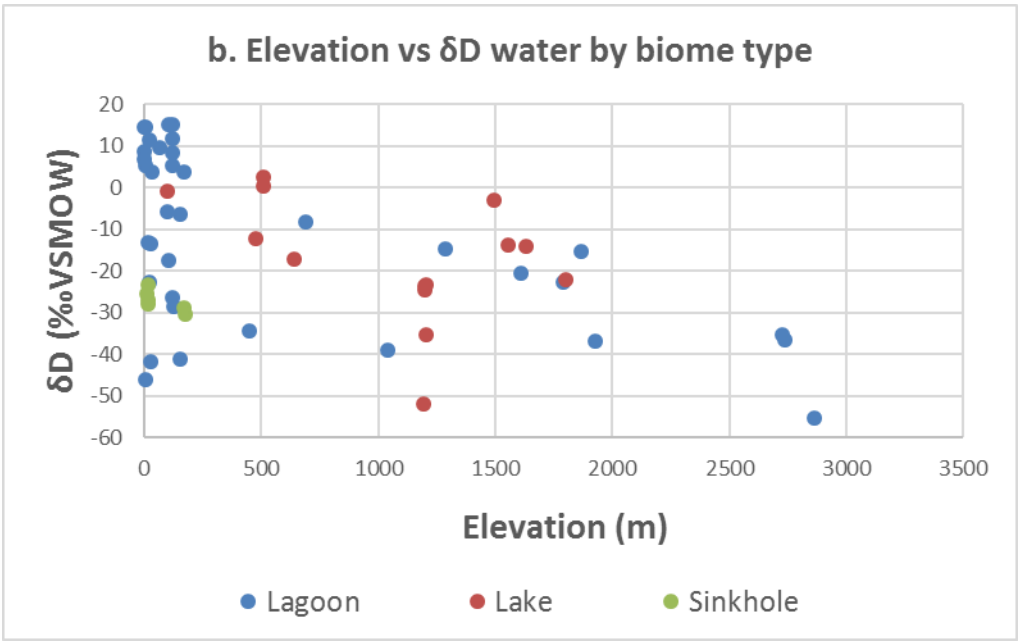

Figure 19 – a.) Elevation vs δD of water (‰ VSMOW) and b.) elevation vs. δD of water (‰ VSMOW) separated by reservoir type in Eastern Mesoamerica.

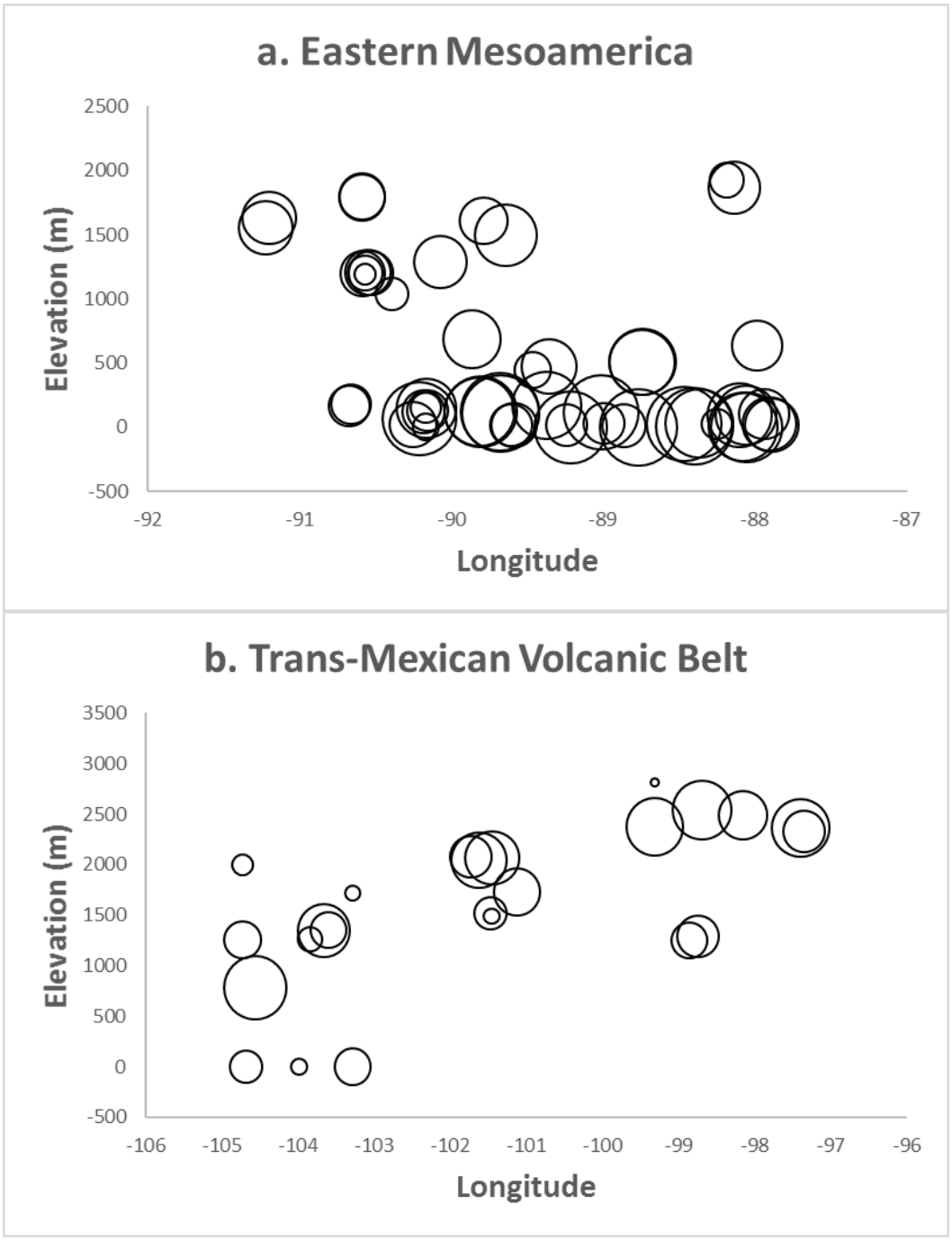

Figure 20 – A relative scale of δD_{water} values represented by bubbles plotted against longitude and elevation in a.) Eastern Mesoamerica and b.) the Trans-Mexican Volcanic Belt. The smaller the bubble, the lighter the δD_{water} value.

In Figure 21, δD_{water} plotted based on basin type also shows no significant trend, besides sinkhole δD values around -20 to -30‰ clustered at low elevations <500m (Figures 16 and 18). Lagoon and lake basins have a wide range of δD values, while sinkholes have a small range, but fall near the median of δD values (Figure 21). There is no significant trend in δD values of meteoric waters vs. basin type based on the error bars in Figure 21. A regression analysis of basin type vs. δD_{water} in Eastern Mesoamerica gives a p-value of 0.075 (Table 5), indicating an insignificant impact of basin type on δD_{water} values.

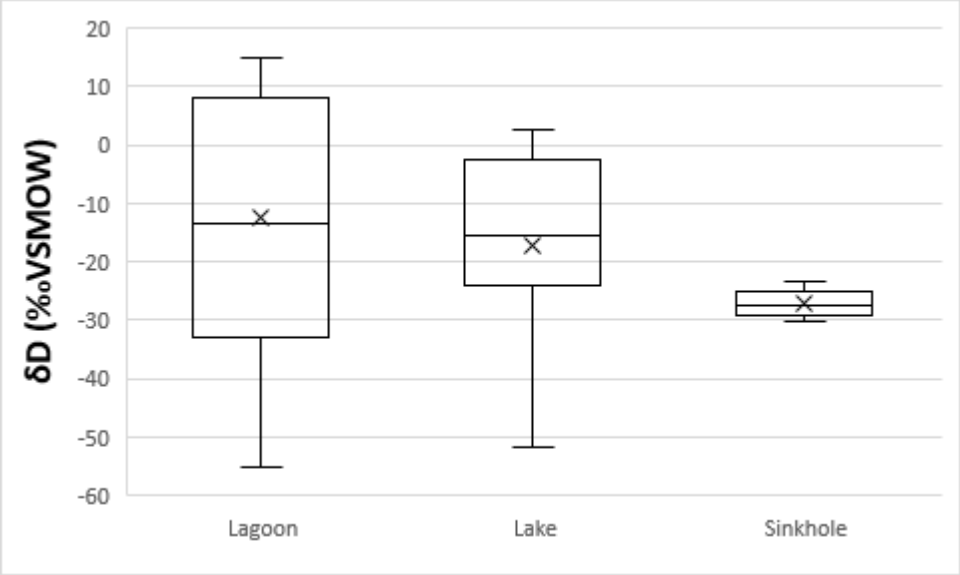

Figure 21 – Box-and-whisker plots of δD_{water} of study sites based on lake type in Eastern Mesoamerica.

Figures 22 and 23 show the correlations of δD_{water} from Transects A-D vs longitude and elevation, respectively. δD_{water} values from Transect A have no significant correlation with longitude, with an R^2 value of 0.39 and p-value of 0.37, nor does it have a significant correlation with elevation, with an R^2 value of 0.51 and p-value of 0.28 (Table 5). However, a multiple regression analysis of longitude and elevation vs δD_{water} from Transect A gives a significant R^2 value of 0.99, indicating a strong correlation, but a p-value of 0.0902 indicating no significant impact of longitude and elevation on δD_{water} values from the lakes. δD_{water} from Transect B has no significant correlation with longitude or elevation (Figures 22 and 23; Table 5). δD_{water} values from Transect C have a positive correlation with longitude with an R^2 value of 0.81 and a p-value of 0.006 (Figure 22; Table 5). δD_{water} values from Transect C has weak correlation with elevation with an R^2 value of 0.57, but a regression analysis of elevation vs δD_{water} has a p-value of 0.049, indicating a significant impact of elevation on δD_{water} values from lakes in the transect. A multiple regression analysis of longitude and elevation vs δD_{water} of Transect C has an R^2 value of 0.81, indicating a significant correlation, however it has a p-value of 0.089, indicating no significant impact of longitude and elevation on δD_{water} values of lakes in Transect C (Table 5). δD_{water} values from Transect D have no significant correlation with longitude and/or elevation (Figures 22 and 23; Table 5).

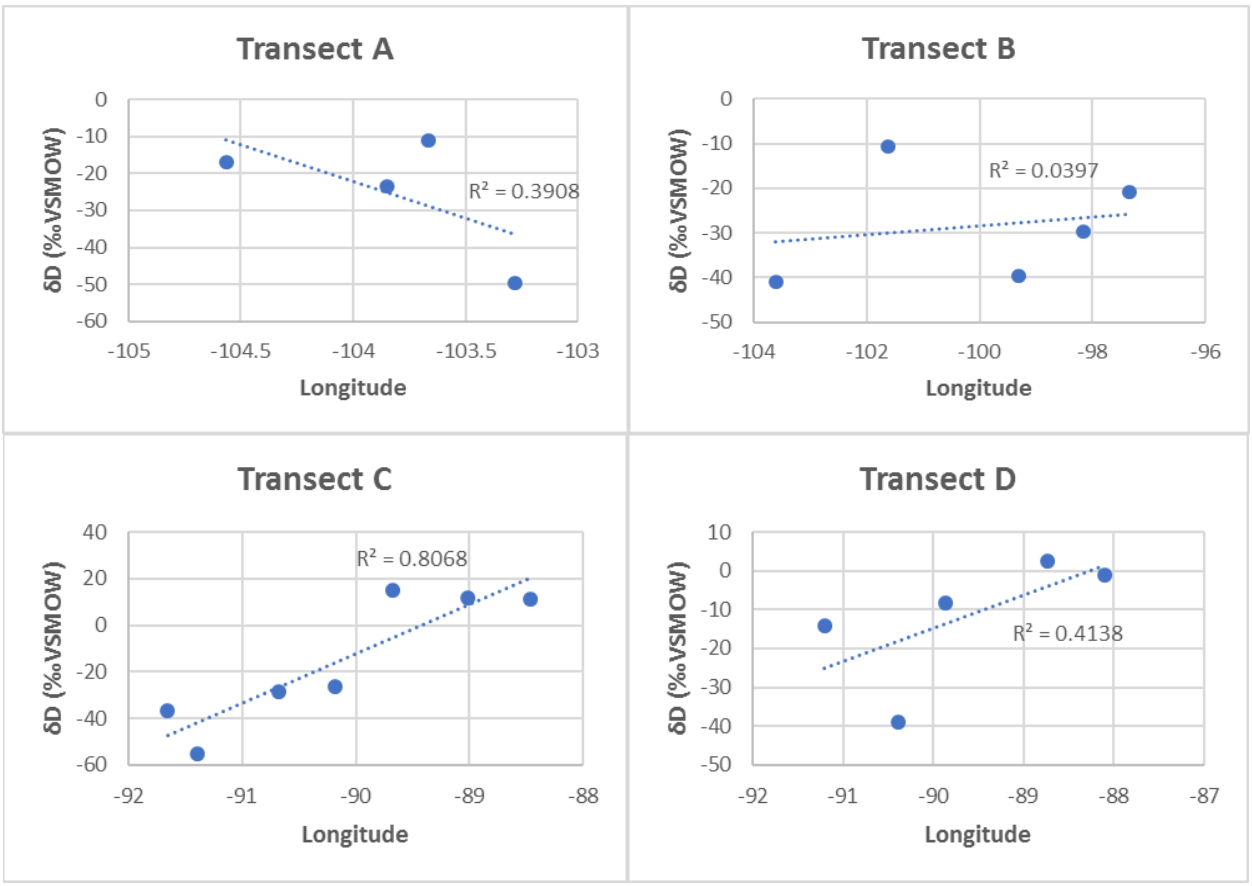

Figure 22 – Longitude vs δD_{water} values of Transects A, B, C, and D across Mesoamerica.

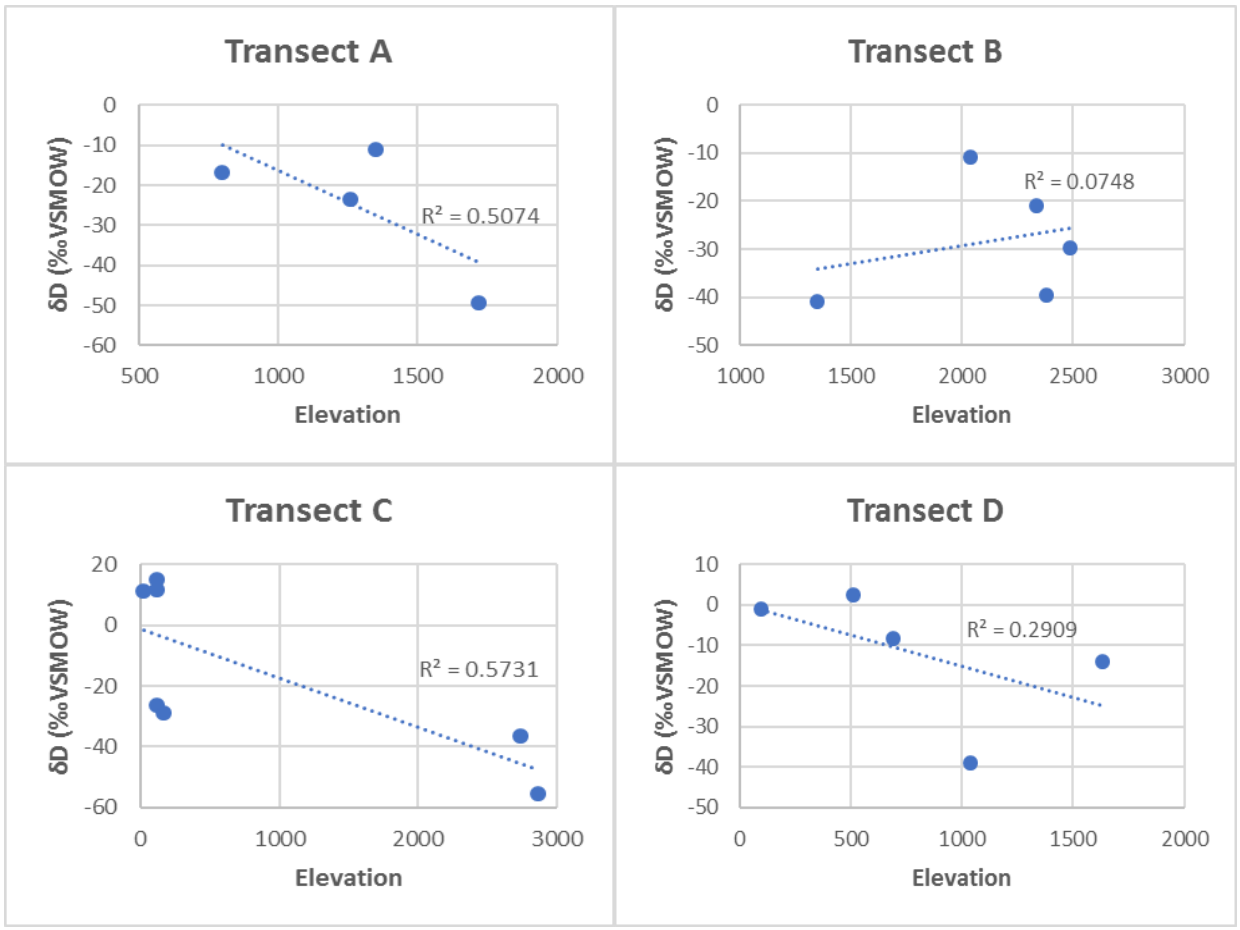

Figure 23 - Elevation vs δD_{water} values of Transects A, B, C, and D across Mesoamerica.

4.0 DISCUSSION

4.1 SOURCES AND ABUNDANCES OF FAMES FROM LAKE SEDIMENTS IN MESOAMERICA

Potential sources of FAMES can be identified based on their carbon chain lengths (Meyers, 1997). Fatty acids found on plant leaf waxes have an even-over-odd carbon chain length predominance (Eglinton and Eglinton, 2008). With a CPI range of 0.733 to 0.954 from the lake sediment surface samples, the entire suite of samples across Mesoamerica exhibits an even-over odd predominance of fatty acids indicating the input of natural organic matter to the lake sediments. The even-over-odd predominance also confirms the reliable acquisition of FAMES from the sediment samples during the extraction of fatty acids and methylation of the samples, as well as the lack of significant contamination from petroleum or plastics during sampling and analysis.

N-alkanoic acids of C_{24}-C_{36} carbon chain lengths are major components of waxy coatings on land-plant leaves, flowers, and pollen (Rieley et al., 1991; Meyers, 1997; Eglinton and Eglinton, 2008). Shorter chain length *n*-alkanoic acids, such as C_{12}, C_{14}, and C_{16}, are produced by all plants, however they are dominant lipid components in algae and other aquatic sources (Cranwell et al., 1987; Meyers, 1997).

The presence of short-chained fatty acids is important in identifying the conditions of the lake sediments and sources of the fatty acids. The surface sediments from this study had high amounts of C_{16} and C_{18}, indicating either an algal or microbial contribution of fatty acids to the sediments (Alfaro et al., 2006) or possible contamination from some plastics or petroleum products during extraction and methylation of the lipids (Gireeshkumar et al., 2015); however, these were not the dominant chain lengths in the vast majority of the samples (Table 9). Since C_{16} and C_{18} fatty acids are common contaminants (e.g. petroleum biomarkers), they were not analyzed further due to potentially unreliable results.

The significant terrestrial FAMES for this study were identified as C_{26}, C_{28}, and C_{30} chain length due to their presence in all lake sediment surface samples in the Mesoamerican sample suite. The average ACL of terrestrial FAMES for all lake surface sediment sample FAMES was 27.78. Due to the common co-elution of C_{26} with other compounds in the chromatograms for many of the lake sediment samples, and the lower relative abundance of the C_{30} compound, C_{28} was identified as the best chain length for analysis of δD. Hou et al. (2008) found after analysis of hydrogen isotope ratios of C_{26}, C_{28}, and C_{30} *n*-alkanoic acids that the δD values of the biomarkers are strongly inter-correlated across all samples, giving statistically significantly similar results. C_{28} is commonly used in δD studies (e.g. Hou et al., 2008; Feakins et al., 2016) of leaf waxes due to their prevalence in sediment samples, identifiable link to waxy leaf coatings of higher plants and strong indication of terrestrial organic matter input (Wannigama et al., ,1981; Nichols et al., 1985; Reiley et al., 1991; Gireeshkumar et al., 2015).

Rommerskirchen et al. (2003; 2006) measured average chain length of leaf waxes from marine sediment cores targeting the last glacial/interglacial cycle across a latitudinal gradient from 4^{o} 47’ south to 25^{o} 30’ south, from the rainforests of the Congo to the deserts of Namibia,

respectively. Rommerskirchen et al. (2003; 2006) found a significant decrease in ACL with a decrease in latitude in cores taken off the coast of Southwest Africa along the continental margin, which corresponded to a decrease in carbon isotope values and a shift in vegetation type during the last glacial. Higher carbon isotope values indicating more C_4 photosynthetic plant contribution was marked by higher ACL during the glacial near the present-day Namibian desert extending further northward (Rommerskirchen et al., 2003; Rommerskirchen et al., 2006). However, in this study, ACL had no significant correlation with biome type (Figure 13), possibly due to the subtle changes in biome type, since forest biomes are typically dominant in C_3 photosynthetic plants and contributing similar fatty acid chain lengths to the lake sediments (Magill et al., 2013). The analysis of carbon isotopes to determine C_3 vs C_4 photosynthetic inputs to lake surface sediments, rather than the biome type of the region, should be conducted for a more significant interpretation of fatty acid contribution and for further analysis of δD values of leaf waxes.

4.2 INFLUENCE OF BIOME ON FATTY ACID ABUNDANCES AND AQUATIC:TERRESTRIAL RATIOS

Aquatic:terrestrial ratios were measured to determine the source of fatty acids to the lake sediments. The majority of lakes in the Mesoamerican sample suite exhibit larger terrestrial inputs of fatty acids relative to aquatic sources; however, the large terrestrial contribution to fatty acids could be due to diagenesis of smaller chain-lengths (i.e. C_{12}-C_{18}), making terrestrial inputs of fatty acids to lake sediments overestimated (Bourbonniere and Meyers, 1996). *N*-alkanoic fatty acids are a significant indicator for terrestrial leaf wax sources, and therefore diagenesis of

shorter chain-lengths does not affect the interpretation of the data in this study. Additionally, leaf waxes are dominantly terrestrially derived, and therefore lake sediments would expectedly exhibit a larger terrestrial dominance. In Figure 16, aquatic:terrestrial ratios were plotted against lake source type to determine if there is any correlation between lake type and input source of fatty acids, however no significant trend was observed. This could be due to either larger contributions of terrestrial input to the lake systems, or increased diagenesis of aquatically-sourced fatty acids (Bourbonniere and Meyers, 1996).

There was no trend observed between biome-type and aquatic:terrestrial values (Figure 15), indicating insignificant impact of vegetation to fatty acid abundances in the lake sediment samples or potentially the impact of multiple factors. The biome-type vs. aquatic:terrestrial values were also compared within the major regions (Trans-Mexican Volcanic Belt and Eastern Mesoamerica); however, there was still no significance correlation between biome type and the aquatic:terrestrial ratio (Figure 15). Six of the lake sediment surface samples showed a higher aquatic input than terrestrial with values >0.5 (Figure 14). There was also no observable trend in biome type for the 6 lake surface sediment samples that had higher aquatic inputs (Figures 11 and 12), likely due to other factors contributing to the influx of aquatically-sourced fatty acids to the lake surface sediments, such as higher algal productivity or less river and runoff input into the lake (Silliman et al., 1996).

Diefendorf et al. (2011) measured *n*-alkanoic acid abundances directly from four different plant functional types: deciduous angiosperms, evergreen angiosperms, deciduous gymnosperms, and evergreen gymnosperms. Based on plant-functional type, there is a significant difference in abundance of C_{22}-C_{30} even carbon chain *n*-alkanoic acids (Diefendorf et al., 2011). This indicates that biome-type should have an impact on distribution of chain-length abundances across biome-

type if the plant functional type varies. However, since many terrestrial plant-types also have a dominance in lower-carbon chain lengths, similar to aquatic macrophytes, it's possible that the aquatic dominance of FAMES (C_{20} and C_{22}) in the 6 lake sediment surface samples from this study could be from an increase in evergreen gymnosperms, which have significantly more C_{22} *n*-alkanoic acids than the other plant functional types. This plant functional type would be present in a coniferous forest biome, which Figures 11 and 12 shows that there is an aquatic dominance in some lake surface sediments in this region, but we also see a dominance in samples from the Dry Broadleaf Forest Biome and the Desert and Xeric Shrubland biome.

Overall, aquatic:terrestrial ratios of fatty acids is not an effective indicator for lake or environmental conditions based on the data collected for this study. However, a more detailed survey of vegetation and lake trophic levels and systems would increase the understanding of aquatic:terrestrial values and distributions across Mesoamerica. The aquatic:terrestrial ratio data did confirm terrestrial fatty acid input into the lake surface sediments for reliable future δD leaf wax analysis.

4.3 HYDROGEN ISOTOPE COMPOSITION OF METEORIC WATER IN MESOAMERICAN LAKE SITES

The Eastern Mesoamerican lowlands and Trans-Mexican Volcanic Belt local evaporation lines both lie below the Global Meteoric Water Line (Figure 14). Both regions have distinct LELs with intercepts at the GMWL indicating regional precipitation with δD_{water} values near -70‰ in the TMVB (Leng et al., 2005) and -35‰ in the Eastern Mesoamerican lowlands (Douglas et al., 2012). These different intercept values indicate a lighter δD_{water} precipitation source for the

TMVB than the lowlands, which is consistent with the modern climate system trajectories in the region (Figure 2; Higgins et al., 1998; Metcalfe et al., 2000).

δD_{water} values of lake waters were not analyzed from Eastern Mesoamerica for this study, so the data had to be extrapolated from a LEL using the $\delta^{18}O$ values analyzed from the lake samples. Douglas et al. (2012) reported values from two other studies to compare against his δD_{water} values (i.e. Lachniet and Patterson, 2009; and Hodell et al., 2012). Similar to Douglas et al. (2012), Lachniet and Patterson (2009) and Hodell et al. (2012) collected a suite of samples across Eastern Mesoamerica through northern Central America from rivers and lakes. Douglas et al. (2012) reports that the water samples from Guatemala and Honduras in their study was collected in May and June 2009 before the start of the wet season, while the water samples collected in Mexico and part of Guatemala in August 2008 was during the wet season. The Guatemalan water samples from the Lachneit and Patterson (2009) and Hodell et al. (2012) studies were also collected during the wet seasons, while the Belize water samples in Lachneit and Patterson (2009) were collected during the dry season in February 2009 (Douglas et al., 2012). The date of collection of the lake waters from Eastern Mesoamerica for this study was August to October 2013, spanning the wet and dry seasons. δD_{water} in the region is particularly sensitive to seasonality due to the massive precipitation differences in the wet and dry season (Douglas et al., 2012). In the wet season, D-depleted water is preferentially rained out, therefore impacting the δD_{water} values of the region (Simpson et al., 1972; Ingraham, 1998). An integrated local evaporation line with the data from both wet and dry seasons is more appropriate to use than the local evaporation line with solely samples from the dry season or the wet season (Figure 14).

When δD_{water} values of the meteoric waters are compared to longitude across Mesoamerica (Figure 18), the δD_{water} becomes progressively D-depleted further westward, away from the source of the moisture. These results agree with Rayleigh distillation, the concept that as water vapor moves inland and away from the source through atmospheric transport, the heavier water isotopes are preferentially rained out, which results in lighter water isotope values furthest from the source (Ingraham, 1998; Alley and Cuffey, 2001; Hou et al., 2008). The lowest δD_{water} value in the Mesoamerican transect was from Laguna Zempoala (23 Zmpl) within the Trans-Mexican Volcanic Belt with a value of -67.2‰ (Table 4). Although it wasn't furthest away from the eastern water source, it is the highest lake in the Trans-Mexican Volcanic Belt with an altitude of 2817 m (Table 4). It is likely that the continental and elevation effects combined are causing the low value of δD_{water} in the lake (Ingraham, 1998; Alley and Cuffey, 2001). The western TMVB is also impacted by the southern extent of the NAM (Metcalfe et al., 2000) receiving meteoric water from both the Pacific Ocean from the west and the Gulf of Mexico/Atlantic Ocean from the east. Different sources of moisture could impact the δD_{water} value of the lakes due to the differing distances from the source and different initial isotope signatures of the source water.

In the Eastern Mesoamerican transect, Laguna Magdalena (14 Mdll2) had the lowest δD_{water} value (Table 4). Laguna Magdalena is one of the most westward lakes in the transect, but it also has the highest elevation in the Eastern Mesoamerican transect with an elevation with 2864 m (Table 3). The correlation in Figure 18 has a weak R^2 value of 0.19, however many of these samples were also taken at different latitudes (Figure 1), varying the extent of different climate system impacts and elevation. In a regression analysis of δD_{water} vs longitude, the p-value is 0.01. With a p-value of less than 0.05, there is a significant impact of longitude on

δD_{water} values. With the lowest δD_{water} values in the Eastern Mesoamerican and Trans-Mexican Volcanic Belt transects being the lakes at highest elevations, it is clear that the elevation effect has an impact on δD_{water} values in the region, however elevation vs δD_{water} has a p-value of 0.099, making this correlation insignificant across the entire Mesoamerican transect. Multiple factors influencing δD_{water}, including evaporative enrichment of lake water or whether the lake is exhibiting outflow, is likely why the correlation with distance from the ocean water source and elevation is insignificant. Figure 20 shows a relative scale of δD_{water} against elevation and longitude. The p-value of the independent variables (elevation and longitude combined) vs. δD_{water} is 0.024, which is less than 0.05 indicating a significant impact of elevation and longitude together on δD_{water} across the Mesoamerican transect.

The δD_{water} in Eastern Mesoamerica was plotted against elevation (Figure 19). Overall, there was a weak negative correlation between δD_{water} and elevation, with a low R^2 value of 0.0769, indicating no significant correlation. Although the correlation was insignificant, the overall negative trend indicates lighter values of δD_{water} with increasing elevation. This is expected because the elevation effect causes heavier δD_{water} values at lower elevations and lighter δD_{water} values with increasing elevation (Alley and Cuffey, 2000). When compared to reservoir type (Figures 16 and 18), whether the meteoric water sample was taken from a lagoon vs. a lake seems to have an insignificant effect on the δD_{water} values of the meteoric lake waters with a p-value of 0.075. Figure 19 shows that lagoons found near sea level, where there is more influence from ocean source water, have a large range of hydrogen isotope compositions. There is an extensive range of δD_{water} values at lower elevations, ranging from about -50‰ to about 20‰ near sea level – this could be due to a range of effects, including from open vs closed lake systems, distance from oceanic water source, or less local evaporation.

Further analyses were completed along small lake transects of δD_{water} to determine effects of climate systems on δD_{water} values of the Mesoamerican region. Transect B, spanning the length of the TMVB, showed no significant impact of longitude on δD_{water} values (Figure 22; Table 5). This is surprising, because due to the continental effect, δD_{water} values should be getting lighter with lakes further from the source of water vapor from the trade winds. However, Figure 22 shows no clear decrease in δD_{water}, indicating the impact of other factors contributing to the δD_{water} values of the lakes including evaporative enrichment of lakes or whether the lakes are an open or closed system. Transect D along the Guatemalan Mountain Range also had no significant correlation or impact of longitude or elevation on δD_{water} values, however this is not surprising. Due to the location of the lakes in Transect D with respect to the trade winds/ITCZ, the primary climate system delivering precipitation to the lakes (Figures 2 and 11), there must be other factors impacting the δD_{water} values of the lake, potentially the orographic effect, which would cause the lakes on the leeward side of the mountains to receive less precipitation and possibly experience more evaporation (Alley and Cuffey, 2001).

Transect A was taken along a longitudinal and elevation gradient, with lakes spanning distances from their primary precipitation source, the NAM (Figures 2 and 11). With an R^2 value of 0.99, the correlation of longitude and elevation together vs. δD_{water} is significant. It is likely that the correlation gives a highly significant value due to the small sample size in the analysis. However, due to the p-value of 0.90, there was no significant impact from longitude or elevation, indicating other factors potentially impacting the δD_{water} values of the lakes. Other factors could include a significant evaporative enrichment, as many lakes in this region dry out for part of the year due to regular droughts (Mendoza et al., 1997), or impact of precipitation δD_{water} values from the ITCZ (Metcalfe, 2000).

Lakes from Transect C were also taken along a longitudinal and elevation gradient, with lakes spanning distance from the primary source of precipitation in the Yucatan peninsula into the mountains of Guatemala (Figures 2 and 11). This transect had the strongest correlation with longitude, with an R^2 value of 0.81 and p-value of 0.006, indicating a strong continental effect on δD_{water} values of the lakes. Although elevation had a weak correlation with δD_{water} values, the p-value of 0.049 indicates a strong impact of elevation on δD_{water}. In the multiple regression analysis of elevation and longitude vs. δD_{water} in Transect C, the R^2 value is significant at 0.81, but the p-value is >0.05, making the impact of elevation and longitude together on δD_{water} insignificant. There are likely other factors contributing to the δD_{water} trend observed in Transect C. Further analysis of the lake systems would increase our understanding of δD_{water} patterns of the region, for example determining impact of local aridity or closed vs open system lakes.

However, for a proper analysis of precipitation δD_{water} values and their translation into leaf wax δD, river or groundwater values should be analyzed in tandem to isolate the evaporative effects on leaf wax δD and δD_{water} values of lakes (Douglas et al., 2012). The continental and elevation effects, along with aridity, will likely influence the leaf δD values across Mesoamerica. Previous studies have published a shift in leaf wax δD values (δD_{wax}) with a changing elevation, implying that the elevation effect in δD_{water} is being translated into δD_{wax} (Bai et al., 2015; Feakins et al., 2016). Bai et al. (2015) reported an altitudinal lapse rate among three elevation transects, with 76 soil samples total, in the Himalayan Mountains. The soil δD_{wax} was compared to δD_{water} from rivers in the transects with shifts in vegetation from lower elevation to higher elevation. Overall, Bai et al. (2015) found a small difference in the translation of δD_{water} in δD_{wax}. Within their Zayu-Bomi transect in the eastern Himalayas, the biomes changed up transect from a pine forest at about 1000 to 2300m in elevation, to an oak broadleaf forest, to a

spruce needle leaf forest and shrubs, to a high-cold scrub meadow higher than 4000m in elevation (Bai et al., 2015). In this transect, Bai et al. (2015) found a fractionation of δD_{wax} and δD_{water} ($\varepsilon_{wax/water}$‰) difference of -102.4‰ at the 2400m in elevation within the oak broadleaf forest and -110.1‰ at the spruce needle leaf forest/shrub and high-cold scrub meadow biome boundary around 4100m in elevation. Bai et al. (2015) demonstrates the impact of elevation, as well as the change in biomes and vegetation type in the fractionation of δD between meteoric waters and leaf waxes.

5.0 POTENTIAL FUTURE STUDIES

Future research extending this study will analyze the fidelity with which leaf waxes record δD values of meteoric water over a broad geographic area to assess what effects changing ecosystems from the tropical lowlands to the arid highlands has on the H isotope composition of leaf waxes in surface sediments of lakes spanning Mesoamerica. This will provide a basis for a future quantitative analysis of downcore leaf wax δD from lacustrine sediment cores throughout this important and climatically sensitive region, ultimately deriving precipitation patterns through time. The results will give us a better understanding of how lake water δD, and therefore precipitation, is recorded in biomarkers in a range of climates and ecosystems to produce a proxy that can be applied to long sediment cores from important sites, such as Lake Petén Itzá in Guatemala and Lake Chalco near Mexico City.

5.1 MESOAMERICAN CALIBRATION

The lake surface sediment fatty acids are continuing to be analyzed for leaf wax δD and compared to δD of meteoric waters for a complete calibration of δD across Mesoamerica. To analyze a complete δD calibration of Mesoamerica, multiple calibrations for different regions (e.g. TMVB vs Yucatan Lowlands) will have to be developed and applied to the Mesoamerican core tops if the effects of environmental factors are significant. Hou et al. (2008) demonstrates

gradient/transect effects on δD values based on local meteorological effects, as well as local climates (Figure 24). Using the multi-calibration will resolve the degree at which δD of leaf waxes reflect the δD of local water in different areas of Mesoamerica, and will be used to verify the accuracy of downcore analyses of δD coupled with ecosystem proxies from previously published results, such as pollen and $\delta^{13}C$ biomarker data (Correa-Metrio et al., 2012; Pierce, 2012), to determine the overall environmental conditions of the past. The Mesoamerican calibration will provide a more integrated calibration across a dry to humid transect along the atmospheric circulation track of moisture coming in from the Gulf of Mexico and will incorporate a broader vegetation composition. The multi-calibration approach will allow for the interpretation of leaf wax δD to be applied downcore during periods of changing ecosystems in response to changes in rain-out history of climate systems to be interpreted within the context of known modern patterns, as influenced by orographic and continental effects, providing a more refined understanding of changing rainfall patterns in the past.

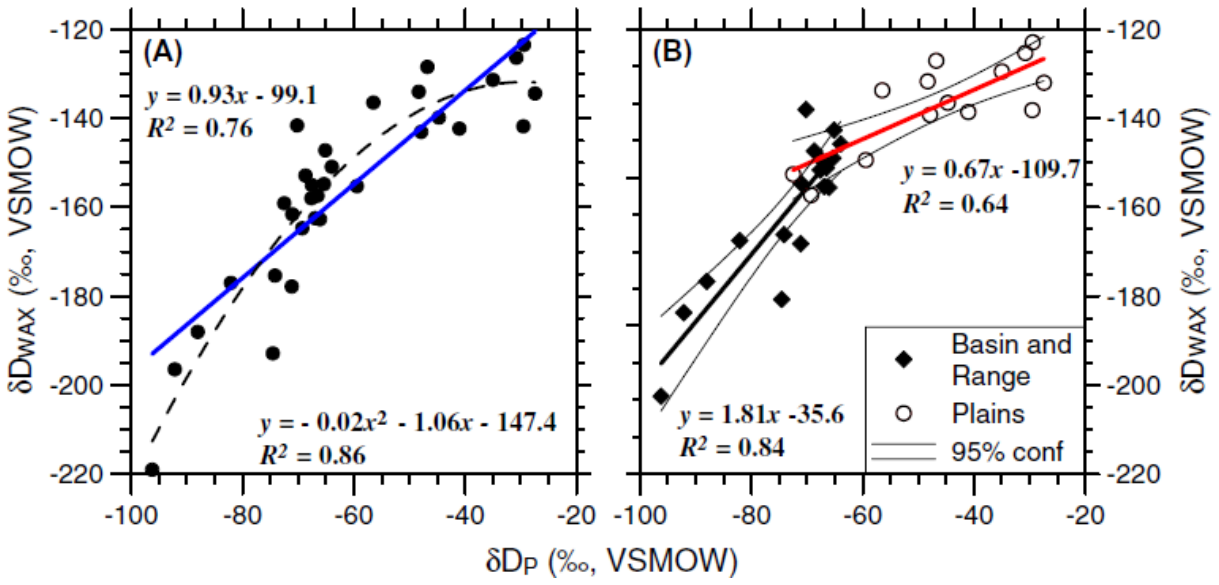

Figure 24 – The correlation between the δD of leaf wax fatty acids and δD of precipitation from sample sites ranging from Arizona through Texas. Graph A shows the correlation of the entire transect, along with linear and polynomial regression lines. Graph B analyzes the Basin and Range transect, covering Arizona and most of New Mexico, and the Plains transect, from northeastern New Mexico through Texas, to show the climate and aridity effects on the correlations (figure from Hou et al., 2008).

The quantitative analysis of δD can be affected by the vegetation type, due to the very different apparent fractionation patterns of δD in C_4 photosynthetic grasses compared to C_3 photosynthetic shrubs and trees (Sachse et al., 2012; Tierney et al., 2017). Therefore, it is important to use a multi-proxy approach, specifically determining $\delta^{13}C$ values of the leaf waxes due to its implication for photosynthetic pathways.

By using a multi-proxy approach with $\delta^{13}C$ of leaf waxes, along with multiple δD calibrations across Mesoamerica, we will be able to better interpret how to quantifiably determine the δD value of leaf waxes downcore due to the significant differences in fractionation between in arid environments. Overall, this allows for a more accurate interpretation for the application of the δD leaf wax proxy.

5.2 DOWNCORE ANALYSES OF HYDROGEN ISOTOPE COMPOSITION OF LEAF WAXES

Using the Mesoamerican leaf wax δD calibration, future studies will be able to demonstrate the use of these novel geochemical proxies. Developing a detailed set of climate records using a modern calibration of proxies across current wet and arid regions of Mesoamerica will enhance our understanding of variations in tropical North American climate and regional climate to determine how regional climate forcings can behave independently of global forcings. We need to analyze how changes in ocean dynamics are linked to continental climate to better understand the impacts of future climate change. This can be accomplished by looking at long climate records from lake sediments to reconstruct past hydroclimate variability during changing global conditions and comparing them to global climate records, such as the Greenland ice core and the

ocean record from the Cariaco Basin (Figure 25; e.g. Dansgaard et al., 1993; Peterson and Haug, 2006). Using emerging paleoclimate proxies that are rigorously studied in modern systems, researchers can compile data to further understand precipitation from the past and determine how abrupt climate shifts in these high-risk regions may influence hydrological systems. Overall, this comprehensive study of the Mesoamerican δD calibration with a multi-proxy approach to downcore lake sediments will help identify major shifts in climate in the past and have implications for modeling the future of modern climate change.

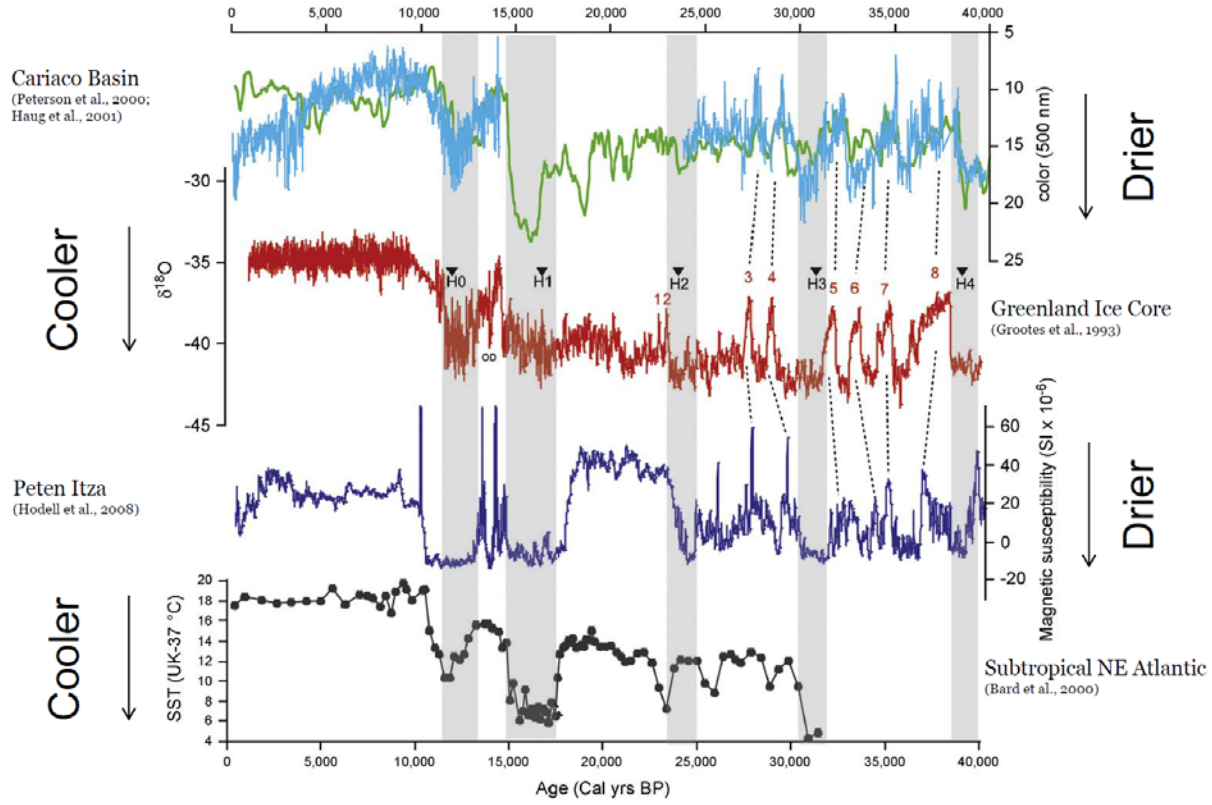

Figure 25 – Climate records recording global climate changes through time (graph from Hodell et al., 2008; data from Grootes et al., 1993; Bard et al., 2000; Peterson et al., 2000; Haug et al., 2001; Hodell et al., 2008).

6.0 CONCLUSION

Mesoamerica is impacted by a suite of climate systems and environmental conditions, causing a complex interpretation of leaf wax fatty acids and δD_{water} across the dynamic transect. For this reason, the study was split into two primary regions, the Trans-Mexican Volcanic Belt and Eastern Mesoamerica.

Several environmental factors impact the abundance and distribution of fatty acid leaf waxes and hydrogen isotope values of meteoric waters across a broad regional landscape. There is no significant trend in aquatic:terrestrial ratio in lake surface sediments across transects (Trans-Mexican Volcanic Belt vs Eastern Mesoamerica), elevation, biome type, or reservoir type as terrestrial sources tend to produce more leaf waxes than aquatic sources and contribute more fatty acids to the lake surface sediments. However, we can conclude that terrigenous input is the primary source of fatty acid methyl esters across the significant majority of Mesoamerican sample sites with little contaminant input. The successful recovery of terrestrial FAMES allows for a trustworthy interpretation of δD biomarker values.

The δD_{water} samples from lakes in Eastern Mesoamerica were not correlated with elevation. Meanwhile, the δD_{water} samples exhibited a weak negative correlation with longitude, indicating a decrease in δD_{water} westward, away from the primary oceanic precipitation source. Transects A-D, across different longitudinal and elevational gradients, showed varying impacts of continental and elevation effects on δD_{water}. Transect A showed no significant impact on

continental and elevation effects from the NAM, likely indicating an impact from both NAM and ITCZ on δD_{water} values, or stronger evaporative enrichment in this historically dry region. Transect B showed no correlation with longitude, which contradicted expectations that a continental effect would have a large impact on δD_{water} values. Transect C showed significant impact of continental and elevation effects on δD_{water} values. Transect D showed no continental or elevation impacts, which was expected due to relatively equal distance of sites from the water vapor source. It is likely that elevation, distance from source water, the influence of various climate systems (e.g. the NAM vs the ITCZ), and the evaporative effect of the lake sample sources contribute to the weak correlations found in much of the results. However, this study demonstrates the multiple potential factors that influence the hydrogen isotope signature of water and its interpretation in leaf wax δD composition in lake sediments.

Overall, this study is a crucial step in the analysis of leaf wax δD and their interpretation of the δD of precipitation in this climatically complex region. By understanding the extent of fractionation between leaf wax δD and meteoric δD, as well as the various environmental and regional effects on leaf wax δD, this work has the potential to contribute to the understanding of how climate, particularly precipitation, has changed through time in Mesoamerica when a complete δD calibration is applied to downcore studies.

APPENDIX

DATA TABLES AND CALCULATION RESULTS

Table 6 – Lake samples, corresponding codes, coordinates, elevation, and basin type of each lake sample.

Sample (Lake)	Code	Latitude	Longitude	Elevation (m)	Basin Type
Alberca	6 Ccc	19.04	-88.18	6	Lagoon
Alchichica	15 Alch	19.37	-97.40	2363	Lake
Alfajayucan	6 CCr	20.77	-103.99	-	Lake
Aljojuca	4 Apq47	13.69	-88.74	509	Lake
Amarillo	20 Aml	16.98	-91.60	850	Lake
Apastepeque 47m	4 MA4	18.23	-96.94	78	Reservoir
Apastepeque litoral 1	10 Apql1	13.69	-88.74	5112	Lake
Aramuaca litoral	14 Arm	13.43	-88.10	96	Lake
Atezca	17 Atzc	20.81	-98.75	1290	Lake
Atitlán 90m	21 Atn	14.68	-91.22	1556	Lake
Atitlán litoral 2	21 Atnl2	14.66	-91.20	1633	Lake
Atlanglatepec	7 Cbo	18.89	-98.11	2158	Lake
Atotonilco	22 Atdlc	20.40	-103.67	1349	Lake
Bahia de Oro Amatitlán 90cm	7 Lcd	17.02	-91.59	812	Lake
Balam 7	3 Blm	16.13	-91.78	1457	Lagoon
Belize 1	3 Blz1	17.24	-88.97	-	-
Belize 2	12 Blz2	17.30	-88.49	-	-
Caballo	7 Pzs5	16.34	-90.17	152	Lagoon
Calderas 26m	11 Cds26	14.41	-90.59	1790	Lagoon
Calderas litoral	6 Chn	19.88	-88.77	1	Lagoon
Camaleon	14 Cmn	20.06	-103.28		Lake

Table 6 (continued)

Sample (Lake)	Code	Latitude	Longitude	Elevation (m)	Basin Type
Cenote azul	14 Azl	18.65	-90.64	18	Sinkhole
Cenote colac	11 Clc	20.91	-88.87	11	Sinkhole
Cenote Oxolá	4 Qxll3	16.92	-89.81	120	Lagoon
Cenote Sabak Ha	16 Sbk	20.58	-89.59	18	Sinkhole
Cenote Yumku	4 Alj	19.44	-99.32	2378	Lake
Centro Colorada	6 Cgt	14.38	-88.18	1925	Lagoon
Chan Laguna	23 CLg	18.48	-90.21	67	Lagoon
Chanmico 40m	23 Cmo	13.78	-89.35	477	Lake
Chicabal 10m	22 Ccl10	14.79	-91.66	2726	Lagoon
Chicabal litoral 1	22 Ccll1	14.79	-91.65	2739	Lagoon
Chicabal litoral 4	8 GSM	19.93	-89.00	32	Cave
Chiligatoro 5.5m	7 Atl	19.55	-98.16	2488	Lake
Comandador litoral	18 Cdr	13.96	-90.25	20	Lagoon
Corralero	10 Crl	16.24	-98.18	8.1	Lake
Crooked Tree Lagoon	23 CTL	17.78	-88.53	-	-
Cuetzalan	13 Ctz	20.01	-97.53	1045	Lake
El Centenario Tequisquiapan	15 ECT	20.50	-99.91	1891	Reservoir
El Estudiante	24 Eet	17.09	-96.66	1640	Presa
El pino 7m	12 Epn	14.34	-90.39	1038	Lagoon
Esmeralda F-60-m	20 Esd	16.12	-91.73	1473	Lagoon
Espino 5m	12 Esp	13.95	-89.87	689	Lagoon
Este centro Amatitlán 16m	8 Lag	21.21	-104.73	1256	Lake
Finca de Escamilla 1m	3 FdE	14.45	-90.53	1200	Lake
Grande litoral	9 Rqn	19.93	-99.34	2132	Reservoir
Gruta San Miguel	8 OCA	14.48	-90.59	1196	Lake
Guija 2	5 MVa	14.36	-88.14	1866	Lagoon
Ipala 25m	18 Ipl	14.56	-89.64	1495	Lake
Jocotal 3m	24 Jct	13.34	-88.25	26	Lagoon
Juanacatlan	10 Jnctln	20.63	-104.74	1999	Lake
Jucutuma 2m	12 Juc	15.51	-87.90	27	Lagoon
La Avispa	13 Asp	15.99	-95.53	15	Lake
La Cofradía Chica	20 Cca	20.11	-99.85	2426	Reservoir
La Huaracha	17 Hra	19.96	-99.69	2644	Reservoir
La Nopala	11 Npl	20.25	-99.66	2360	Reservoir

Table 6 (continued)

Sample (Lake)	Code	Latitude	Longitude	Elevation (m)	Basin Type
La Soledad	9 Tecm	20.41	-98.69	2539	Lake
La Vega	12 LaVeg	20.67	-103.85	1260	Lake
Lacaudon	7 Qxl25	16.92	-89.81	120	Lagoon
Lachua 35 m	19 Lch	15.92	-90.67	170	Sinkhole
Lachua litoral	11 Lchl	15.92	-90.66	177	Sinkhole
Lago Tenexac	18 Tnk	19.49	-98.00	22548	Lake
Laguna camp.	19 Cmp	18.04	-90.99	43	Lagoon
Laguna Chacanbacab	17 Ccb	18.48	-89.09	109	Lagoon
Laguna Chica	9 Sld	19.97	-97.45	732	Reservoir
Laguna Chichancanab	7 BOA	14.49	-90.57	1203	Lake
Laguna de Chacchoben	6 Cdsl	14.41	-90.59	1800	Lake
Laguna Emiliano Zapata	21 Ezp	19.20	-88.47	23	Lagoon
Laguna Grande	13 Grd	18.61	-97.27	2514	Lake
Laguna Kaná	13 Kna	19.50	-88.40	5	Lagoon
Laguna la Perdida	22 Prd	18.03	-90.58	49	Lagoon
Laguna Lourdes	15 LLd	20.49	-100.03	1891	Lake
Laguna Miguel Hidalgo	21 Mhd	18.79	-88.37	31	Lagoon
Laguna San José	12 SJs	18.37	-89.01	118	Lagoon
Laguna Señor	5 Gja	14.26	-89.54	-	-
Laguna Sijil Noh Ha	10 SNh	19.47	-88.06	0	Lagoon
Laguna verde 12m	16 Vrd	13.89	-89.79	1609	Lagoon
Laguna Yalahau	11 Yhu	20.66	-89.22	2	Lagoon
Las Pozas	17 Pzs	16.35	-90.17	-	-
Las pozas 23 m	19 Pzs23	16.34	-90.17	152	Lagoon
Las pozas 5m	7 Wha	16.98	-91.60	850	Lake
Lequi 2	13 Lq2	16.08	-91.46	1500	Lagoon
Loma Bonita	5 SGer	20.04	-103.28	1720	Lake
Madre vieja 1m	5 SJB	14.04	-90.08	1285	Lagoon
Magdalena 2.8m	19 Mdl2.8	15.54	-91.40	2863	Lagoon
Magdalena litoral 1	18 Mdl l1	15.54	-91.39	2852	Lagoon
Magdalena litoral 2	14 Mdl l2	15.54	-91.40	2864	Lagoon
Manialtepec	17 Mlt	15.94	-97.19	18	Lake
Metapan 6m	10 Mtp	14.31	-89.47	450	Lagoon
Meztitlan	27 Mztln	20.68	-98.87	1255	Lake

Table 6 (continued)

Sample (Lake)	Code	Latitude	Longitude	Elevation (m)	Basin Type
Miguel Aleman 1	23 MA1	18.24	-96.42	78	Reservoir
Miguel Aleman 4	4 Oxl	20.68	-89.24	18	Sinkhole
Naha	3 Nha	16.98	-91.60	830	Lago
Negritos super	11 Ngr	13.28	-87.94	102	Lagoon
Ocatolito Reserve 2	10 OcR2	16.94	-91.60	930	Lake
Ocom	12 Ocm	19.47	-88.05	-	-
Ocotalito reserva	10 OcR1	16.94	-91.60	930	Lake
Oeste Centro Amatitlán 20 m	8 Tmt	19.45	-97.99	2550	Lake
Olomega 2.5m	9 Grdl1	13.89	-90.17	5	Lagoon
Olomega litoral	17 Olol1	13.29	-88.06	96	Lagoon
Paiasquito	16 Psq	16.13	-91.75	1462	Laguna
Patzcuaro	24 Ptzc	19.56	-101.63	2039	Reservoir
Petexbatún super	19 Ptx	16.42	-90.19	120	Lagoon
Piedra Azul	20 Paz	17.04	-96.52	1720	Lake
Presa Benito Juarez	18 PBJ	16.46	-95.44	139	Reservoir
Presa Matias Romero	20 PMR	17.28	-96.93	1745	Reservoir
Quechulac	11 Qchl	19.37	-97.35	2333	Lake
Quexil 25m	8 Ccll4	14.79	-91.66	2742	Lagoon
Quexil litoral 3	4 Txy	19.83	-99.40	2224	Presa
Requena	9 Spn10	16.98	-89.68	105	Lagoon
Rio villalobos super	19 RVl	14.48	-90.57	1193	Lake
Rosario litoral	14 Rso	16.53	-90.16	126	Lagoon
Sabanita	22 Sbt	18.40	-88.57	-	-
Sacnab 9m	22 Scb	17.06	-89.37	170	Lagoon
Salina Cruz	15 SCz	16.17	-95.23	1.5	Reservoir
Salpeten 10m	9 Zpn	20.66	-99.49	1556	Presa
Salpeten litoral1	17 Spnl1	16.99	-89.68	120	Lagoon
Salpeten litoral2	15 Spnl2	16.98	-89.68	105	Lagoon
San Francisco Yosocuta	16 SFY	17.74	-97.82	1511	Reservoir
San Jose Aguilar	15 SJA	18.37	-89.01	-	-
San Juan Bautista litoral	5 Yjal1	14.88	-87.95	640	Lake
San Juanico	3 Smart	20.42	-103.90	-	Lake
San Martin Hidalgo	3 Ymk	20.58	-89.61	16	Sinkhole
San Pedro Lagunilla	8 Olo2.5	13.31	-88.06	66	Lagoon

Table 6 (continued)

Sample (Lake)	Code	Latitude	Longitude	Elevation (m)	Basin Type
Santa Ana	6 Alb	19.21	-101.46	1491	Lake
Santa Elena	16 Sea	19.91	-99.60	2585	Lake
Santa Gertrudis	5 StA	20.21	-98.21	2200	Reservoir
Santa Maria del Oro	18 SMarDel	21.37	-104.56	779	Lake
Sayula	20 Svla	19.45	-103.61	1349	Lake
Supitlan	16 Sup	20.15	-98.39	2135	Lake
Tacambaro	13 PTcmb	19.21	-101.47	1517	Lake
Taxhimay 1	5 Lba	18.12	-95.84	16	Presa
Tecuitlapa	1 Tectp	19.12	-97.54	-	Lake
Tejocotal	20 Tcl	20.14	-98.14	2143	Reservoir
Tenango	24 Tng	20.20	-97.99	1306	Reservoir
Teometitla	9 LCh	18.60	-97.27	2459	Lake
Tepeltitic	25 Tpltc	21.28	-104.69	-	Lake
Teremendo	21 Trmd	19.81	-101.45	2065	Lake
Ticamaya 2m	23 Tcy	15.55	-87.89	17	Lagoon
Valsequillo 1	18 Vsq	18.91	-98.11	2065	Reservoir
Waha	8 ECA	14.45	-90.55	1204	Lake
Xi-bana	24 Xbn	17.13	-91.67	630	Lagoon
Yala	21 Yla	16.09	-91.65	1460	Lagoon
Yaxha	14 Yxh	17.06	-89.39	164	Lagoon
Yaxha	15 dp	16.97	-91.58	963	Lake
Yegüey	24 Ygy	16.12	-97.72	24	Lake
Yojoa litoral1	6 Alf	20.44	-99.36	1877	Reservoir
Yojoa litoral3	13 Yjal3	14.93	-88.00	637	Lake
Yojoa punto2	21 Yjap2	14.86	-87.98	639	Lake
Yuriria	14 Yri	20.24	-101.13	1729	Lake
Zempoala	23 Zmpl	19.44	-99.32	2817	Lake
Zirahuen	19 Zrhn	19.45	-101.73	2082	Lake

Table 7 – Lakes samples and biome type (as indicated by Olson et al., 2001).

Sample (Lake)	Code	Biome
Alberca	6 Ccc	Moist Broadleaf Forest
Alchichica	15 Alch	Desert and Xeric Shrubland
Alfajayucan	6 CCr	Coniferous Forest
Aljojuca	4 Apq47	Coniferous Forest
Amarillo	20 Aml	Moist Broadleaf Forest
Apastepeque 47m	4 MA4	Moist Broadleaf Forest
Apastepeque litoral 1	10 Apql1	Coniferous Forest
Aramuaca litoral	14 Arm	Dry Broadleaf Forest
Atezca	17 Atzc	Moist Broadleaf Forest
Atitlán 90m	21 Atn	Coniferous Forest
Atitlán litoral 2	21 Atnl2	Coniferous Forest
Atlanglatepec	7 Cbo	Coniferous Forest
Atotonilco	22 Atdlc	Dry Broadleaf Forest
Bahia de Oro Amatitlán 90cm	7 Lcd	Moist Broadleaf Forest
Balam 7	3 Blm	Coniferous Forest
Belize 1	3 Blz1	Moist Broadleaf Forest
Belize 2	12 Blz2	Moist Broadleaf Forest
Caballo	7 Pzs5	Moist Broadleaf Forest
Calderas 26m	11 Cds26	Coniferous Forest
Calderas litoral	6 Chn	Moist Broadleaf Forest
Camaleon	14 Cmn	Dry Broadleaf Forest

Table 7 (continued)

Sample (Lake)	Code	Biome
Cenote azul	14 Azl	Moist Broadleaf Forest
Cenote colac	11 Clc	Dry Broadleaf Forest
Cenote Oxolá	4 Qxll3	Moist Broadleaf Forest
Cenote Sabak Ha	16 Sbk	Dry Broadleaf Forest
Cenote Yumku	4 Alj	Coniferous Forest
Centro Colorada	6 Cgt	Moist Broadleaf Forest
Chan Laguna	23 CLg	Moist Broadleaf Forest
Chanmico 40m	23 Cmo	Coniferous Forest
Chicabal 10m	22 Ccl10	Moist Broadleaf Forest
Chicabal litoral 1	22 Ccll1	Moist Broadleaf Forest
Chicabal litoral 4	8 GSM	Dry Broadleaf Forest
Chiligatoro 5.5m	7 Atl	Coniferous Forest
Comandador litoral	18 Cdr	Dry Broadleaf Forest
Corralero	10 Crl	Mangrove
Crooked Tree Lagoon	23 CTL	Coniferous Forest
Cuetzalan	13 Ctz	Moist Broadleaf Forest
El Centenario Tequisquiapan	15 ECT	Desert and Xeric Shrubland
El Estudiante	24 Eet	Dry Broadleaf Forest
El pino 7m	12 Epn	Coniferous Forest
Esmeralda F-60-m	20 Esd	Moist Broadleaf Forest
Espino 5m	12 Esp	Coniferous Forest
Este centro Amatitlán 16m	8 Lag	Coniferous Forest
Finca de Escamilla 1m	3 FdE	Coniferous Forest
Grande litoral	9 Rqn	Desert and Xeric Shrubland
Gruta San Miguel	8 OCA	Coniferous Forest
Guija 2	5 MVa	Moist Broadleaf Forest
Ipala 25m	18 Ipl	Coniferous Forest
Jocotal 3m	24 Jct	Dry Broadleaf Forest
Juanacatlan	10 Jnctln	Coniferous Forest
Jucutuma 2m	12 Juc	Dry Broadleaf Forest
La Avispa	13 Asp	Dry Broadleaf Forest
La Cofradía Chica	20 Cca	Coniferous Forest
La Huaracha	17 Hra	Coniferous Forest
La Nopala	11 Npl	Coniferous Forest

Table 7 (continued)

Sample (Lake)	Code	Biome
La Soledad	9 Tecm	Desert and Xeric Shrubland
La Vega	12 LaVeg	Dry Broadleaf Forest
Lacaudon	7 Qxl25	Moist Broadleaf Forest
Lachua 35 m	19 Lch	Moist Broadleaf Forest
Lachua litoral	11 Lchl	Moist Broadleaf Forest
Lago Tenexac	18 Tnk	Coniferous Forest
Laguna camp.	19 Cmp	Moist Broadleaf Forest
Laguna Chacanbacab	17 Ccb	Moist Broadleaf Forest
Laguna Chica	9 Sld	Coniferous Forest
Laguna Chichancanab	7 BOA	Coniferous Forest
Laguna de Chacchoben	6 Cdsl	Coniferous Forest
Laguna Emiliano Zapata	21 Ezp	Moist Broadleaf Forest
Laguna Grande	13 Grd	Coniferous Forest
Laguna Kaná	13 Kna	Moist Broadleaf Forest
Laguna la Perdida	22 Prd	Moist Broadleaf Forest
Laguna Lourdes	15 LLd	Desert and Xeric Shrubland
Laguna Miguel Hidalgo	21 Mhd	Moist Broadleaf Forest
Laguna San José	12 SJs	Moist Broadleaf Forest
Laguna Señor	5 Gja	Dry Broadleaf Forest
Laguna Sijil Noh Ha	10 SNh	Moist Broadleaf Forest
Laguna verde 12m	16 Vrd	Moist Broadleaf Forest
Laguna Yalahau	11 Yhu	Dry Broadleaf Forest
Las Pozas	17 Pzs	Moist Broadleaf Forest
Las pozas 23 m	19 Pzs23	Moist Broadleaf Forest
Las pozas 5m	7 Wha	Moist Broadleaf Forest
Lequi 2	13 Lq2	Moist Broadleaf Forest
Loma Bonita	5 SGer	Dry Broadleaf Forest
Madre vieja 1m	5 SJB	Moist Broadleaf Forest
Magdalena 2.8m	19 Mdl2.8	Coniferous Forest
Magdalena litoral 1	18 Mdl l1	Coniferous Forest
Magdalena litoral 2	14 Mdl l2	Coniferous Forest
Manialtepec	17 Mlt	Mangrove
Metapan 6m	10 Mtp	Dry Broadleaf Forest
Meztitlan	27 Mztln	Desert and Xeric Shrubland

Table 7 (continued)

Sample (Lake)	Code	Biome
Miguel Aleman 1	23 MA1	Moist Broadleaf Forest
Miguel Aleman 4	4 Oxl	Dry Broadleaf Forest
Naha	3 Nha	Moist Broadleaf Forest
Negritos super	11 Ngr	Dry Broadleaf Forest
Ocatolito Reserve 2	10 OcR2	Moist Broadleaf Forest
Ocom	12 Ocm	Moist Broadleaf Forest
Ocotalito reserva	10 OcR1	Moist Broadleaf Forest
Oeste Centro Amatitlán 20 m	8 Tmt	Coniferous Forest
Olomega 2.5m	9 Grdl1	Dry Broadleaf Forest
Olomega litoral	17 Olol1	Dry Broadleaf Forest
Paiasquito	16 Psq	Coniferous Forest
Patzcuaro	24 Ptzc	Coniferous Forest
Petexbatún super	19 Ptx	Moist Broadleaf Forest
Piedra Azul	20 Paz	Dry Broadleaf Forest
Presa Benito Juarez	18 PBJ	Dry Broadleaf Forest
Presa Matias Romero	20 PMR	Coniferous Forest
Quechulac	11 Qchl	Desert and Xeric Shrubland
Quexil 25m	8 Ccll4	Moist Broadleaf Forest
Quexil litoral 3	4 Txy	Coniferous Forest
Requena	9 Spn10	Moist Broadleaf Forest
Rio villalobos super	19 RVl	Coniferous Forest
Rosario litoral	14 Rso	Moist Broadleaf Forest
Sabanita	22 Sbt	Moist Broadleaf Forest
Sacnab 9m	22 Scb	Moist Broadleaf Forest
Salina Cruz	15 SCz	Dry Broadleaf Forest
Salpeten 10m	9 Zpn	Desert and Xeric Shrubland
Salpeten litoral1	17 Spnl1	Moist Broadleaf Forest
Salpeten litoral2	15 Spnl2	Moist Broadleaf Forest
San Francisco Yosocuta	16 SFY	Dry Broadleaf Forest
San Jose Aguilar	15 SJA	Moist Broadleaf Forest
San Juan Bautista litoral	5 Yjal1	Moist Broadleaf Forest
San Juanico	3 Smart	-
San Martin Hidalgo	3 Ymk	-
San Pedro Lagunilla	8 Olo2.5	Dry Broadleaf Forest

Table 7 (continued)

Sample (Lake)	Code	Biome
Santa Ana	6 Alb	Coniferous Forest
Santa Elena	16 Sea	Coniferous Forest
Santa Gertrudis	5 StA	Coniferous Forest
Santa Maria del Oro	18 SMarDel	Dry Broadleaf Forest
Sayula	20 Svla	Coniferous Forest
Supitlan	16 Sup	Desert and Xeric Shrubland
Tacambaro	13 PTcmb	Coniferous Forest
Taxhimay 1	5 Lba	Moist Broadleaf Forest
Tecuitlapa	1 Tectp	-
Tejocotal	20 Tcl	-
Tenango	24 Tng	Moist Broadleaf Forest
Teometitla	9 LCh	Coniferous Forest
Tepeltitic	25 Tpltc	Coniferous Forest
Teremendo	21 Trmd	Coniferous Forest
Ticamaya 2m	23 Tcy	Dry Broadleaf Forest
Valsequillo 1	18 Vsq	Coniferous Forest
Waha	8 ECA	Coniferous Forest
Xi-bana	24 Xbn	Moist Broadleaf Forest
Yala	21 Yla	Moist Broadleaf Forest
Yaxha	14 Yxh	Moist Broadleaf Forest
Yaxha	15 dp	Moist Broadleaf Forest
Yegüey	24 Ygy	Dry Broadleaf Forest
Yojoa litoral1	6 Alf	Desert and Xeric Shrubland
Yojoa litoral3	13 Yjal3	Moist Broadleaf Forest
Yojoa punto2	21 Yjap2	Moist Broadleaf Forest
Yuriria	14 Yri	Dry Broadleaf Forest
Zempoala	23 Zmpl	Coniferous Forest
Zirahuen	19 Zrhn	Coniferous Forest

Table 8 – Sediment weights and injection volumes of each sample in GC-FID for abundance analysis.

Sample	Androstane added (ul)	Sediment wt (g)	Ratio of FAMES split	Dilution (ul)	Injection (ul)
1 Tectp	30	6.043	0.50	100	1
10 Apql1	30	5.29	0.33	100	1
10 Crl	30	4.93	0.33	100	1
10 Jnctln	50	3.077	0.50	100	0.5
10 Mtp	30	4.76	0.27	100	1
10 OcR1	30	4.95	0.33	100	1
10 OcR2	50	1.97	0.23	100	0.5
10 SNh	30	4.67	0.33	100	1
11 Cds26	30	4.84	0.33	100	1
11 Clc	30	4.71	0.33	100	0.5
11 Lchl	30	5.07	0.33	100	1
11 Ngr	100	4.83	0.17	200	0.5
11 Npl	30	5.88	0.33	100	1
11 Qchl	200	2.9901	0.50	400	0.5
11 Yhu	30	4.71	0.33	100	1
12 Blz2	30	4.74	0.33	100	1
12 Epn	30	4.76	0.33	100	1
12 Esp	30	4.93	0.33	100	1
12 Juc	100	2.59	0.13	200	0.5
12 LaVeg	100	4.04	0.50	200	0.5
12 Ocm	30	4.41	0.33	100	1
12 SJs	100	3.02	0.33	200	0.5
13 Asp	50	5.51	0.20	100	0.5
13 Ctz	50	4.73	0.33	100	0.5
13 Grd	30	4.87	0.33	100	1
13 Kna	30	4.69	0.33	100	0.5
13 Lq2	30	4.56	0.33	100	1
13 PTcmb	100	6.077	0.25	200	0.5
13 Yjal3	30	5.02	0.33	100	1
14 Arm	30	4.95	0.33	100	1
14 Azl	30	4.27	0.33	100	1
14 Cmn	30	4.94	0.33	100	1
14 Mdll2	30	5.37	0.33	100	1

Table 8 (continued)

Sample	Androstane added (ul)	Sediment wt (g)	Ratio of FAMES split	Dilution (ul)	Injection (ul)
14 Rso	30	4.86	0.33	100	1
14 Yri	100	4.182	0.50	200	0.5
14 Yxh	50	2.22	0.27	100	0.5
15 Alch	30	6.019	0.50	100	1
15 dp	30	4.11	0.33	100	1
15 ECT	100	4.89	0.30	200	0.5
15 LLd	30	5.12	0.33	100	1
15 SCz	30	4.99	0.33	100	1
15 SJA	30	4.7	0.33	100	1
15 Spnl2	30	4.64	0.33	100	1
16 Psq	100	5.64	0.27	200	0.5
16 Sbk	30	4.77	0.33	100	1
16 SEa	100	3.5	0.23	100	1
16 SFY	30	4.59	0.33	100	1
16 Sup	100	1.95	0.20	100	0.5
16 Vrd	100	4.97	0.33	200	0.5
17 Atcz	50	4.507	0.50	100	0.5
17 Ccb	100	4.67	0.33	200	0.5
17 Hra	30	4.64	0.33	100	1
17 Mlt	50	2.71	0.13	100	0.5
17 Olol1	30	4.77	0.33	100	1
17 Pzs	50	3.76	0.33	100	0.5
17 Spnl1	100	5.53	0.33	100	0.5
18 Cdr	100	4.79	0.33	100	0.5
18 Ipl	100	5.95	0.13	200	0.5
18 Mdll1	30	4.74	0.33	100	1
18 PBJ	30	5.02	0.33	100	1
18 SMarDel	100	4.96	0.50	200	0.5
18 Tnk	30	4.46	0.33	100	1
18 Vsq	50	5.14	0.33	200	0.5
19 Cmp	100	4.91	0.33	100	0.5
19 Lch	30	4.61	0.33	100	1
19 Mdl2.8	30	4.87	0.33	100	1
19 Ptx	30	5.14	0.33	100	1

Table 8 (continued)

Sample	Androstane added (ul)	Sediment wt (g)	Ratio of FAMES split	Dilution (ul)	Injection (ul)
19 Pzs23	100	4.84	0.07	200	0.5
19 RVl	30	4.94	0.33	100	1
19 Zrhn	30	4.425	0.50	100	1
20 Aml	100	3.75	0.33	200	0.5
20 Cca	30	4.94	0.33	100	1
20 Esd	200	4.88	0.20	200	0.5
20 PAz	30	5.15	0.33	100	1
20 PMR	100	5.64	0.10	200	0.5
20 Svla	30	6	0.50	100	1
20 Tcl	300	4.02	0.33	400	0.5
21 Atn	30	4.82	0.33	100	1
21 Atnl1	50	5.45	0.33	100	0.5
21 Ezp	100	4.85	0.33	200	0.5
21 MHd	100	3.49	0.33	200	0.5
21 Trmd	100	3	0.38	200	0.5
21 Yjap2	50	4.31	0.23	100	0.5
21 Yla	100	5.31	0.23	200	0.5
22 Atdlc	30	6.077	0.50	100	1
22 Ccl10	50	4.78	0.33	100	0.5
22 Ccll2	30	5.33	0.33	100	1
22 Prd	100	2.72	0.33	100	0.5
22 Sbt	50	4.98	0.33	100	0.5
22 Scb	30	2.8	0.33	100	0.5
23 Clg	100	4.84	0.33	100	0.5
23 Cmo	30	4.98	0.33	100	1
23 CTL	30	4.94	0.33	100	1
23 MA1	50	4.34	0.23	100	1
23 Tcy	100	3.59	0.33	100	0.5
23 Zmpl	100	2.045	0.50	200	0.5
24 EEt	30	4.47	0.33	100	1
24 Jct	50	4.04	0.30	100	0.5
24 Ptzc	30	4.0801	0.50	100	1
24 Tng	30	4.64	0.33	100	1
24 Xbn	30	4.92	0.33	100	1

Table 8 (continued)

Sample	Androstane added (ul)	Sediment wt (g)	Ratio of FAMES split	Dilution (ul)	Injection (ul)
24 Ygy	30	5.17	0.33	100	1
25 Tpltc	200	2.522	0.50	400	0.5
27 Mztln	30	5.989	0.50	100	1
3 Blm	30	5.23	0.33	100	1
3 Blz1	30	4.93	0.33	100	1
3 FdE	30	5.51	0.23	100	1
3 Nha	30	5.02	0.33	100	1
3 SMart	30	6.088	0.50	100	1
3 Ymk	30	4.97	0.33	100	1
4 Alj	200	5	0.50	400	0.5
4 Apq47	30	5.14	0.27	100	1
4 MA4	30	4.83	0.33	100	1
4 Oxl	30	4.99	0.33	100	1
4 Oxll3	100	5.62	0.23	100	0.5
4 Txy	30	4.56	0.33	100	1
5 Gja	30	4.89	0.33	100	1
5 LBa	50	5.28	0.33	100	0.5
5 MVa	300	3.24	0.33	300	0.5
5 SGer	30	5.064	0.50	100	1
5 SJB	50	5.35	0.33	100	0.5
5 StA	100	4.79	0.27	200	0.5
5 Yjal1	30	4.87	0.33	100	1
6 Alb	100	5	0.50	200	0.5
6 Alf	50	4.69	0.33	100	0.5
6 Ccc	50	0.83	0.33	100	0.5
6 Ccr	100	4.82	0.17	200	0.5
6 Cdsl	30	4.99	0.33	100	1
6 Cgt	30	4.77	0.33	100	1
6 Chn	30	4.69	0.33	100	1
7 Atl	30	5	0.50	100	1
7 BOA	100	4.6	0.13	100	0.5
7 Cbo	30	4.49	0.33	100	1
7 Lcd	100	4.3	0.20	200	0.5
7 Pzs5	50	2.05	0.33	100	0.5

Table 8 (continued)

Sample	Androstane added (ul)	Sediment wt (g)	Ratio of FAMES split	Dilution (ul)	Injection (ul)
7 Qxl2.5	50	1.48	0.33	100	0.5
7 Wha	30	5.17	0.33	100	1
8 Ccll4	50	5.19	0.33	100	0.5
8 ECA	100	4.81	0.07	200	0.5
8 GSM	50	5.47	0.33	100	0.5
8 Lag	100	6	0.50	200	0.5
8 OCA	30	4.85	0.33	100	1
8 Olo2.5	30	4.64	0.33	100	1
8 Tmt	30	2.88	0.33	200	1
9 Grdl1	50	5.94	0.23	100	0.5
9 LCh	30	4.99	0.33	100	1
9 Rqn	30	4.82	0.33	100	1
9 Sld	30	4.74	0.33	100	1
9 Spn10	50	4.82	0.33	100	0.5
9 Tecm	200	5.052	0.50	400	0.5
9 Zpn	30	4.81	0.33	100	1

Table 9 – Abundances of FAMES in lake sediment surface samples across Mesoamerica.

Sample	Androstane (ng)	C16 (ng/g sediment)	C18 (ng/g sediment)	C19 (ng/g sediment)	C20 (ng/g sediment)	C21 (ng/g sediment)
10 Apql1	1200	850.35	704.90	0.00	142.66	0.00
10 Crl	1200	4164.07	2271.56	26.50	717.22	186.38
10 Jnctln	2000	9592.57	4624.93	576.13	2081.70	826.53
10 Mtp	1200	3259.57	1432.85	139.16	441.41	188.43
10 OcR1	1200	2201.09	1738.04	145.65	580.43	209.78
10 OcR2	2000	4185.78	2457.40	208.84	1250.48	474.06
10 SNh	1200	4292.93	3516.03	198.91	670.11	320.38
11 Cds26	1200	4705.14	2593.40	260.63	1997.54	1001.07
11 Clc	1200	7943.35	2856.65	132.41	1630.58	280.45
11 Lchl	1200	803.81	719.43	0.00	164.48	0.00
11 Ngr	4000	14489.48	3917.78	548.76	1487.57	862.33
11 Npl	1200	3790.02	1979.39	97.26	878.58	376.17
11 Qchl	8000	23282.17	3964.87	0.00	1979.38	534.56
11 Yhu	1200	1105.44	1391.96	0.00	363.12	118.20
12 Blz2	1200	1585.06	926.99	0.00	766.55	228.18
12 Epn	1200	5953.72	3067.39	543.98	1179.70	574.02
12 Esp	1200	1913.86	2184.34	119.88	425.90	187.95
12 Juc	4000	11291.12	1745.07	0.00	1179.28	532.89
12 LaVeg	4000	5820.82	1946.73	0.00	1317.19	0.00
12 Ocm	1200	2633.48	951.07	164.23	326.18	207.15
12 SJs	4000	12535.59	2652.54	216.95	1384.75	569.49
13 Asp	2000	6810.10	2633.30	158.09	940.13	465.86
13 Ctz	2000	15202.58	3509.92	193.82	1227.50	442.09
13 Grd	1200	4891.29	2495.68	352.89	1143.82	552.16
13 Kna	1200	18024.77	3957.92	419.44	1045.01	223.70
13 Lq2	1200	9051.31	3028.50	0.00	1038.95	405.46
13 PTcmb	4000	16158.07	2183.68	379.07	1011.34	787.41
13 Yjal3	1200	692.23	736.61	0.00	105.86	0.00
14 Arm	1200	4683.94	4452.90	98.25	598.11	212.15
14 Azl	1200	9237.85	1854.64	381.56	509.73	111.15
14 Cmn	1200	15941.33	3338.50	135.15	1326.35	550.65
14 Mdll2	1200	1660.65	1478.69	83.88	1220.97	473.51
14 Rso	1200	19037.92	4153.11	164.49	1364.01	285.69

Table 9 (continued)

Sample	Androstane (ng)	C16 (ng/g sediment)	C18 (ng/g sediment)	C19 (ng/g sediment)	C20 (ng/g sediment)	C21 (ng/g sediment)
14 Yri	4000	14076.24	3987.59	632.98	3356.38	1000.00
14 Yxh	2000	6372.25	2587.20	231.56	1168.54	477.77
15 Alch	1200	1780.28	404.16	0.00	91.35	0.00
15 dp	1200	4918.58	2028.32	98.23	515.93	145.58
15 ECT	4000	45287.12	8300.91	354.47	2760.14	1202.05
15 LLd	1200	2076.94	957.71	0.00	385.06	136.00
15 SCz	1200	13116.70	1545.55	478.96	318.87	195.23
15 SJA	1200	10407.07	4868.25	345.89	1895.75	426.73
15 Spnl2	1200	18112.34	2495.97	91.88	441.91	169.99
16 Psq	4000	21921.80	4131.45	286.19	2086.52	698.84
16 Sbk	1200	1813.11	2248.74	0.00	463.87	157.31
16 SEa	4000	104753.14	13517.43	923.29	3324.97	1252.44
16 SFY	1200	5817.81	2882.59	0.00	1016.19	360.32
16 Sup	4000	17781.73	3082.78	0.00	680.79	319.74
16 Vrd	4000	18975.86	6955.38	1082.66	4857.35	2177.03
17 Atcz	2000	40969.07	6503.68	0.00	2006.87	818.85
17 Ccb	4000	9854.85	3034.87	228.09	1445.81	654.10
17 Hra	1200	5044.57	2378.11	294.05	1172.40	596.67
17 Mlt	2000	5500.51	2767.11	0.00	364.66	197.14
17 Olol1	1200	1983.99	1376.34	62.78	353.23	159.96
17 Pzs	2000	6450.73	2743.68	211.05	1245.67	292.94
17 Spnl1	4000	3849.65	1204.32	0.00	289.90	144.18
18 Cdr	4000	7343.01	2604.51	184.01	828.65	443.35
18 Ipl	4000	2592.83	1378.49	374.50	1498.01	919.52
18 Mdll1	1200	5822.55	4598.39	0.00	1367.09	575.14
18 PBJ	1200	1605.55	942.65	0.00	221.16	93.06
18 SMarDel	4000	6194.77	2781.95	0.00	1791.92	1303.56
18 Tnk	1200	2900.19	2244.32	178.03	788.44	373.80
18 Vsq	2000	7348.34	2731.90	193.74	1630.14	636.01
19 Cmp	4000	17888.72	2673.95	205.93	1121.16	446.18
19 Lch	1200	852.97	1555.21	0.00	163.58	0.00
19 Mdl2.8	1200	3224.59	2271.04	146.45	1489.62	667.76
19 Ptx	1200	18997.70	3097.38	234.35	478.12	221.78
19 Pzs23	4000	7971.37	3751.91	440.84	1356.87	791.98

Table 9 (continued)

Sample	Androstane (ng)	C16 (ng/g sediment)	C18 (ng/g sediment)	C19 (ng/g sediment)	C20 (ng/g sediment)	C21 (ng/g sediment)
19 RVl	1200	8137.69	5732.41	0.00	1224.12	201.26
19 Zrhn	1200	1500.53	778.63	0.00	339.93	150.26
20 Aml	4000	14125.00	5456.52	472.83	2926.63	1225.54
20 Cca	1200	3835.58	1828.06	94.23	1034.89	351.93
20 Esd	8000	33266.43	3848.49	0.00	2149.56	639.69
20 PAz	1200	4947.27	2533.46	127.71	1329.43	405.56
20 PMR	4000	46941.79	10349.25	576.12	4931.34	776.12
20 Svla	1200	296.22	313.15	0.00	97.93	0.00
21 Atn	1200	2539.95	1382.57	196.25	865.42	402.14
21 Atnl1	2000	2863.91	1249.42	0.00	553.65	299.12
21 Ezp	4000	24313.81	9811.15	610.82	1966.94	1012.05
21 MHd	4000	42529.37	4835.71	1460.32	962.70	392.06
21 Trmd	4000	9110.33	7856.28	254.37	1662.32	582.51
21 Yjap2	2000	8390.94	3435.04	769.96	2202.62	1505.36
21 Yla	4000	26021.79	2898.58	313.50	1495.39	829.84
22 Atdlc	1200	1916.29	712.47	0.00	197.63	126.66
22 Ccl10	2000	7456.03	1839.20	169.60	1253.14	515.08
22 Ccll2	1200	1088.18	1046.45	0.00	307.09	126.84
22 Prd	4000	8363.42	2481.56	202.70	915.14	483.36
22 Sbt	2000	7203.40	2655.34	213.68	1149.75	485.47
22 Scb	1200	3587.35	1875.88	175.64	604.22	313.35
23 Clg	4000	18595.16	2478.30	146.08	941.57	402.34
23 Cmo	1200	3835.58	1828.06	94.23	1034.89	351.93
23 CTL	1200	7996.42	2747.28	0.00	240.26	168.91
23 MA1	2000	6698.47	2408.61	204.30	726.99	319.94
23 Tcy	4000	11278.13	2886.55	0.00	1391.58	403.48
23 Zmpl	4000	10501.34	3377.34	435.33	2686.89	913.47
24 EEt	1200	1789.34	1214.59	0.00	442.28	195.32
24 Jct	2000	8723.85	1527.61	172.35	881.32	418.33
24 Ptzc	1200	1570.90	1164.05	138.09	381.17	216.26
24 Tng	1200	12280.94	7369.90	252.84	1558.53	548.49
24 Xbn	1200	1896.90	2136.52	0.00	316.95	120.29
24 Ygy	1200	2660.63	1905.88	57.01	307.33	157.47
25 Tpltc	8000	37396.93	4740.03	1043.95	2698.47	834.07

Table 9 (continued)

Sample	Androstane (ng)	C16 (ng/g sediment)	C18 (ng/g sediment)	C19 (ng/g sediment)	C20 (ng/g sediment)	C21 (ng/g sediment)
27 Mztln	1200	2205.43	984.22	0.00	322.90	167.14
3 Blm	1200	3910.26	2069.39	120.77	798.00	314.26
3 Blz1	1200	16790.36	6378.31	403.21	1777.51	685.94
3 FdE	1200	5842.24	2286.51	135.37	754.20	241.22
3 Nha	1200	5212.82	1671.63	117.62	559.28	213.20
4 Alj	8000	7853.39	2638.90	0.00	2259.06	779.68
4 Apq47	1200	3952.42	2103.16	155.37	778.11	392.84
4 MA4	1200	3521.53	1866.07	133.03	456.37	265.61
4 Oxl	1200	1168.62	1091.81	199.86	199.86	0.00
4 Oxll3	4000	20168.98	4420.79	317.25	953.41	301.51
4 Txy	1200	5087.24	2338.29	195.81	1608.38	578.29
5 Gja	1200	57410.31	18383.51	115.46	27596.56	627.49
5 LBa	2000	11814.34	2618.44	277.62	847.24	384.83
5 MVa	12000	39848.59	9704.06	916.72	6037.16	2997.94
5 SGer	1200	3841.47	2199.15	175.46	1189.28	455.85
5 SJB	2000	5255.44	2055.28	170.85	2858.46	762.98
5 StA	4000	14880.28	3528.17	0.00	2147.89	978.87
5 Yjal1	1200	4387.42	1782.73	102.35	917.27	372.28
6 Alb	4000	12661.75	3964.63	464.26	2359.62	816.51
6 Alf	2000	7478.02	4371.12	386.86	2385.93	1081.91
6 Ccc	2000	10591.68	2775.63	121.23	559.71	179.73
6 Ccr	4000	23266.74	4191.55	314.25	1441.08	592.59
6 Cdsl	1200	1471.71	1090.47	0.00	524.05	257.79
6 Cgt	1200	4727.22	2812.42	422.82	2415.60	677.55
6 Chn	1200	10761.46	3977.56	278.05	1545.85	350.73
7 Atl	1200	4563.64	1658.59	0.00	783.16	367.00
7 BOA	4000	11012.31	4154.02	327.74	1140.81	479.96
7 Cbo	1200	1677.03	2410.21	0.00	576.33	191.18
7 Lcd	4000	36446.24	3590.52	444.04	764.57	381.55
7 Pzs5	2000	12002.43	3493.53	227.35	2330.10	363.27
7 Qxl2.5	2000	31869.98	9248.16	223.86	1050.31	309.78
7 Wha	1200	639.50	595.68	0.00	83.04	0.00
8 Ccll4	2000	7624.81	2484.78	141.55	2485.54	916.29
8 ECA	4000	24588.74	10070.99	340.75	2311.41	603.88

Table 9 (continued)

Sample	Androstane (ng)	C16 (ng/g sediment)	C18 (ng/g sediment)	C19 (ng/g sediment)	C20 (ng/g sediment)	C21 (ng/g sediment)
8 GSM	2000	4603.06	3640.82	216.33	688.78	208.16
8 Lag	4000	17881.75	3665.69	493.43	1290.51	550.36
8 OCA	1200	96.17	1604.62	86.64	409.82	125.63
8 Olo2.5	1200	2769.54	2564.96	208.63	510.24	244.20
8 Tmt	1200	12272.36	2327.64	176.82	1508.79	506.50
9 Grdl1	2000	5435.12	2837.49	415.06	3270.57	921.82
9 LCh	1200	11488.38	4180.24	232.69	1747.42	715.97
9 Rqn	1200	6763.83	3024.66	156.82	932.06	327.65
9 Sld	1200	2475.61	2208.29	0.00	458.05	169.76
9 Spn10	2000	4078.39	2438.76	108.87	538.92	278.72
9 Tecm	8000	25215.63	5768.75	646.88	3640.63	1856.25
9 Zpn	1200	2.77	1402.11	0.00	474.23	133.68

Table 9 (continued)

Sample	C22 (ng/g sediment)	C23 (ng/g sediment)	C24 (ng/g sediment)	C25 (ng/g sediment)	C26 (ng/g sediment)	C27 (ng/g sediment)
10 Apql1	448.95	181.12	522.38	131.47	337.06	0.00
10 Crl	983.08	593.71	2822.60	704.19	2451.65	458.98
10 Jnctln	8786.21	2308.75	13849.34	2442.44	9472.68	1125.73
10 Mtp	922.04	630.88	2203.24	561.48	1970.73	352.92
10 OcR1	1736.96	804.35	4290.22	1082.61	4467.39	725.00
10 OcR2	3229.98	1583.60	8576.55	2011.53	9675.85	1752.72
10 SNh	2973.91	714.95	8188.86	753.26	6100.27	481.79
11 Cds26	7690.87	4761.32	16587.26	4859.86	14383.42	3558.56
11 Clc	4450.74	1806.78	1.00	1526.32	5589.23	623.46
11 Lchl	555.66	175.92	1064.12	238.14	1798.57	190.94
11 Ngr	2963.67	2082.22	9424.47	2948.37	11642.45	2944.55
11 Npl	2729.79	1095.65	3690.82	600.32	2798.71	363.93
11 Qchl	6103.09	1680.03	13684.61	1429.55	7667.05	571.21
11 Yhu	938.06	539.95	2112.53	416.08	1740.90	226.00
12 Blz2	1508.15	561.80	1187.78	291.85	745.16	153.82
12 Epn	2510.42	1066.04	4763.46	1164.28	5384.57	766.44
12 Esp	543.37	321.69	1153.61	364.46	1488.55	312.65
12 Juc	3347.04	2939.14	12271.38	2383.22	6287.83	725.33
12 LaVeg	4629.54	3893.46	15012.11	4067.80	14518.16	2237.29
12 Ocm	1015.16	330.76	2544.21	274.11	2038.34	441.77
12 SJs	3811.86	2108.47	12589.83	4222.03	19072.88	4755.93
13 Asp	7021.52	1429.37	9710.94	956.03	4334.89	507.95
13 Ctz	3125.06	1740.66	6953.39	1453.62	5794.19	927.55
13 Grd	3736.06	1232.48	7096.42	1229.85	5254.72	658.38
13 Kna	2246.60	864.45	2948.07	647.14	2269.77	337.95
13 Lq2	2958.67	1619.00	7521.38	1994.54	5933.02	741.09
13 PTcmb	2341.75	1309.92	5665.57	1326.02	6390.05	1096.23
13 Yjal3	294.77	135.66	467.19	112.84	401.27	95.09
14 Arm	1339.81	640.22	1767.34	391.90	998.65	197.57
14 Azl	1214.09	443.78	2132.51	443.25	1941.06	264.57
14 Cmn	4493.24	1486.64	7959.35	1236.46	4742.17	793.92
14 Mdll2	4181.74	2017.14	6714.32	2124.01	5585.34	1394.14
14 Rso	2711.18	994.15	4038.16	777.23	2797.27	345.33

Table 9 (continued)

Sample	C22 (ng/g sediment)	C23 (ng/g sediment)	C24 (ng/g sediment)	C25 (ng/g sediment)	C26 (ng/g sediment)	C27 (ng/g sediment)
14 Yri	9210.99	3523.05	22576.24	3819.15	18219.86	2345.74
14 Yxh	3926.72	1401.07	8785.54	1761.60	8802.15	1538.84
15 Alch	275.36	80.18	520.48	0.00	267.47	0.00
15 dp	1184.07	477.43	2788.05	581.86	2809.29	498.67
15 ECT	8592.36	5693.58	12258.37	2813.71	6768.02	992.52
15 LLd	765.44	485.11	1165.61	299.09	843.07	146.42
15 SCz	786.12	393.06	0.00	545.99	1538.39	361.82
15 SJA	5173.72	2178.69	10668.80	2054.11	8680.29	829.60
15 Spnl2	3306.14	899.07	5049.60	635.34	2500.06	275.64
16 Psq	5204.66	2379.37	14517.47	2777.04	10846.92	1138.10
16 Sbk	1339.16	682.69	0.00	720.00	2219.50	563.70
16 SEa	8736.40	3375.17	20002.79	2772.66	11737.80	2131.10
16 SFY	2523.89	1040.49	4719.03	866.40	2931.17	438.06
16 Sup	1773.90	942.85	5172.16	1063.20	5750.40	505.61
16 Vrd	16178.49	6340.89	42425.75	9082.66	35833.21	3201.17
17 Atcz	5657.34	1872.36	10144.33	1504.17	6735.40	972.02
17 Ccb	5766.26	3883.13	20755.89	4769.09	25694.63	4955.70
17 Hra	3443.93	2373.35	10690.56	2261.06	6887.87	1396.99
17 Mlt	920.33	295.20	3127.68	338.10	2233.91	341.16
17 Olol1	789.99	648.04	1653.14	476.07	1262.78	182.35
17 Pzs	2298.27	872.84	3565.25	593.87	3019.97	326.90
17 Spnl1	986.89	478.80	3330.76	683.11	4492.68	465.69
18 Cdr	2216.73	1352.27	6599.57	1979.62	9477.00	1070.70
18 Ipl	3847.01	1512.35	9880.48	1556.97	6739.44	1090.04
18 Mdll1	4179.98	1920.14	6259.61	1550.06	4978.83	1197.24
18 PBJ	456.10	232.07	848.44	209.10	770.32	155.10
18 SMarDel	12400.95	2105.46	13077.43	2381.00	22194.77	1666.51
18 Tnk	2727.55	1179.96	4179.58	1015.03	2555.68	524.86
18 Vsq	5256.36	2307.24	10792.56	1616.44	6726.03	939.33
19 Cmp	2449.30	1861.67	8288.09	2360.89	8034.32	1483.10
19 Lch	538.66	167.09	0.00	569.04	1853.16	329.50
19 Mdl2.8	5547.54	2496.72	7944.26	2275.96	6786.34	1711.48
19 Ptx	1096.96	505.13	2442.72	522.72	2873.72	461.15
19 Pzs23	3427.48	2301.53	6937.02	1700.38	8776.72	1414.12

Table 9 (continued)

Sample	C22 (ng/g sediment)	C23 (ng/g sediment)	C24 (ng/g sediment)	C25 (ng/g sediment)	C26 (ng/g sediment)	C27 (ng/g sediment)
19 RVl	2066.08	560.05	2184.42	374.62	928.64	146.23
19 Zrhn	847.99	316.29	1305.60	332.57	1164.80	236.95
20 Aml	9845.11	3529.89	19429.35	3967.39	14730.98	2024.46
20 Cca	2535.61	839.06	2627.38	481.39	1548.24	284.33
20 Esd	4897.38	2201.36	12682.42	2307.54	10235.03	1007.45
20 PAz	3309.49	1234.52	4618.79	935.38	3553.40	658.10
20 PMR	10588.06	1753.73	7523.88	979.10	2574.63	317.91
20 Svla	126.35	97.33	231.54	91.28	268.41	0.00
21 Atn	2704.83	1138.07	4660.86	979.62	3393.30	529.22
21 Atnl1	2878.77	805.39	5512.31	747.79	4600.09	563.86
21 Ezp	3035.02	2235.92	9749.51	3264.78	18424.21	3108.99
21 MHd	2785.71	1348.41	5688.10	992.06	3591.27	393.65
21 Trmd	5372.34	2664.55	12025.44	2055.33	8298.89	1130.68
21 Yjap2	5025.03	1992.85	7829.56	2181.17	9748.51	2382.60
21 Yla	5433.36	2353.73	16031.85	3461.86	18694.05	3136.63
22 Atdlc	344.49	267.52	1125.20	347.77	2024.93	185.08
22 Ccl10	5475.50	1910.80	7145.73	1898.24	17194.72	1131.91
22 Ccll2	908.48	307.65	914.60	296.52	999.17	282.06
22 Prd	2993.70	1651.57	13703.15	2531.93	14416.79	2661.47
22 Sbt	4938.76	2253.02	9255.25	2135.90	7944.57	1052.30
22 Scb	1888.52	890.87	9369.56	1347.54	8659.95	1287.12
23 Clg	3419.03	2207.01	8998.33	2530.05	8021.70	1639.40
23 Cmo	2535.61	839.06	2627.38	481.39	1548.24	284.33
23 CTL	572.06	312.03	1384.81	397.13	1779.37	321.06
23 MA1	2356.24	767.95	4155.04	651.28	3674.36	682.40
23 Tcy	2731.02	2207.69	9883.81	2838.98	8380.60	1379.69
23 Zmpl	7728.81	3350.58	22007.14	3099.02	9857.27	1652.10
24 EEt	1097.85	578.11	2302.34	562.39	1437.98	313.19
24 Jct	1556.60	1179.01	4931.45	1388.95	5644.34	760.67
24 Ptzc	804.56	425.11	2260.20	386.88	2471.33	338.94
24 Tng	4032.11	1475.59	6060.20	1210.70	3182.61	690.30
24 Xbn	868.74	312.17	1446.30	319.81	1236.28	281.62
24 Ygy	778.64	435.48	1657.19	402.35	1273.85	257.92
25 Tpltc	5745.83	2668.48	15084.16	6402.73	19745.14	7781.94

Table 9 (continued)

Sample	C22 (ng/g sediment)	C23 (ng/g sediment)	C24 (ng/g sediment)	C25 (ng/g sediment)	C26 (ng/g sediment)	C27 (ng/g sediment)
27 Mztln	713.58	372.06	1704.53	315.14	1098.58	218.89
3 Blm	1964.64	1156.30	3413.84	974.15	2242.54	498.08
3 Blz1	3112.45	1367.07	6384.74	1379.92	6667.47	1095.58
3 FdE	1452.93	637.66	3129.26	662.60	3110.94	501.78
3 Nha	1668.80	952.31	4166.07	684.26	3382.85	515.17
4 Alj	14473.97	2029.15	25392.75	2345.69	17909.20	1426.07
4 Apq47	2285.05	1054.74	6091.58	1157.68	6903.79	915.79
4 MA4	1504.85	812.63	2791.43	610.60	2723.34	569.11
4 Oxl	778.80	404.68	1875.57	589.68	2202.62	504.61
4 Oxll3	1768.48	1124.87	5100.02	1284.74	5423.90	668.46
4 Txy	4289.52	2086.86	6510.48	1456.00	4371.05	814.48
5 Gja	2942.96	973.88	3964.26	438.49	2137.46	382.82
5 LBa	2080.63	953.15	4268.90	1081.72	3473.52	757.90
5 MVa	32886.44	16757.05	103507.23	21794.91	90194.08	11380.59
5 SGer	3079.27	1614.10	4690.55	947.81	3012.69	528.07
5 SJB	5564.49	3491.62	9759.63	1833.33	6167.50	800.67
5 StA	7669.01	3795.77	15866.20	3725.35	11161.97	2626.76
5 Yjal1	2570.79	1540.30	6422.81	1494.88	5934.75	808.53
6 Alb	7534.27	2231.39	22316.88	1731.76	9672.81	1463.52
6 Alf	11566.87	5079.13	22806.11	4267.47	17609.44	3023.60
6 Ccc	1724.97	1121.23	5284.68	1167.67	4397.47	518.09
6 Ccr	4357.65	2853.72	11389.45	3037.79	8733.26	1348.30
6 Cdsl	1593.95	870.80	2396.97	552.50	1861.42	364.30
6 Cgt	4711.62	2319.42	10673.50	2051.70	9720.43	1362.02
6 Chn	3335.12	1298.05	4044.39	720.98	2646.34	262.93
7 Atl	2152.19	1125.25	4214.81	742.09	2265.32	315.15
7 BOA	2505.48	967.09	5877.77	811.28	5445.27	676.07
7 Cbo	1581.44	757.31	2582.83	474.25	1762.41	264.50
7 Lcd	2179.75	971.88	4292.59	1038.78	3311.16	699.14
7 Pzs5	3115.70	976.54	4832.52	1049.35	4819.58	766.99
7 Qxl2.5	2410.40	1715.09	5786.32	939.51	5908.42	741.66
7 Wha	197.21	95.72	535.70	110.72	705.81	69.77
8 Ccll4	6330.29	2426.94	7044.90	2583.71	6952.05	1527.40
8 ECA	4509.23	1094.18	10831.99	1031.71	7956.46	885.94

Table 9 (continued)

Sample	C22 (ng/g sediment)	C23 (ng/g sediment)	C24 (ng/g sediment)	C25 (ng/g sediment)	C26 (ng/g sediment)	C27 (ng/g sediment)
8 GSM	1851.02	894.90	5050.00	1133.67	5170.41	878.57
8 Lag	2875.91	1262.77	7486.13	1741.61	8916.79	1776.64
8 OCA	761.59	314.51	1079.57	233.94	674.95	150.76
8 Olo2.5	1198.38	733.42	3154.45	1166.85	5472.78	991.37
8 Tmt	3063.69	1984.71	4448.92	808.92	1582.17	257.83
9 Grdl1	3633.24	2930.00	8330.74	1462.96	6402.78	594.35
9 LCh	7478.93	2704.29	21848.35	1833.19	7842.14	1342.45
9 Rqn	2317.44	1168.33	4453.14	967.89	3076.07	605.45
9 Sld	1180.00	511.71	1674.63	444.88	1220.00	282.44
9 Spn10	1493.74	780.62	3346.76	683.72	4415.90	567.23
9 Tecm	18300.00	6543.75	39240.63	3262.50	12825.00	1796.88
9 Zpn	1371.26	370.60	2043.24	280.42	1348.32	162.56

Table 9 (continued)

Sample	C28 (ng/g sediment)	C29 (ng/g sediment)	C30 (ng/g sediment)	C31 (ng/g sediment)	C32 (ng/g sediment)	C33 (ng/g sediment)	C34 (ng/g sediment)
10 Apql1	367.83	100.00	460.14	0.00	212.59	0.00	0.00
10 Crl	2249.10	458.53	1411.08	182.34	336.83	0.00	163.92
10 Jnctln	6606.90	903.98	2791.51	263.13	820.16	319.36	2579.31
10 Mtp	2365.64	283.86	1118.45	171.43	469.17	0.00	0.00
10 OcR1	3653.26	841.30	2635.87	416.30	1302.17	0.00	263.04
10 OcR2	8775.14	1381.17	3903.91	456.12	1203.07	149.90	292.12
10 SNh	2222.28	272.28	763.86	116.58	194.84	0.00	352.99
11 Cds26	10899.46	2768.38	5884.88	1089.49	2169.76	0.00	320.49
11 Clc	4186.97	884.10	3098.52	371.16	1176.02	0.00	184.54
11 Lchl	1004.77	182.36	597.14	123.72	381.88	0.00	0.00
11 Ngr	14667.30	1957.93	6678.78	738.05	1493.31	0.00	2405.35
11 Npl	1971.01	268.60	1066.67	133.98	479.23	0.00	94.69
11 Qchl	5095.07	449.03	1722.79	0.00	589.54	0.00	1560.90
11 Yhu	1278.49	194.80	848.23	112.53	466.19	0.00	0.00
12 Blz2	921.39	283.70	1296.26	337.69	1469.44	231.75	673.85
12 Epn	3569.96	614.61	1523.14	194.86	384.84	0.00	513.94
12 Esp	1811.45	304.82	1121.08	209.04	619.28	0.00	168.07
12 Juc	6930.92	475.33	2501.64	246.71	955.59	373.36	0.00
12 LaVeg	14062.95	987.89	4164.65	0.00	0.00	0.00	2450.36
12 Ocm	928.76	161.37	292.99	0.00	62.95	0.00	0.00
12 SJs	22781.36	6350.85	8000.00	2800.00	618.64	0.00	1271.19
13 Asp	2765.20	348.92	1125.35	128.16	297.47	0.00	0.00
13 Ctz	4955.24	738.35	2267.65	296.26	595.29	0.00	111.68
13 Grd	3668.47	366.93	1528.31	118.51	501.24	0.00	101.83
13 Kna	1886.28	400.27	1974.17	269.24	969.11	0.00	160.59
13 Lq2	3288.60	272.21	1202.14	98.34	230.88	0.00	714.73
13 PTcmb	7095.50	1039.15	1817.78	245.88	824.00	0.00	1198.68
13 Yjal3	459.59	115.37	429.16	92.55	292.23	0.00	0.00
14 Arm	699.06	298.52	1439.14	133.33	392.98	99.33	207.29
14 Azl	1522.00	357.10	1700.16	244.36	928.25	0.00	0.00
14 Cmn	3756.52	286.64	880.67	106.86	157.78	0.00	674.49
14 Mdll2	4333.93	1008.57	2569.79	470.80	1051.86	137.32	194.14
14 Rso	1825.25	357.35	1498.20	177.96	521.84	0.00	245.77

Table 9 (continued)

Sample	C28 (ng/g sediment)	C29 (ng/g sediment)	C30 (ng/g sediment)	C31 (ng/g sediment)	C32 (ng/g sediment)	C33 (ng/g sediment)	C34 (ng/g sediment)
14 Yri	16682.62	1274.82	4210.99	375.89	547.87	196.81	4778.37
14 Yxh	8502.20	1786.03	5866.15	980.95	3064.97	0.00	700.54
15 Alch	236.58	0.00	175.47	0.00	90.03	0.00	0.00
15 dp	2675.66	650.44	1898.23	316.37	820.35	125.66	224.34
15 ECT	4798.74	760.93	3218.59	437.97	1734.54	0.00	0.00
15 LLd	602.34	138.08	496.05	83.89	235.00	0.00	80.76
15 SCz	1302.17	299.35	1070.50	115.18	252.49	0.00	0.00
15 SJA	5885.37	679.18	3382.00	303.48	915.74	0.00	1578.35
15 Spnl2	1159.08	179.67	572.47	59.52	141.72	0.00	86.67
16 Psq	5123.13	482.53	1680.53	0.00	381.03	0.00	0.00
16 Sbk	1968.40	718.99	2247.73	462.86	1139.50	0.00	0.00
16 SEa	9997.21	853.56	2744.77	306.83	658.30	0.00	1283.12
16 SFY	2041.30	311.74	996.76	0.00	176.52	0.00	89.07
16 Sup	5513.98	183.73	931.46	96.85	196.55	0.00	811.82
16 Vrd	15862.47	1369.42	3801.02	333.58	792.98	0.00	1117.78
17 Atcz	5682.87	554.74	2505.65	341.68	837.51	318.11	1649.48
17 Ccb	25202.64	3394.91	6844.49	1291.23	997.17	0.00	7489.16
17 Hra	5032.20	705.15	1669.15	183.66	292.15	0.00	424.43
17 Mlt	2118.49	412.67	1510.73	257.41	673.14	0.00	146.07
17 Olol1	1545.59	162.69	1216.38	86.26	292.08	0.00	90.08
17 Pzs	1734.35	380.16	695.74	114.51	200.40	0.00	679.09
17 Spnl1	3781.03	702.39	1093.29	150.35	248.27	0.00	0.00
18 Cdr	7086.14	601.42	1436.25	0.00	185.24	0.00	718.74
18 Ipl	3400.80	435.06	970.52	0.00	278.88	0.00	0.00
18 Mdll1	4207.59	947.99	2944.07	561.33	1552.82	217.49	410.13
18 PBJ	817.42	179.80	688.75	103.40	334.90	0.00	107.42
18 SMarDel	11325.42	938.72	3186.70	421.85	1064.13	193.82	2441.81
18 Tnk	3230.06	494.80	1627.75	132.56	450.87	0.00	132.56
18 Vsq	5195.69	591.00	2367.91	0.00	610.57	0.00	0.00
19 Cmp	7014.04	670.83	1977.12	165.37	268.33	0.00	2030.16
19 Lch	1146.25	262.90	674.20	116.85	267.58	0.00	0.00
19 Mdl2.8	5953.55	1379.23	4006.56	697.27	1800.00	0.00	173.22
19 Ptx	2508.69	454.24	1227.64	245.03	587.43	0.00	0.00
19 Pzs23	7341.60	1719.47	4412.21	696.56	2000.00	335.88	761.45

Table 9 (continued)

Sample	C28 (ng/g sediment)	C29 (ng/g sediment)	C30 (ng/g sediment)	C31 (ng/g sediment)	C32 (ng/g sediment)	C33 (ng/g sediment)	C34 (ng/g sediment)
19 RVl	875.88	172.61	838.19	115.33	525.38	0.00	208.04
19 Zrhn	1565.67	198.60	749.21	97.72	296.85	0.00	178.11
20 Aml	8845.11	3948.37	2402.17	298.91	0.00	0.00	0.00
20 Cca	1939.50	231.07	1242.20	108.16	375.69	0.00	96.69
20 Esd	4786.01	564.58	2087.41	0.00	429.91	0.00	0.00
20 PAz	4684.95	925.02	3415.34	339.41	1147.65	0.00	0.00
20 PMR	2274.63	558.21	2267.16	202.99	740.30	0.00	0.00
20 Svla	357.28	0.00	310.13	0.00	143.27	0.00	0.00
21 Atn	2335.66	371.58	926.54	102.95	194.64	0.00	118.23
21 Atnl1	3704.60	339.99	1066.42	125.41	356.71	0.00	114.26
21 Ezp	24192.77	2465.68	10399.55	708.32	1627.35	0.00	2795.18
21 MHd	1807.14	260.32	760.32	80.95	160.32	0.00	911.11
21 Trmd	11233.07	924.64	4326.87	452.78	1902.70	459.14	5863.28
21 Yjap2	10406.44	2143.03	2636.47	419.55	682.96	0.00	0.00
21 Yla	13681.48	2449.29	7914.50	1257.33	3488.68	378.88	697.40
22 Atdlc	955.96	147.41	417.65	61.69	138.13	0.00	95.00
22 Ccl10	3235.55	0.00	879.40	209.80	298.37	157.04	2454.77
22 Ccll2	962.45	144.09	448.40	96.80	272.04	0.00	79.00
22 Prd	16149.93	2372.41	4558.92	483.36	822.79	0.00	467.77
22 Sbt	5439.43	874.39	3569.96	448.82	1384.00	158.25	317.39
22 Scb	7622.95	1586.42	1717.10	207.96	231.85	0.00	0.00
23 Clg	7176.13	848.08	1843.91	248.75	342.24	0.00	0.00
23 Cmo	1939.50	231.07	1242.20	108.16	375.69	0.00	96.69
23 CTL	2030.80	231.66	847.13	112.18	232.52	0.00	65.33
23 MA1	3794.14	469.80	1172.93	209.49	491.57	0.00	1462.28
23 Tcy	12612.99	1147.30	4322.05	419.95	1234.22	0.00	1098.81
23 Zmpl	8833.18	1434.43	6024.98	820.70	2483.50	0.00	765.39
24 EEt	1150.61	181.85	621.89	0.00	193.08	0.00	0.00
24 Jct	6161.38	507.64	2487.27	222.48	691.74	103.41	0.00
24 Ptzc	1890.44	202.00	519.26	67.33	131.81	0.00	176.32
24 Tng	2521.74	402.68	1220.07	0.00	262.21	0.00	315.72
24 Xbn	1267.78	322.67	1033.89	220.53	687.35	111.69	287.35
24 Ygy	1567.60	212.85	830.23	112.40	356.20	118.91	92.85
25 Tpltc	32035.43	1556.39	7719.25	915.84	2259.63	0.00	5955.71

Table 9 (continued)

Sample	C28 (ng/g sediment)	C29 (ng/g sediment)	C30 (ng/g sediment)	C31 (ng/g sediment)	C32 (ng/g sediment)	C33 (ng/g sediment)	C34 (ng/g sediment)
27 Mztln	1171.02	193.01	658.21	86.42	239.59	0.00	113.32
3 Blm	2052.71	387.32	1458.88	209.84	644.54	0.00	96.41
3 Blz1	5302.01	432.13	1168.67	0.00	218.47	0.00	1619.28
3 FdE	2605.09	554.20	1956.23	293.64	775.06	99.24	187.79
3 Nha	2440.15	442.79	1547.79	229.59	691.61	0.00	0.00
4 Alj	8189.92	573.09	1929.20	0.00	613.08	0.00	1979.18
4 Apq47	8247.79	759.16	2996.84	394.11	1315.58	72.63	917.68
4 MA4	2611.95	443.29	1171.14	214.21	618.71	0.00	1439.91
4 Oxl	2568.48	678.87	2065.52	365.86	686.30	0.00	0.00
4 Oxll3	3333.20	661.83	1457.86	165.67	311.45	0.00	290.74
4 Txy	4041.14	588.95	2009.90	141.71	402.29	0.00	0.00
5 Gja	1454.98	415.81	804.12	96.22	122.34	0.00	576.63
5 LBa	2790.15	570.93	1329.70	259.32	489.00	67.99	104.60
5 MVa	51452.17	677.22	17417.76	1602.20	2931.87	0.00	14634.55
5 SGer	3063.47	520.17	2743.58	346.40	1756.28	0.00	346.40
5 SJB	5613.90	856.78	3220.27	546.06	1597.99	0.00	463.15
5 StA	7021.13	1049.30	2619.72	0.00	873.24	0.00	0.00
5 Yjal1	4583.16	633.90	1852.45	198.29	347.97	0.00	635.18
6 Alb	13391.30	1099.48	3997.05	591.01	2085.48	331.61	3347.09
6 Alf	19257.75	1177.23	4973.62	233.23	844.98	0.00	1964.83
6 Ccc	3304.58	331.72	1826.30	144.75	347.41	0.00	680.34
6 Ccr	10039.66	583.61	2475.12	0.00	456.42	0.00	2898.62
6 Cdsl	1811.20	414.52	1472.31	268.68	877.46	0.00	94.40
6 Cgt	6354.37	934.01	2312.49	305.85	509.46	0.00	245.20
6 Chn	1669.27	319.51	1338.54	182.44	533.66	0.00	115.12
7 Atl	2000.67	237.04	976.43	98.99	317.17	0.00	338.05
7 BOA	4772.78	294.60	1250.95	0.00	338.48	0.00	0.00
7 Cbo	2482.60	284.92	1767.98	128.07	670.07	0.00	0.00
7 Lcd	2437.79	707.96	882.19	110.27	183.05	0.00	351.41
7 Pzs5	3797.73	560.68	1944.98	309.87	872.98	158.58	322.01
7 Qxl2.5	3830.41	1085.36	1119.28	0.00	159.41	0.00	113.06
7 Wha	582.41	78.42	514.94	0.00	222.01	0.00	0.00
8 Ccll4	4643.07	730.59	2159.06	398.02	904.11	0.00	98.93
8 ECA	3905.35	478.94	1408.42	227.17	507.34	427.83	21372.46

Table 9 (continued)

Sample	C28 (ng/g sediment)	C29 (ng/g sediment)	C30 (ng/g sediment)	C31 (ng/g sediment)	C32 (ng/g sediment)	C33 (ng/g sediment)	C34 (ng/g sediment)
8 GSM	4200.00	1051.02	3411.22	613.27	1568.37	220.41	405.10
8 Lag	11013.14	848.18	3045.26	313.87	675.91	185.40	2569.34
8 OCA	694.01	143.83	442.74	0.00	130.83	0.00	0.00
8 Olo2.5	7616.44	629.11	2037.74	155.26	327.49	0.00	473.85
8 Tmt	1146.50	111.59	778.34	57.83	357.71	0.00	0.00
9 Grdl1	4250.51	512.48	2365.94	233.32	664.76	121.98	269.34
9 LCh	7173.90	565.32	2065.88	147.67	492.23	0.00	431.08
9 Rqn	2977.93	479.79	2113.89	212.38	855.21	0.00	247.68
9 Sld	1484.88	242.44	796.10	78.05	207.32	0.00	0.00
9 Spn10	5613.50	897.11	1218.29	211.21	400.65	0.00	166.58
9 Tecm	8484.38	787.50	2596.88	0.00	403.13	0.00	4728.13
9 Zpn	1284.64	159.00	863.81	82.66	329.86	0.00	0.00

Table 10 – Calculations of Carbon Preference Index (CPI), Average Chain Length (ACL), and Aquatic:Terrestrial ratios from abundances of FAMES.

Sample	CPI (C20-C33)	ACL (C26-C32)	Aquatic:Terrestrial
10 Apql1	0.86	28.80	0.39
10 Crl	0.81	27.89	0.26
10 Jnctln	0.84	27.49	0.43
10 Mtp	0.81	28.03	0.25
10 OcR1	0.82	28.13	0.23
10 OcR2	0.82	27.71	0.22
10 SNh	0.89	26.93	0.35
11 Cds26	0.77	27.75	0.30
11 Clc	0.83	27.98	0.37
11 Lchl	0.86	27.77	0.23
11 Ngr	0.81	27.89	0.16
11 Npl	0.83	27.76	0.43
11 Qchl	0.89	27.37	0.41
11 Yhu	0.83	28.02	0.31
12 Blz2	0.79	29.57	0.45
12 Epn	0.82	27.43	0.31
12 Esp	0.81	28.35	0.22
12 Juc	0.81	27.78	0.28
12 LaVeg	0.83	27.37	0.20
12 Ocm	0.84	27.03	0.35
12 SJs	0.77	27.61	0.13
13 Asp	0.87	27.39	0.55
13 Ctz	0.82	27.66	0.31
13 Grd	0.85	27.50	0.38
13 Kna	0.83	28.46	0.39
13 Lq2	0.81	27.20	0.33
13 PTcmb	0.81	27.64	0.23
13 Yjal3	0.82	28.77	0.29
14 Arm	0.79	28.69	0.42
14 Azl	0.84	28.53	0.30
14 Cmn	0.84	27.26	0.43

Table 10 (continued)

Sample	CPI (C20-C33)	ACL (C26-C32)	Aquatic:Terrestrial
14 Rso	0.83	27.92	0.43
14 Yri	0.86	27.35	0.30
14 Yxh	0.83	28.24	0.23
15 Alch	0.95	28.23	0.40
15 dp	0.82	28.18	0.24
15 ECT	0.77	27.99	0.47
15 LLd	0.78	28.11	0.41
15 SCz	0.73	28.02	0.27
15 SJA	0.85	27.63	0.34
15 Spnl2	0.86	27.25	0.53
16 Psq	0.84	27.07	0.34
16 Sbk	0.74	28.61	0.27
16 SEa	0.84	27.39	0.38
16 SFY	0.83	27.49	0.41
16 Sup	0.87	27.29	0.22
16 Vrd	0.84	26.92	0.33
17 Atcz	0.84	27.68	0.39
17 Ccb	0.82	27.43	0.15
17 Hra	0.80	27.33	0.31
17 Mlt	0.86	28.19	0.23
17 Olol1	0.81	28.25	0.27
17 Pzs	0.83	27.32	0.42
17 Spnl1	0.84	27.40	0.16
18 Cdr	0.84	27.16	0.19
18 Ipl	0.83	27.08	0.38
18 Mdll1	0.79	28.16	0.37
18 PBJ	0.81	28.45	0.28
18 SMarDel	0.88	27.11	0.35
18 Tnk	0.81	27.99	0.38
18 Vsq	0.84	27.58	0.38
19 Cmp	0.81	27.36	0.22
19 Lch	0.76	27.67	0.21
19 Mdl2.8	0.78	28.09	0.36
19 Ptx	0.82	27.87	0.24

Table 10 (continued)

Sample	CPI (C20-C33)	ACL (C26-C32)	Aquatic:Terrestrial
19 Pzs23	0.79	27.97	0.24
19 RVl	0.85	28.61	0.52
19 Zrhn	0.82	28.09	0.31
20 Aml	0.80	27.05	0.39
20 Cca	0.83	28.17	0.46
20 Esd	0.85	27.17	0.34
20 PAz	0.83	28.34	0.34
20 PMR	0.87	28.30	0.62
20 Svla	0.89	28.61	0.24
21 Atn	0.81	27.39	0.40
21 Atnl1	0.87	27.42	0.34
21 Ezp	0.84	27.83	0.12
21 MHd	0.82	27.21	0.43
21 Trmd	0.84	27.99	0.29
21 Yjap2	0.78	27.51	0.29
21 Yla	0.83	27.83	0.20
22 Atdlc	0.82	27.25	0.18
22 Ccl10	0.86	26.55	0.30
22 Ccll2	0.79	28.00	0.39
22 Prd	0.84	27.54	0.14
22 Sbt	0.82	27.82	0.33
22 Scb	0.84	27.29	0.17
23 Clg	0.80	27.37	0.26
23 Cmo	0.83	28.17	0.46
23 CTL	0.82	27.81	0.20
23 MA1	0.84	27.67	0.32
23 Tcy	0.83	27.88	0.18
23 Zmpl	0.84	28.08	0.35
24 EEt	0.80	27.75	0.37
24 Jct	0.83	27.76	0.19
24 Ptzc	0.84	27.33	0.25
24 Tng	0.81	27.60	0.48
24 Xbn	0.80	28.55	0.31
24 Ygy	0.80	28.13	0.28

Table 10 (continued)

Sample	CPI (C20-C33)	ACL (C26-C32)	Aquatic:Terrestrial
25 Tpltc	0.81	27.76	0.17
27 Mztln	0.81	28.02	0.31
3 Blm	0.78	28.16	0.37
3 Blz1	0.83	27.24	0.32
3 FdE	0.82	28.09	0.27
3 Nha	0.83	27.89	0.29
4 Alj	0.91	26.97	0.44
4 Apq47	0.86	27.87	0.19
4 MA4	0.80	27.91	0.29
4 Oxl	0.80	28.33	0.17
4 Oxll3	0.81	27.36	0.26
4 Txy	0.80	27.71	0.41
5 Gja	0.93	27.52	0.50
5 LBa	0.79	27.71	0.33
5 MVa	0.85	27.17	0.26
5 SGer	0.82	28.61	0.38
5 SJB	0.81	28.03	0.40
5 StA	0.80	27.37	0.38
5 Yjal1	0.82	27.47	0.28
6 Alb	0.88	27.90	0.33
6 Alf	0.84	27.49	0.32
6 Ccc	0.83	27.62	0.25
6 Ccr	0.82	27.51	0.27
6 Cdsl	0.79	28.45	0.35
6 Cgt	0.83	27.32	0.33
6 Chn	0.83	27.92	0.48
7 Atl	0.81	27.76	0.41
7 BOA	0.87	27.40	0.29
7 Cbo	0.84	28.40	0.32
7 Lcd	0.78	27.39	0.36
7 Pzs5	0.84	27.80	0.37
7 Qxl2.5	0.81	27.19	0.29
7 Wha	0.89	28.25	0.18
8 Ccll4	0.78	27.59	0.43

Table 10 (continued)

Sample	CPI (C20-C33)	ACL (C26-C32)	Aquatic:Terrestrial
8 ECA	0.87	27.20	0.38
8 GSM	0.81	28.19	0.22
8 Lag	0.84	27.62	0.20
8 OCA	0.81	28.03	0.42
8 Olo2.5	0.84	27.64	0.14
8 Tmt	0.78	27.95	0.54
9 Grdl1	0.81	27.60	0.37
9 LCh	0.87	27.45	0.41
9 Rqn	0.82	28.17	0.34
9 Sld	0.80	28.00	0.37
9 Spn10	0.83	27.59	0.20
9 Tecm	0.86	27.22	0.53
9 Zpn	0.87	28.09	0.40

BIBLIOGRAPHY

Adams, D.K., and Comrie, A.C., 1997, The Northern American Monsoon: Bulletin of the American Meteorological Society, v. 78, p. 2197-2215.

Aichner, B., Herzschuh, U., Wilkes, H., Vieth, A., and Bohner, J., 2010, δD values of n-alkanes in Tibetan lake sediments and aquatic macrophytes – A surface sediment study and application to a 16 ka record from Lake Koucha: Organic Geochemistry, v. 41, p. 779-790.

Alfaro, A.C., Thomas, F., Sergent, L., and Duxbury, M., 2006, Identification of trophic interactions within an estuarine food web (northern New Zealand) using fatty acid biomarkers and stable isotopes: Estuarine, Coastal and Shelf Science, v. 70, p. 271-286.

Alley, R. B., and Cuffey, K. M., 2001, Oxygen- and hydrogen-isotopic ratios of water in precipitation: beyond paleothermometry: Reviews in Mineralogy and Geochemistry, v. 43, p. 527-553.

Bai, Y., Fang, X., Jia, G., Sun, J., Wen, R., and Ye, Y., 2015, Different altitude effect of leaf wax *n*-alkane δD values in surface soils along two vapor transport pathways, southeastern Tibetan Plateau: Geochimica et Cosmochimica Acta, v. 170, p. 94-107.

Bard, E., Rostek, F., Turon, J.-L., and Gendreau, S., 2000, Hydrological impact of Heinrich events in the subtropical Northeast Atlantic: Science, v. 289, p. 1321-1324.

Bourbonniere, R.A., and Meyers, P.A., 1996, Sedimentary geolipid records of historical changes in the watersheds and productivities of Lakes Ontario and Erie: Limnology and Oceanography, v. 41, no. 2., p. 352-359.

Bradbury, J. P., 2000, Limnological history of Lago de Patzcuaro, Michoacan, Mexico for the past 48,000 years: impacts of climate and man: Palaeogeography, Palaeoclimatology, Palaeoecology, v. 163, p. 69-95.

Bray, E.E., and Evans, E.D., 1961, Distribution of *n*-paraffins as a clue to recognition of source beds: Geochimica et Cosmochimica Acta, v. 22, p. 2-15.

Castaneda, I.S., and Schouten, S., 2011, A review of molecular organic proxies for examining modern and ancient lacustrine environments: Quaternary Science Reviews, v. 30, no. 21-22, p. 2851-2891.

Chikaraishi, Y., and Naraoka, H., 2003, Compound-specific δD-δ^{13}C analyses of *n*-alkanes extracted from terrestrial and aquatic plants: Phytochemistry, v. 63, p. 361-371.

Correa-Metrio, A., Bush, M.B., Cabrera, K.R., Sully, S., Brenner, M., Hodell, D.A., Escobar, J., and Guilderson, T., 2012, Rapid climate change and no-analog vegetation in lowland Central America during the last 86,000 years: Quaternary Science Reviews, v. 38, p. 63-75.

Cranwell, P.A., 1982, Lipids of aquatic sediments and sedimenting particulates: Progressive Lipid Research, v. 21, p. 271-308.

Cranwell, P.A., Eglinton, G., and Robinson, N., 1987, Lipids of aquatic organisms as potential contributors to lacustrine sediments – II.: Organic Geochemistry, v. 11., p. 513-527.

Dansgaard, W., 1964, Stable isotopes in precipitation: Tellus, v. 16, no. 4, p. 436-468.

Dansgaard, W., Johnsen, S.J., Clausen, H.B., Dahl-Jensen, D., Gundestrup, N.S., Hammer, C.U., Hvidberg, C.S., Steffensen, J.P., Sveinbjornsdottir, A.E., Jouzel, J., and Bond, G., 1993, Evidence for general instability of past climate from a 250-kyr ice-core record: Nature, v. 364, p. 218-220.

Diefendorf, A.F., Freeman, K.H., Wing, S.L., and Graham, H.V., 2011, Production of *n*-alkyl lipids in living plants and implications for the geologic past: Geochimica et Cosmochimica Acta, v. 75, p. 7472.

Douglas, P.M.J., Pagani, M., Brenner, M., Hodell, D.A., and Curtis, J.H., 2012, Aridity and vegetation composition are important determinants of leaf-wax δD values in southeastern Mexico and Central America: Geochimica et Cosmochimica Acta, v. 97, p. 24-45.

Eglinton, T.I., and Eglinton, G., 2008, Molecular proxies for paleoclimatology: Earth and Planetary Science Letters, v. 275, p. 1-16.

Feakins, S. J., and Sessions, A. L., 2010, Controls on the D/H ratios of plant leaf waxes in an arid ecosystem: Geochimica et Cosmochimica Acta, v. 74, no. 7, p. 2128-2141.

Feakins, S.J., Patrick Bentley, Lisa, Salinas, N., Shenkin, A., Blonder, B., Goldsmith, G.R., Ponton, C., Arvin, L.J., Wu, M.S., Peters, T., West, A.J., Martin, R.E., Enquist, B.J., Asner, G.P., and Malhi, Y., 2016, Plant leaf biomarkers capture gradients in hydrogen isotopes of precipitation from the Andes and Amazon: Geochimica et Cosmochimica Acta, v. 182, p. 155-172.

García-Lopez, J., and Allue, C., 2013, Modelling future no-analog climate distributions: A world-wide phytoclimatic niche-based survey: Global and Planetary Change, v. 101, p. 1-11.

Garcin, Y., Schwab, V.F., Gleixner, G., Kahmen, A., Todou, G., Sene, O., Onana, J.-M., Achoudong, G., and Sachse, D., (2012) Hydrogen isotope ratios of lacustrine sedimentary n-alkanes as proxies of tropical African hydrology: insights from a calibration transect across Cameroon: Geochimica et Cosmochimica Acta, v. 79, p. 106-126.

Gibson, J.J., and Edwards, T.W.D., 2002, Regional water balance trends and evaporation-transpiration partitioning from stable isotope survey of lakes in northern Canada: Global Biogeochemical Cycles, v. 16, no. 2, p. 1-9.

Gireeshkumar, T.R., Deepulal, P.M., and Chandramohanakumar, N., 2015, Distribution of sources of aliphatic hydrocarbons and fatty acids in surface sediments of a tropical

estuary south west coast of India (Cochin estuary): Environmental Monitoring and Assessment, v. 187, no. 56, p. 1-17.

Gotsch, S.G., Asbjornsen, H., Holwerda, F., Goldsmith, G.R., Weintraub, A.E., and Dawson, T.E., 2014, Foggy days and dry nights determine crown-level water balance in a seasonal tropical montane cloud forest: Plant, Cell & Environment, v. 37, p. 261-272.

Grootes, P.M., Stuiver, M., White, J.W.C., Johnsen, S., Jouzel J., 1993, Comparison of oxygen isotope records from the GISP2 and GRIP Greenland ice cores: Nature, v. 366, p. 552-554.

Haug, G. H., Hughen, K. A., Sigman, D. M., Peterson, L. C., and Rohl, U., 2001, Southward Migration of the Intertropical Convergence Zone Through the Holocene: Science, v. 293, p. 1304-1308.

Higgins, R.W., Mo, K.C., and Yao, Y., 1998, Interannual variability of the US summer precipitation regime with emphasis on the southwestern monsoon: Journal of Climate, v. 11, p. 2582–2606.

Hodell, D.A., Anselmetti, F.S., Ariztegui, D., Brenner, M., Curtis, J.H., Gilli, A., Grzesik, D.A., Guilderson, T.J., Muller, A.D., Bush, M.B., Corres-Metrio, A., Escobar, J., and Kutterolf, S., 2008, A 85-ka record of climate change in lowland Central America: Quaternary Science Reviews, v. 27, p. 1152-1165.

Hodell, D.A., Turchyn, A.V., Wiseman, C.J., Escobar, J., Curtis, J.H., Brenner, M., Gilli, A., Mueller, A.D., Anselmetti, F., Ariztegui, D., and Brown, E.T., 2012, Late Glacial temperature and precipitation changes in the lowland Neotropics by tandem measurement of $\delta^{18}O$ in biogenic carbonate and gypsum hydration water: Geochimica et Cosmochimica Acta, v. 77, p. 352-368.

Hou, J. Z., D'Andrea, W. J., MacDonald, D., and Huang, Y., 2007, Hydrogen isotopic variability in leaf waxes among terrestrial and aquatic plants around Blood Pond, Massachusetts (USA): Organic Geochemistry, v. 38, p. 977-984.

Hou, J. Z., D'Andrea, W., and Huang, Y., 2008, Can sedimentary leaf waxes record D/H ratios of continental precipitation? Field, model and experimental assessments: Geochimica et Cosmochimica Acta, v. 72, p. 3503-3517.

Huang, Y., Shuman, B., Wang, Y., and Webb, T., 2004, Hydrogen isotope ratios of individual lipids in lake sediments as novel tracers of climatic and environmental change: a surface sediment test: Journal of Paleolimnology, v. 31, p. 363-375.

Ingraham, N. L., 1998, Isotopic Variations in Precipitation *in* Isotope Tracers *in* Kendall, C., and McDonnell, J. J., eds., Isotope Tracers in Catchment Hydrology: Amsterdam, Elsevier Science B.V., p. 87-118.

IPCC, 2007: Climate Change 2007: The Physical Science Basis. Contribution of Working Group I to the Fourth Assessment Report of the Intergovernmental Panel on Climate Change [Solomon, S., D. Qin, M. Manning, Z. Chen, M. Marquis, K.B. Averyt, M.Tignor and H.L. Miller (eds.)]. Cambridge University Press, Cambridge, United Kingdom and New York, NY, USA.

IPCC, 2013, Climate Change 2013: The Physical Science Basis, Contribution of Working Group I to the Fifth Assessment Report of the Intergovernmental Panel on Climate Change [Stocker, T.F., D. Qin, G.-K. Plattner, M. Tignor, S.K. Allen, J. Boschung, A. Nauels, Y. Xia, V. Bex and P.M. Midgley (eds.)]. Cambridge University Press, Cambridge, United Kingdom and New York, NY, USA, 1535 pp, doi:10.1017/CBO9781107415324.

Killops, S.D., and Killops, V.J., 2004, An introduction to Organic Geochemistry: Wiley-Blackwell, 408 p.

Lachniet, M.S., and Patterson, W.P., 2009, Oxygen isotope values of precipitation and surface waters in northern Central America (Belize and Guatemala) are dominated by temperature and amount effects: Earth and Planetary Science Letter, v. 284, p. 435-446.

Leng, M.J., Metcalfe, S.E., and Davies, S.J., 2005, Investigating Late Holocene climate variability in central Mexico using carbon isotope ratios in organic materials and oxygen isotope ratios from diatom silica within lacustrine sediments: Journal of Paleolimnology, v. 34, p. 413-431.

Liu, W., and Huang, Y., 2005, Compound-specific D/H ratios and molecular distributions of higher plant leaf waxes as novel paleoenvironmental indicators in the Chinese Loess Plateau: Organic Geochemistry, v. 36, p. 851-860.

Liu, W., Yang, H., and Li, L., 2006, Hydrogen isotopic composition of *n*-alkanes from terrestrial plants correlate with their ecological life forms: Oecologia, v. 150, p. 330-338.

Lounejeva Baturina, E., Morales Puente, P., Cabadas Báez, H.V., Cienfuegos Alvarado, E., Sedov, S., Vallejo Gómez, E., and Solleiro Rebolledo, E., 2006, Late Pleistocene to Holocene environmental changes from $\delta^{13}C$ determinations in soils at Teotihuacan, Mexico: Geofisica Internacional, v. 45, p. 85-98.

Lozano-García, M.S., and Xelhuantzi-López, M.S., 1997, Some problems in the Late Quaternary pollen records of Central Mexico: Basins of Mexico and Zacapu: Quaternary International, v.43/44, p. 117-123.

Lyle, M., Huesser, L., Ravelo, C., Yamamoto, M., Barron, J., Diffenbaugh, N.S., Herbert, T., and Andreasen, D., 2012, Out of the tropics: The Pacific, Great Basin Lakes, and Late Pleistocene water cycle in the Western United States: Science, v. 337, p. 1629-1633.

Magill, C.R., Ashley, G.M., and Freeman, K.H., 2013, Ecosystem variability and early human habitats in eastern Africa: Proceedings of the National Academy of Sciences, v. 110, no. 4, p. 1167-1174.

McGee, D., Donohoe, A., Marshall, J., and Ferreira, D., 2014, Changes in ITCZ location and cross-equatorial heat transport at the Last Glacial Maximum, Heinrich Stadial 1, and the mid-Holocene: Earth and Planetary Science Letters, v. 290, p. 69-79.

McInerney, F.A., Helliker, B.R., and Freeman, K.H., 2011, Hydrogen isotope ratios of leaf wax *n*-alkanes in grasses are insensitive to transpiration: Geochimica et Cosmochimica Acta, v. 75, p. 541-554.

Mendoza, V. M., Villanueva, E. E., and Adem, J., 1997, Vulnerability of basins and watersheds in Mexico to global climate change: Climate Research, v. 9, p. 139-145.

Metcalfe, S.E., 1997, Paleolimnological records of climate change in México – Frustrating past, promising future?: Quaternary International, v. 43/44, p. 111-116.

Metcalfe, S. E., O'Hara, S. L., Caballero, M., and Davies, S. J., 2000, Records of Late Pleistocene-Holocene climatic change in Mexico – a review: Quaternary Science Reviews, v. 19, p. 699-721.

Meyers, P.A., 1997, Organic geochemical proxies of paleoceanographic, paleolimnologic, and paleoclimatic processes: Organic Geochemistry, v. 27, p. 213-250.

Nichols, P.D., Smith, G.A., Antworth, L.P., Hanson, R.S., and White, D.C., 1985, Phospholipid and lipopolysaccharide normal and hydroxy fatty acids as potential signatures for methane-oxidizing bacteria: FEMS Microbial Ecology, v. 31, p. 327-335.

Olson, D.M., Dinerstein, E., Wikramanayake, E.D., Burgess, N.D., Powell, G.V.N., Underwood, E.C., D'Amico, J.A., Itoua, I., Strand, H.E., Morrison, J.C., Loucks, C.J., Allnutt, T.F., Ricketts, T.H., Kura, Y., Lamoureux, J.F., Wettengel, W.W., Hedao, P., and Kassem, K.R., 2001, Terrestrial ecoregions of the world: A new map of life on Earth: BioScience, v. 51, p. 933-938.

Peterson, L.C., Haug, G.H., Hughen, K.A., Rohl, U., 2000, Rapid changes in the hydrologic cycle of the tropical Atlantic during the Last Glacial: Science, v. 290, p. 1947-1951.

Peterson, L.C., and Haug, G.H., 2006, Variability in the mean latitude of the Atlantic Intertropical Convergence Zone as recorded by riverine input of sediments to the Cariaco Basin (Venezuela): Palaeogeography, Palaeoclimatology, Palaeoecology, v. 234, p. 97-113.

Pierce, M.L., 2012, A 40,000 year geochemical record from Lake Chalco, Mexico [Master's thesis]: Duluth, University of Minnesota, 127 p.

Polissar, P. J., and Freeman, K. H., 2010, Effects of aridity and vegetation on plant-wax δD in modern lake sediments: Geochimica et Cosmochimica Acta, v. 74, p. 5785-5797.

Poynter, J., and Eglinton, G., 1990, Molecular composition of three sediments from Hole 717C: the Bengal Fan: *in* Cochran, J.R., Stow, D.A.V., et al., Proceeding of the Ocean Drilling Program, Science Results, 116, College Station, TX, p.155-161.

Rezanka, T., and Sigler, K., 2009, Odd-numbered very-long-chain fatty acids from the microbial, animal and plant kingdoms: Progress in Lipid Research, v. 48, p. 206-238.

Rieley, G., Collier, R.J., Jones, D.M., and Eglinton, G., 1991, The biogeochemistry of Ellesmere Lake, U.K. – I: Source correlation of leaf wax inputs to the sedimentary record: Organic Geochemistry, v. 17, p. 901-912.

Rommerskirchen, F., Eglinton, G., Dupont, L., Gunter, U., Wenzel, C., and Rullkotter, J., 2003, A north to south transect of Holocene southeast Atlantic continental margin sediments: Relationship between aerosol transport and compound-specific $\delta^{13}C$ land plant biomarker and pollen records: Geochemistry, Geophysics, Geosystems, v. 4, no. 12, GC000451.

Rommerskirchen, F., Eglinton, G., Dupont, L., and Rullkotter, J., 2006, Glacial/interglacial changes in southern Africa: compound-specific $\delta^{13}C$ land plant biomarker and pollen records from southeast Atlantic continental margin sediments: Geochemistry, Geophysics, Geosystems, v. 7 Q08010, doi:10.1029/2005GC00122.

Ruddiman, 2013, Earth's Climate (3nd ed): W.H. Freeman, 464 pages.

Sachse, D., Radke, J., and Gleixner, G., 2004, Hydrogen isotope ratios of recent lacustrine sedimentary *n*-alkanes record modern climate variability: Geochimica et Cosmochimica Acta, v. 68, p. 4877-4889.

Sachse, D., Radke, J., and Gleixner, G., 2006, δD values of individual *n*-alkanes from terrestrial plants along a climatic gradient – implications for the sedimentary biomarker record: Organic Geochemistry, v. 37, p. 469-483.

Sachse, D., Billault, I., Bowen, G. J., Chikaraishi, Y., Dawson, T.E., Feakins, S.J., Freeman, K.H., Magill, C.R., McInerney, F.A., van der Meer, M.T.J., Polissar, P., Robins, R.J., Sachs, J.P., Schmidt, H.L., Sessions, A.L., White, J.W.C., West, J.B., and Kahmen, A., 2012, Molecular paleohydrology: Interpreting the hydrogen-isotopic composition of lipid biomarkers from photosynthesizing organisms: Annual Review of Earth and Planetary Sciences, v. 40, p. 221-249.

Schimmelmann, A., Lewan, M.D., and Wintsch, R.P., 1999, D/H isotope ratios of kerogen, bitumen, oil, and water in hydrous pyrolysis of source rocks containing kerogen types I, II, and III: Geochimica et Cosmochimica Acta, v. 63, p. 3751-3766.

Seager, R., M. Ting, I. Held, Y. Kushnir, J. Lu, G. Vecchi, H.P. Huang, N. Harnik, A. Leetmaa, N.C. Lau, C. Li, J. Velez, N. Naik, 2007, Model Projections of an Imminent Transition to a More Arid Climate in Southwestern North America, Science, v. 316, p. 1181-1184.

Sessions, A. L., Burgoyne, T. W., Schimmelmann, A., and Hayes, J. M., 1999, Fractionation of hydrogen isotopes in lipid biosynthesis: Organic Geochemistry, v. 30, no. 9, p. 1193-1200.

Silliman, J.E., Meyers, P.A., and Bourbonniere, R.A., 1996, Record of postglacial organic matter delivery and burial in sediments of Lake Ontario: Organic Geochemistry, v. 24, no. 4, p. 463-472.

Simpson, E. S., Thorud, D. B., and Friedman, I., 1972, Distinguishing seasonal recharge to groundwater by deuterium analysis in southern Arizona: World Water Balance, v. 3, p. 623-633.

Tierney, J.E., Pausata, F.S.R., and deMenocal, P.B., 2017, Rainfall regimes of the Green Sahara: Science Advances, v.3, p. 1-9.

Wannigama, G.P., Volkman, J.K., Gillan, F.T., Nichols, P.D., and Johns, R.B., 1981, A comparison of lipid components of the fresh and dead leaves and pneumatophores of the mangrove Avicennia marina: Phytochemistry, v. 20, p. 659-666.

Xia, Z-H., Xu, B-Q., Mugler, I., Wu, G-J., Gleixner, G., Sachse, D., and Zhu, L-P., 2008, Hydrogen isotope ratios of terrigenous *n*-alkanes in lacustrine surface sediment of the Tibetan Plateau record the precipitation signal: Geochemical Journal, v. 42, p. 331-338.